Improving Nonviral Gene Transfer and Cellular Reprogramming with Microfluidic Nanomanufacturing

by

Christopher Lawrence Grigsby

Department of Biomedical Engineering
Duke University

Date:_____

Approved:

_____
Kam W. Leong, Supervisor

_____
William M. Reichert

_____
Ashutosh Chilkoti

_____
Charles A. Gersbach

_____
Dwight D. Koeberl

Dissertation submitted in partial fulfillment of
the requirements for the degree of Doctor
of Philosophy in the Department of
Biomedical Engineering in the Graduate School
of Duke University

2014

ABSTRACT

Improving Nonviral Gene Transfer and Cellular Reprogramming with Microfluidic Nanomanufacturing

by

Christopher Lawrence Grigsby

Department of Biomedical Engineering
Duke University

Date:_____

Approved:

_____
Kam W. Leong, Supervisor

_____
William M. Reichert

_____
Ashutosh Chilkoti

_____
Charles A. Gersbach

_____
Dwight D. Koeberl

An abstract of a dissertation submitted in partial fulfillment of the requirements for the degree of Doctor of Philosophy in the Department of Biomedical Engineering in the Graduate School of Duke University

2014

Abstract

The success of gene medicine ultimately depends on the efficient intracellular delivery and sustained expression of nucleic acid therapeutics, yet nonviral gene delivery performed with cationic polymer carriers has been chronically hindered by the slow release of nucleic acid payloads at their targets, as well as the transient nature of exogenous transgene expression. Polymer-nucleic acid nanocomplexes prepared with passive gene carriers using traditional bulk methods have proven inadequate for most translational applications. The objective of this work is to improve nonviral gene transfer through the selection, formulation, and application of improved nanoparticulate delivery systems.

After screening a number of number of cationic polymer delivery vectors ranging from natural to synthetic, high molecular weight to low, binary and ternary, we identified a bioreducible linear poly(amido amine) able to give sustained, robust expression of both DNA and RNA through serial dosing. We next turned our attention to the process of nanocomplex assembly. Traditional assembly via bulk mixing is poorly controlled, and the poor quality of these nanocomplexes is a significant impediment to the establishment of robust structure-function relationships and the advancement of efficacious nonviral gene delivery. So, we developed an emulsion-based microfluidic nanomanufacturing platform to better control the self-assembly process, and thus the physical properties of nanocomplexes. Confined mixing within picoliter droplets

generates self-assembled nanocomplexes that are more uniform and more effective. This microfluidic nanomanufacturing approach possesses broad utility in the production of polymer-nucleic acid nanocomplexes; we demonstrated that its benefits extend to multiple gene carriers, a range of nucleic acid payloads, and translationally relevant cell types. Then, we applied the improved nanomanufactured particles to begin to address an unmet clinical need, namely the lack of a safe and ethical source of cells to treat neurodegenerative diseases. Nonviral cellular reprogramming strategies eliminate the integration of viral DNA sequences and represent a potentially safer alternative to viral transdifferentiation methods to generate therapeutic cells. Using nanomanufactured polymer-nucleic acid nanocomplexes, we improved the efficiency of nonviral cellular reprogramming of fibroblasts directly to functional induced neuronal cells.

Nonviral gene therapy will continue to demand more sophisticated delivery systems to continue to progress. Microfluidic nanomanufacturing represents a reproducible and scalable platform to synthesize more uniform nanocomplexes that not only improves their performance but may also help establish clearer structure-function relationships that will inform future carrier design. Complementing the innovative chemical and biological approaches to create multifunctional nanoparticles, this study indicates that microfluidic nanomanufacturing can serve as a parallel physical strategy to both optimize the properties of polymer-nucleic acid nanocomplexes and improve their performance in applications with important clinical implications.

To my parents,

Barbara and Brian Grigsby

Contents

List of Tables

List of Figures

Acknowledgements

The research described here was made possible by generous financial support from the National Institutes of Health, the Duke Center for Biomolecular and Tissue Engineering, the American Heart Association, Sigma Xi, BD, the North Carolina State Firemen's Association, the North Carolina Association of Rescue and Emergency Medical Services, the US Fulbright Program, and the Whitaker International Program.

I am grateful to each of the members of my dissertation committee for their time and thoughtful advice during my time at Duke. Dr. Kam Leong has been continually and selflessly supportive as my research advisor, and always granted me the latitude to pursue the projects that I found most interesting. His creativity and optimism were a constant source of inspiration. I would also like to thank the many exceptionally bright labmates, collaborators, and colleagues who contributed significantly to my research endeavors. Especially Andy Adler, Megan Ho, Yihua Loo, Malathi Chellappan, and Jenny Jackman - thank you for sharing your precious time and many skills so freely with me over the years. While at UCSF, Profs. David Gardner, Songcang Chen, and Denis Glenn played an important role in developing my confidence and technical skills as a scientist. Thank you for your enduring support commitment to teaching. Kathy Barbour, Susan Story-Hill, Kristen Rivers, and Carla Sturdivant routinely exceeded the call of duty to make the department efficient and hospitable for all of the students.

My years in graduate school have been the best of my life, and I will always hold dear the memories made with my family and friends - you know who you are. A special thank you to Josie, Titus, and Shasta – it's impossible to imagine coming this far without the pack. You each continue to amaze me, and my world is better, brighter, and furrier with you around. Finally, I thank my parents for their constant encouragement of my academic and personal goals. None of my accomplishments would have been possible without their selfless sacrifice and support. I am grateful for the personal investments that so many have made in my success; to those acknowledged here and those left unacknowledged – my achievements are yours. Thank you.

1. Introduction

As advances in genomics continue to expand the range of targets for therapeutic intervention, nucleic acid-based technologies are poised to play a more prominent role in the treatment of many inherited and acquired diseases. One approach to their delivery has been to use polymers to condense nucleic acids into nanocomplexes, facilitating cellular uptake and preventing degradation en route to target cells. However, engineering polymeric gene delivery vectors to release an intact nucleic acid payload at the optimal time and place remains a formidable challenge. An ideal vector would provide total protection of complexed cargo from degradation prior to releasing it efficiently near or within the nucleus of a target cell. While optimization of polymer properties, such as molecular weight and charge density, has proven largely inadequate in addressing this challenge, applying polymeric carriers that respond to temperature, light, pH, and redox environment to trigger a switch from a tight, protective complex to a more relaxed interaction favoring release at the appropriate time and place has shown promise. After screening a number of polymer delivery systems ranging from natural to synthetic, high molecular weight to low, binary and ternary, we identified a bioreducible linear poly(amido amine) able to give sustained, robust expression of both DNA and RNA through serial dosing. This work strives, through optimization of this carrier's formulation and application, to alleviate the paucity of uniform, potent, biocompatible, and reproducibly generated gene carriers that are able to satisfy the contrary

requirements of adequate protection and efficient release, in order to achieve the primary goal of sustainable and robust transgene expression.

While tremendous effort has been concentrated on carrier design and optimization, the process of nanocomplex assembly has been largely overlooked. Traditional assembly via bulk mixing (i.e. vortex mixing), while convenient, is poorly controlled and results in metastable preparations, variable nanocomplex properties, and inconsistent results. The poor quality of these nanocomplexes is a significant impediment to both the establishment of robust structure-function relationships and the translation of nonviral gene delivery. So, we developed an emulsion-based microfluidic nanomanufacturing platform to better control the self-assembly process, and thus the physical properties of nanocomplexes, through confinement of the complexation reaction to picoliter droplets. Confined mixing within droplets enables the charge neutralization between polyelectrolytes to reach equilibrium, thereby generating self-assembled nanocomplexes that are more uniform and more effective. Nanocomplexes produced by this nanomanufacturing approach were smaller, more monodispersed, lower in zeta potential, and more colloidally stable compared to their bulk-assembled counterparts. The amount of unreacted polymer remaining following assembly was reduced, contributing to diminished cytotoxicity. Most importantly, the improved nanoparticles consistently mediated improved transfection. We applied a quantum dot-FRET nanosensor paired with flow cytometric detection to ascribe the increased

transfection efficiency to specific changes in intracellular behavior, such as uptake and intracellular release. This microfluidic nanomanufacturing approach possesses broad utility in the production of polymer-nucleic acid nanocomplexes; we demonstrated that its benefits extend to custom gene carriers, a range of nucleic acid payloads, and multiple translationally relevant cell types.

The increased transfection efficiency and diminished toxicity of nanomanufactured particles are especially advantageous in applications requiring high levels of transgene expression and repeated administration. One such application is the nonviral direct cellular reprogramming of fibroblasts to neurons. In an effort to address the lack of a safe and ethical source of therapeutic cells to treat neurodegenerative diseases, we developed a nonviral transfection strategy to deliver genes encoding the transcription factors necessary to convert fibroblasts directly to functional neuronal cells. Nonviral cellular reprogramming strategies eliminate the integration of viral DNA sequences and represent a potentially safer alternative to viral transdifferentiation methods. Our method produced neuronal cells with appropriate morphological changes, activation and expression of endogenous neuronal markers, and electrophysiological function. Delivery of the reprogramming factors with microfluidic nanomanufactured particles significantly improved the efficiency of this nonviral neuronal transdifferentiation, which is a critical parameter in the effort to generate a

sufficient supply cells for potential transplantation given the postmitotic, non-proliferative nature of neurons.

The overall objective of this work is to improve nonviral gene delivery through the production of polymer-nucleic acid nanocomplexes using advanced bioprocessing and nanomanufacturing techniques. This dissertation describes efforts to extend, evaluate, and apply a reliable and scalable microfluidic platform to manufacture polymer-nucleic acid nanocomplexes with better-controlled characteristics and improved functional performance. Through the results described here, we have contributed to the improvement of nonviral gene transfer and cellular reprogramming by: 1) selecting and synthesizing a promising polymeric gene carrier while optimizing its delivery strategy to facilitate serial dosing without compounding cytotoxicity, 2) implementing emulsion-based microfluidic nanomanufacturing techniques to improve the physicochemical characteristics and functional performance of the chosen nanoparticles, and 3) applying these more potent nanoparticles to increase the efficiency of nonviral cellular reprogramming of fibroblasts to functional induced neurons. Ultimately, efficacious nonviral gene delivery will depend on the combination of intelligent material design, controlled nanomanufacturing, innovative imaging techniques, and sophisticated model systems to enable the rational design and advancement of polymeric gene delivery systems. We addressed each of these considerations through the following specific aims.

1.1 Specific Aim 1

Screen, select, and synthesize a promising polymeric gene carrier while optimizing its delivery scheme to facilitate serial dosing without compounding cytotoxicity. In this aim, we identified a polymer gene carrier with an inherent response mechanism to changes in the redox environment present in the cytoplasm of cells. This carrier is designed to release its payload efficiently within cells, and then degrade to minimize associated sequelae. Employing this carrier enabled us to optimize and adopt serial dosing schemes to achieve consistently high transgene expression levels without compounding toxicity.

Hypothesis 1: *By synthesizing, screening, and selecting a responsive polymeric gene carrier that mediates very high transfection levels through the efficient release of nucleic acids, we can deliver serial doses to mitigate the problem of transient expression, without prohibitive limitations arising from compounding cytotoxicity.*

1.2 Specific Aim 2

Develop and evaluate the benefits of microfluidic nanomanufacturing with select gene carrier systems, nucleic acid payloads, and translationally relevant cell types to achieve improved nanoparticle physicochemical properties and functional performance. In this aim, we proved the feasibility of improved nanocomplex preparation using a microfluidic nanomanufacturing approach with multiple gene carriers loaded with either plasmid DNA or messenger RNA payloads. We

characterized the physical and chemical properties of these nanomanufactured products and quantified their intracellular release using a quantum dot-FRET flow cytometric detection system. We also tested the transfection capabilities of the improved particles in primary cells, stem cells, and other difficult-to-transfect cell types.

Hypothesis 2: *Nanomanufactured nanoparticles composed of custom polymeric gene carriers and diverse nucleic acids exhibit consistent improvements in physical properties when compared to their counterparts produced by conventional bulk methods. These changes lead to differences in intracellular release and improved functional performance, including superior transfection, in a variety of cell types.*

1.3 Specific Aim 3

Apply nanomanufactured particles to increase the efficiency of nonviral direct cellular reprogramming of fibroblasts to functional induced neurons. In the final aim, we applied the microfluidic nanomanufactured particles to improve nonviral direct cellular reprogramming. We delivered the three transcription factor genes required to directly convert fibroblasts to functional induced neurons, demonstrating that such conversion is feasible without the use of viral delivery methods. The serial dosing approach derived from Specific Aim 1, when paired with the more-potent microfluidic nanomanufactured particles derived from Specific Aim 2, enabled the generation of functional induced neurons with greater efficiency.

Hypothesis 3: *The increased transfection efficiency and diminished toxicity of nanomanufactured particles translates to an increase in the cellular reprogramming efficiency of fibroblasts directly to functional neuronal cells.*

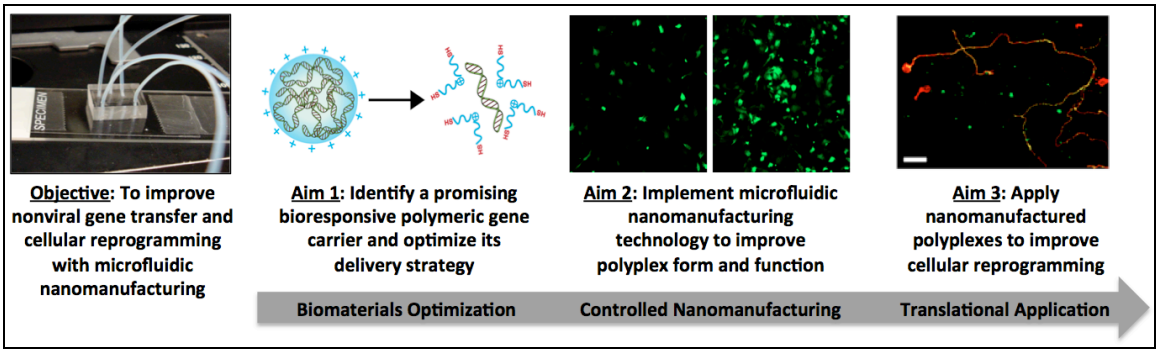

Figure 1. Summary of Specific Aims
To improve nonviral gene transfer and cellular reprogramming, we optimized the formulation of a bioresponsive polymeric gene carrier, implemented a microfluidic nanomanufacturing approach to further improve the form and function of these nanoparticles, and applied them to enhance nonviral direct cellular reprogramming.

2. Background and Motivation

Some of the material in Chapter 2 is included in:

1) Balancing protection and release of DNA: tools to address a bottleneck of non-viral gene delivery. Grigsby CL and Leong KW. 2010. J R Soc Interface. 7 Suppl 1:S67-82

2) Understanding nonviral nucleic acid delivery with quantum dot-FRET nanosensors. Grigsby CL, Ho YP, Leong KW. 2012. Nanomedicine. 7(4):565-77

Gene therapy has the potential to treat a wide variety of inherited and acquired genetic disorders, including diabetes, cystic fibrosis, cancer, and hemophilia [1-3]. The theoretical simplicity of the technique, along with the sequencing of the human genome, gave rise to the field amidst considerable excitement in the 1990's [4]. To treat diseases caused by a missing or aberrant protein, DNA encoding the desired gene is introduced to the nucleus of a cell where it is subsequently processed into a functional protein. In practice, however, this has proven much more difficult than predicted. The lack of safe and effective gene delivery methods has hindered the clinical translation of gene therapy. Many potential barriers exist along the path from the laboratory bench to the nucleus of a cell. First, the DNA must reach the plasma membrane of a target cell and be taken up. The path to target cells is nontrivial, as the extracellular environment contains many molecules able to trap and degrade DNA. Once inside the cell, the DNA

encounters a harsh enzymatic environment that promotes its degradation. In most cases, the administration of naked DNA results in insufficient amounts of intact coding sequence reaching the nucleus. In an effort to increase the amount of intact DNA reaching the nucleus, various techniques have been used with mixed degrees of success. Poration of the plasma membrane has been accomplished using electrical and mechanical means such as electroporation, ultrasound-based sonoporation, and the gene gun. However, for reasons of low efficacy, tissue damage, or poor access to deep tissue, these methods face significant barriers to translation in vivo. The bulk of current research is focused on the use of vectors designed to package and protect a DNA payload for delivery into the cell. Vectors commonly used today range from virus to lipids, peptides, and polymers.

The majority of gene therapy clinical trials have relied on viral vectors for gene transduction due to their high efficiency. However, the high transfection efficiency of viral vectors comes at a cost. Viral vectors pose safety concerns stemming from their immunogenicity and toxicity. Limitations of cell mitosis for retrovirus, contamination of adenovirus, and packaging constraints of adeno-associated virus (AAV) also lessen their appeal. Nonviral vectors composed of cationic polymers, lipids, and peptides able to form ionic complexes with DNA currently achieve lower and transient transgene expression levels, but possess the potential advantages of unrestricted DNA cargo size, ease of synthesis, low immunogenicity, and potential for repeated administration. They

can also address many pharmaceutical considerations better than viral vectors, such as scale-up, storage stability, and quality control. Still, nonviral gene delivery remains prohibitively inefficient for most therapeutic applications. Development of safe and effective nonviral gene carriers is critical to the eventual success of gene therapy.

Polycationic polymers have been extensively investigated as gene delivery vectors because of their versatility. They are able to interact electrostatically with negatively charged nucleic acids to form stable particles, termed polyplexes, with diameters on the order of nanometers. Physical properties of polymers such as rigidity, hydrophilicity, charge density, biodegradability, and molecular weight can be tuned to modulate gene delivery properties such as DNA binding, colloidal stability of ionic complexes, endosomal escape, vector unpacking, cytotoxicity, and transfection efficiency. Also, it is likely that for different target cells and tissues, or different routes of administration, the optimal characteristics of the DNA-polymer nanoparticles would differ in kind. For gene therapy to advance, rational design of gene delivery vectors able to address the individual rate-limiting steps identified along the gene delivery pathway is necessary. These steps include cellular localization and binding, internalization, subcellular trafficking, endosomal escape, unpacking and release, and nuclear translocation (Figure 2). Each must be studied individually and in concert, as changes in the structure of a polymeric vector designed to increase unpacking could adversely influence its behavior during another step up- or downstream. Without considering each

step independently and systematically, advances will remain phenomenological and stochastic. Once each step is understood, the knowledge can be integrated toward the rational design of polymeric gene carriers that address multiple barriers.

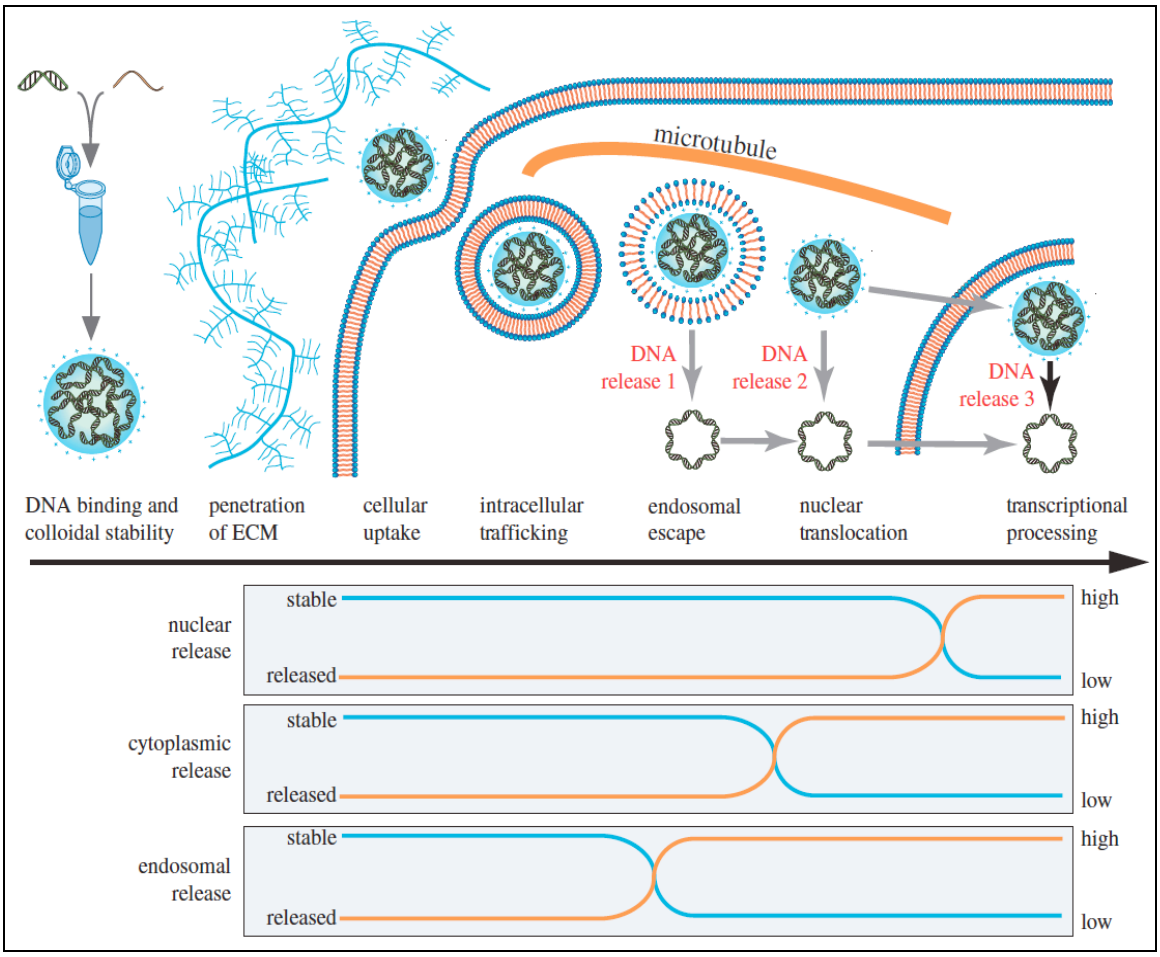

Figure 2. Barriers to Nonviral Gene Delivery
After shuttling a DNA payload into the cell, a carrier must then release it. This happens either (i) in the endocytic vesicle, (ii) in the cytoplasm or (iii) in the nucleus. Ideally, the carrier would switch from a protective element to one favoring release at one of these locations.

One crux of the nonviral gene delivery pathway is the release of intact nucleic acids from the polymer into the cytoplasm or nucleus of a target cell. If release occurs too slowly or not at all, the DNA will not be accessible to the transcriptional machinery and will eventually be lost or diluted out by processes including exocytosis and mitosis. If release occurs too readily, or if the polyplex is not compact enough to resist enzyme penetration, the DNA is susceptible to degradation prior to reaching the nucleus. Various vector design strategies have been tried to achieve release at the right time and place. So far, the competing functionalities of protection and efficient release have proven difficult to engineer into polymeric gene carriers. Fortunately, recent advances in imaging modalities, microscopy, and complex tissue models have begun to help elucidate the barriers encountered by a polyplex on the path to transfection. Both live and fixed cell imaging have advanced such that single particles can be tracked intracellularly in the spatiotemporal domain. Polyplexes can be tagged and tracked to determine their uptake kinetics and subcellular localization at specific time-points, as well as their dissociation status. The ability to resolve structure-function relationships at the subcellular, single-particle level provides valuable information for the rational design of the next generation of polymeric gene carriers. Sections 2.1 through 2.7 of this chapter examine the current rational design strategies to effect appropriate DNA release at the optimal time and place while maintaining adequate DNA protection, as well as the most important imaging techniques and engineering tools that allow for the

characterization and evaluation of these gene carriers. Systematic studies using state of the art imaging techniques and models will enable the rational design of polymeric gene carriers that address the tradeoff between protection and efficient release of DNA, helping to close the gap between engineering phenomena and therapeutic success.

In addition to gene carrier design, the means by which polyplexes are assembled can also impact their form and function. Bulk mixing, the process used by the vast majority researchers to form polyplexes via electrostatic self-assembly, introduces significant variability to the quality of polyplexes because of their metastable preparation and non-equilibrium composition [5]. The heterogeneity resulting from bulk synthesis impedes advances in nonviral gene delivery with respect to rational carrier design, mechanistic understanding, and optimization. The final properties and composition of the product depend on how the polyelectrolytes initially encounter one another, which is determined by chaotic mixing and operator inputs. Irreproducibility is rampant, as slight perturbations of mixing protocols are known to produce particles of differing qualities. The resulting heterogeneity is an impediment to the progress of nonviral gene delivery in multiple ways: 1) It precludes mechanistic understandings of the gene transfer process if only a subpopulation of particles is responsible for an observed behavior; 2) it exacerbates the challenge of establishing precise structure-function relationships; and 3) it hinders the translation of nonviral delivery systems if they cannot be manufactured in a reproducible and scalable manner. Sections 2.8

through 2.10 of this chapter address the basis of the manufacturing issue, as well as some of the most recent attempts to address the problem with a range of engineering approaches.

The primary objective of gene delivery is to have a positive impact on human health, and one of the most pressing unmet clinical needs today is the prevalence and intransigence of neurodegenerative diseases. Patients with Alzheimer's or Parkinson's disease may see temporary improvements with pharmacologic intervention or deep brain stimulation, but the clinical benefits inevitably decline with the progressive loss of neuronal function. Cell replacement therapy has been proposed as a long-term solution. However, finding an appropriate cell source has been a challenge while safety and ethical concerns preclude the use of embryonic stem cells. The translation of therapies derived from induced pluripotent stem cells (iPSC) have been slowed by concerns of teratogenic potential. Recently, the reprogramming of adult cells from one type to another was reported. In 2010, researchers found that expression of three genes encoding transcription factors (Ascl1, Brn2, Myt1l) delivered by lentivirus was sufficient to convert fibroblasts to functional neurons [6]. This exciting revelation brings the prospect of an ethical, practical, and safe neuronal cell therapy one step closer to reality. However, the unpredictable integration of viral DNA sequences into the genome of the cells renders them unsuitable for transplantation. So, there would be significant benefits associated with a non-integrative, nonviral cellular reprogramming approach to

generate a source of therapeutic neuronal cells directly from differentiated somatic cells. While such nonviral direct conversion of fibroblasts to functional neurons greatly reduces the ethical and safety concerns of previous methods, its efficiency must be increased to enable potential translation. Sections 2.11 through 2.13 of this chapter address aspects of cellular reprogramming and relevant recent therapeutic approaches for the treatment of neurodegenerative diseases.

2.1 Release as a Rate-Limiting Barrier

It is intuitive that polyplexes must dissociate in order for the bound DNA to be processed within a target cell. Early computational models of nonviral gene delivery using an integrative systems approach identified the efficient release of DNA from its carrier as a critical step in the transfection process. A first-order mass action model predicted a biphasic dependence of transgene expression on the rate of vector unpacking, which was validated with in vitro transfection data [7]. An optimal intermediate value for the release rate constant was computed when the model was populated with values for polylysine gene carriers taken from the literature. The model predicted a dissociation threshold rate-constant of 10^{-3} minutes^{-1}, above which transfection efficiency is significantly increased. A more recent and comprehensive model arrived at the same conclusion [8]. Some of the data used to create the model were borrowed from an earlier report that proposed vector unpacking as a potential rate-limiting barrier to nonviral gene delivery. In that study, Schaffer et al. found that

fluorescently labeled 180-residue polylysine (MW~28 kDa) remained co-localized with plasmid DNA in the nucleus and perinuclear region of transfected fibroblasts [9] (Figure 3). In contrast, 36- and 19-residue polylysines delivered free plasmid to the nucleus. In vitro transcription assays showed that the shorter polycations freed plasmid more readily for transcription, and cell transfection studies showed that the intermediate polymer length resulted in the highest transgene expression levels. The authors explained that dissociation might occur spontaneously due to thermodynamics, or via competitive displacement of DNA by another anionic species. Genomic DNA in the cell nucleus can participate in polyplex destabilization by ion exchange [9], but it remains unknown precisely which dissociative mechanisms dominate for most carrier systems. Nuclear microinjection of polyethylenimine (PEI)-DNA polyplexes results in high transgene expression levels, showing unpacking can take place in the nucleus [10]. Again, chromosomal DNA may be implicated, or polymerases may mediate DNA release similar to their stripping of histone proteins during DNA replication [11]. Another study demonstrated that RNA found in the cytoplasm could also promote DNA release by ion exchange [12]. Regardless of exactly where and by which processes polymer and payload dissociate, it is certain that inefficient release of DNA precludes efficient transfection.

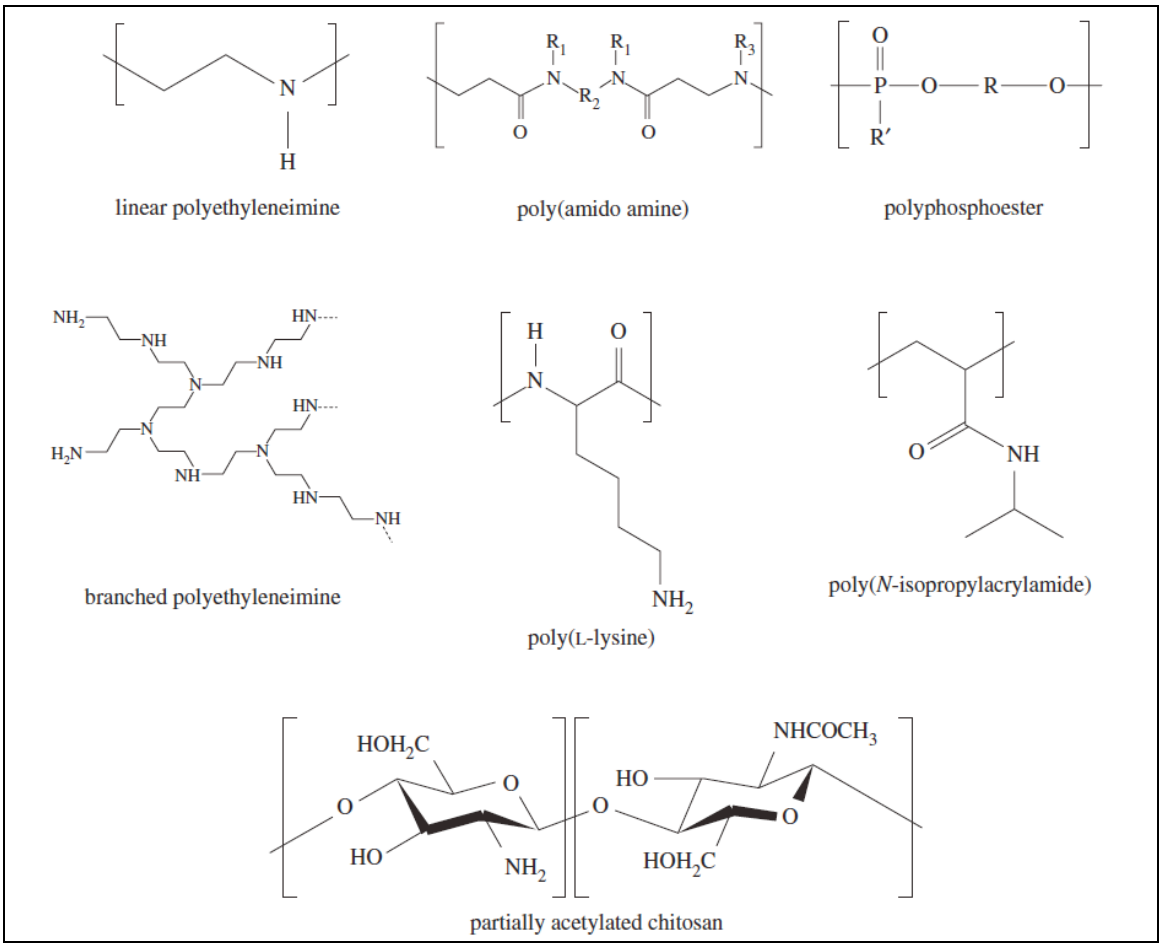

Figure 3. Polymers Commonly Used and Modified for Nonviral Gene Delivery

2.2 Modulating Protection and Release with Polymer Properties

Many physical, chemical, and structural features of a polymeric gene carrier affect its ability to bind, condense, and protect a DNA payload from enzymatic and nonspecific degradation. These same features also play important roles in determining when and where the DNA is released. With many polymeric systems, the abilities to protect and efficiently release DNA are inversely related. One goal of carrier design

should be to strike an optimal balance between protection and release to maximize transfection (Figure 4).

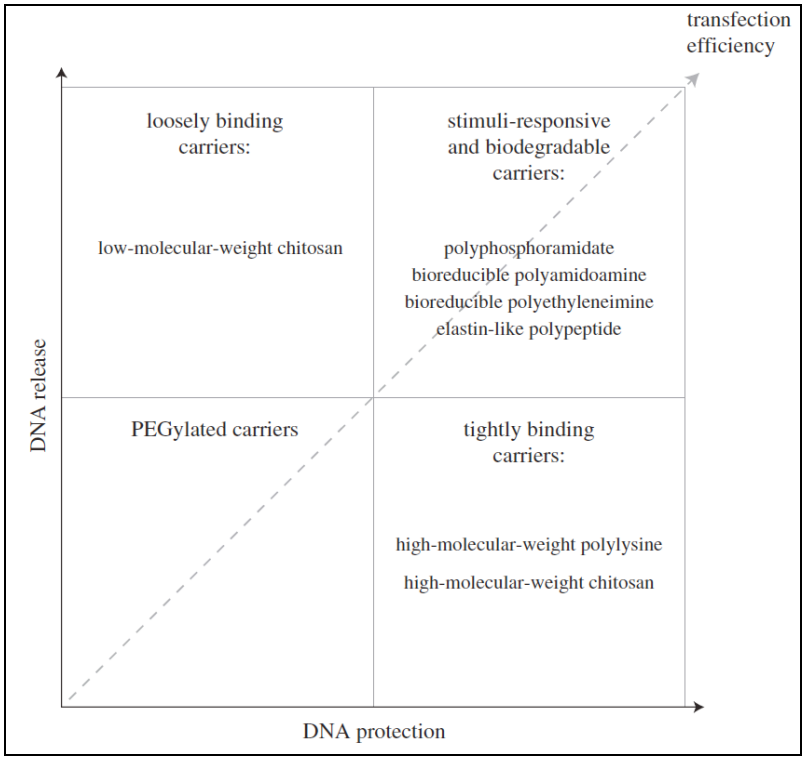

Figure 4. Balancing Protection and Release of Nonviral Gene Carriers
Vectors exhibiting both strong protection of DNA and efficient intracellular release mediate the highest levels of transfection. Vectors capable of only one of these qualities typically do not perform as well. Vectors capable of neither are largely ineffective.

2.2.1 Polymer Length

Molecular weight or length of the polymer chains is one property known to influence the tradeoff between protection and release. For instance, one study demonstrated that polyplexes based on highly defined low molecular weight chitosan oligomers (10- to 50-mers) dissociated more easily than those derived from high

molecular weight (1000-mer) chitosan chains [13]. Below about 14 monomer units, the polyplexes formed were weak and unstable. The more easily dissociated polyplexes also mediated higher transgene expression levels in vitro and in vivo. However, the polyplexes needed to be formed with a much higher polymer-to-DNA ratio (N:P charge ratio as high as 60:1, as opposed to 5:1 for the high molecular weight chitosan) to bind and retain DNA as determined by gel retardation assay. Lower mass ratios resulted in unstable polyplexes, yielding poor transfection results. The decreased ability of the shorter polycations to effectively complex the anionic phosphate groups of DNA can be explained by their lower binding valency combined with the loss of the chain entanglement effect exhibited by the longer polymers. Longer polymer chains more easily entangle free DNA once the initial electrostatic interaction occurs, creating an additional non-ionic, knot-like binding component [14]. Shorter chains are less able to physically entangle molecules of DNA, and the requirement of additional molecules to match the binding strength of longer chains may be energetically unfavorable to polyplex formation.

As discussed previously, Schaffer et al. reported that polylysine of an intermediate length (36 residues) possesses superior gene delivery properties than shorter (19 residues) and longer (180 residues) chains [9]. Dissociation rates and transcription levels were higher in vitro for the smaller chains, whereas longer polymer chains significantly inhibited RNA synthesis. However, once the chains became too

short, transgene expression levels dropped. Premature release and degradation of the plasmid was again the putative culprit. Selecting the optimal chain length of a polymer gene carrier is perhaps the most straightforward and established way to change the release kinetics and DNA protection properties of a polymeric gene carrier, but that alone may not be enough because the structural and charge characteristics of a polymer are also important.

2.2.2 Charge Density and Structural Rigidity

There are few published systematic studies investigating the effects of charge density and stiffness of polymeric gene carriers on their DNA binding affinity and release characteristics. One such study using a series of linear poly(amido amine)s (PAAs) looked at how their physiochemical properties and colloidal stability were affected by changes in charge density and structural rigidity [15]. The authors reported that the DNA binding behavior of the PAAs depended on their molecular structures, showing by gel retardation assays that chains with a single tertiary amino group per monomer bound DNA more weakly than those with two tertiary amino groups. However, when the methylene linker in the diacrylamide segment of the polymer possessing two tertiary amino groups was substituted for a piperazine ring, the DNA binding affinity was greatly diminished. The authors speculated that this decrease in binding is caused by the resultant increase in rigidity from the ring substitution. The increase in rigidity, despite a higher charge density, resulted in decreased colloidal

stability and transfection efficiency. It is difficult to separate the effects of decreased uptake of the larger polyplexes and premature degradation of plasmid when ascribing the blame for the decrease in transfection, but it is likely that both effects contribute.

Another series of studies aimed to improve the transfection efficiency of PEI through the optimization of charge density. Forrest et al. acetylated primary and secondary amines of PEI to varying degrees, decreasing the number of positive charges available to bind DNA at neutral pH [16]. They found that acetylation of 43 percent of the primary amines and 23 percent of the secondary amines of 25 kDa branched PEI decreased the surface charge and increased the size of polyplexes, while mediating up to 21-fold higher transgene expression compared to unmodified PEI. The authors attribute the increase in transfection, at least partially, to more efficient release of DNA from the acetylated PEI. Gabrielson et al. studied 25 kDa branched PEI with even higher degrees of acetylation [17]. They found that acetylation of the primary amines up to 57% increased transfection, while further acetylation resulted in diminished efficacy. This time, the authors' speculation that the decrease in charge density results in more efficient intracellular release of DNA was confirmed via fluorescence imaging techniques. These studies demonstrate that an optimal charge density exists for PEI, and that it alters the polymer-DNA binding and release characteristics.

A recently developed gene carrier is composed of linear PEI with approximately 20 percent of the secondary amines functionalized with hydrolysable methyl ester,

charge-shifting side chains [18]. As ester hydrolysis occurs, negative charges are gradually introduced to the polymer, so that the effective positive charge density is decreased, weakening DNA binding and promoting polyplex dissociation. Higher degrees of side-chain addition resulted in polyplexes that dissociated prematurely, but the carrier with 20 percent substitution mediated 8-fold higher transfection levels than unmodified linear PEI. The authors propose that 20 percent substitution results in the accumulation of negative charges at the proper rate to release DNA intracellularly via competition with other anionic species. Another way of promoting DNA release is the design of biodegradable vectors, such as polyphosphoesters including polyphosphates (PPEs) and polyphosphoramidates (PPAs) [19]. The rationale of using carriers that can be hydrolyzed over time is derived from the desire to promote DNA release. By degrading steadily over time, these carriers can provide sustained release of DNA, improving the bioavailability inside and outside the cell. The release kinetics can be adjusted by varying the polymer-to-DNA ratio, as well as the composition of the backbone and side chains. Polyphosphoesters also offer a high degree of structural versatility, which permits the tailored design of its physiochemical properties. Their efficacy rivals PEI, but with much less associated toxicity. However, a steady degradation means that control over the spatiotemporal release of DNA is lacking. It would be advantageous to trigger DNA release at a specific time and place.

2.2.3 Stimuli-Responsive Strategies

The ideal gene carrier would protect DNA from nucleases and provide unrestricted access to polymerases. Polymers able to respond to biological or environmental cues that signal the right time and place for DNA deprotection and release are perhaps better suited than their unresponsive counterparts for providing such selective enzymatic access. Polyplexes capable of responding to environmental stimuli have the potential to circumvent barriers to delivery in ways that traditional carriers cannot. Many physical stimuli have been studied, including light, heat, sonication, and magnetic fields. Furthermore, some polymers can respond to chemical stimuli such as pH and redox changes. One reason that viruses are such potent gene carriers is their ability to respond to physical and chemical cues in certain subcellular compartments to more efficiently complete the steps of their replication cycle. Many researchers are trying to borrow viral response mechanisms and apply them to polymeric gene carrier designs.

2.2.3.1 Redox-Responsive Polymers

One strategy to facilitate DNA release at the right time and right place is to include bioreducible disulfide linkages in the polymer chain. Disulfide bonds are covalent linkages formed via the oxidation of sulfhydryl (-SH) groups. They are quickly cleaved inside cells, which possess a reducing environment due to high concentrations of reducing enzymes such as glutathione reductase and sulfhydryl species like

glutathione as compared to the extracellular spaces. Consequently, disulfide bonds are relatively stable in plasma and extracellular spaces, but rapidly degrade inside cells. This rapid degradation can lead to the dissociation of a polyplex and DNA release. Disulfide linkages added to polylysine and 25 kDa branched PEI resulted in improved gene carrier properties such as higher transfection levels and diminished cytotoxicity when compared to their unmodified analogues [20, 21]. Lin et al. have shown more recently that a minimal number of disulfide linkages in the main chain of poly(amido amine)s is sufficient to allow efficient intracellular DNA release [22-24]. Again, a side effect of the polymer degradation is a marked decrease in cytotoxicity as compared to the polymer analogues lacking disulfide linkages. The ability of the polymer to protect the DNA prior to cleavage of the disulfide bonds is unaffected. Miyata et al. studied the addition of thiol groups to a polylysine backbone with possible modification of its charge density [25]. Using the reagent that substituted positive charges for disulfide linkages, they created a redox sensitivity that led to efficient intracellular DNA release and 50-fold higher transfection efficiency in cells, as compared to the thiolated polylysine with unaltered positive charges. The balance between charge density and disulfide cross-linking can both play crucial roles in the mediation of efficient gene transfer. These reports demonstrate that the inclusion of disulfide bonds into polymer chains can lead to the fast intracellular degradation of polyplexes, efficient DNA release, sufficient protection, improved transfection, and decreased cytotoxicity.

2.2.3.2 pH-Sensitive Polymers

Polymers sensitive to pH offer another layer of biochemical responsiveness. Decreases in pH are known to occur near tumors, sites of inflammation, and in the endocytic vesicles through which polyplexes travel following endocytosis. A triblock copolymer composed of lactosylated PEG-*block*-polysilamine-*block*-poly[2-(N,N-dimethylamino)ethyl methacrylate] (lac-PEG-PSAO-PAMA) has been developed by Oishi et al. to undergo pH-sensitive conformational changes [26]. When the pH drops from neutral (~7) to slightly acidic (~4) typical of endosomal compartments, the PSAO segments of the 3-layer micelle swell and cause the polyplex to grow in diameter. This conformational change may decrease the binding affinity of the polymer for DNA, allowing intracellular anions to compete with and release the DNA more easily. Prior to release, the tight conformation affords good protection to the bound DNA. The lactose group was incorporated to promote receptor-mediated endocytosis by hepatocytes.

To deliver genes specifically to the acidic interstitium of tumors, PEI-DNA nanoparticles have been further functionalized with a pH-responsive poly(methacryloyl sulfadimethoxine) (PSD)-*block*-PEG (PSD-*b*-PEG) [27]. At a normal physiological pH of 7.4, the nanoparticles mediate very little transfection. The PSD-*b*-PEG layer served to shield the positive surface charges of the PEI-based polyplexes, decreasing both cytotoxicity and the ability of the polyplexes to interact with cell membranes. However at pH 6.6, the polyplexes shed the PSD-*b*-PEG and exhibited the high transfection and

cytotoxicity characteristic of PEI-based systems. Such a high-sensitivity pH-responsive system could be used to shield and protect polyplexes at physiological pH until delivery to an acidic environment, whereupon stripping of the mask makes transfection possible. Despite the fact that the PSD-*b*-PEG used is not easily degraded, the principle shows good promise.

Another strategic alternative to shielding polyplexes with pH-sensitive units and the inclusion of polymer segments that switch conformations upon acidification is the addition of acid-labile linkages within the polymer backbone. Kim et al. introduced imine linkages into a PEI backbone by crosslinking low molecular weight PEI (1.8 kDa) with glutaraldehyde [28]. The half-life of hydrolytic degradation of their polymer decreased two orders of magnitude when the pH was changed from 7.4 (118 hours) to 4.5 (1.1 hours). A DNase protection assay confirmed that the carrier affords sufficient protection from nuclease activity. The system is designed such that DNA is released upon acidification of the endosomal compartment. The acid-labile PEI polyplexes yielded transgene expression levels similar to 25 kDa branched PEI, but with much lower associated toxicity likely due to the degradation into smaller chains.

2.2.3.3 Thermo-Sensitive Polymers

In contrast to the natural environmental stimuli encountered by the polyplexes discussed above, a stimulus can also be applied externally to trigger DNA release. A targeted increase in temperature is one stimulus frequently exploited. Poly(N-

isopropylacrylamide) (PNIPAm) is a widely-used thermo-sensitive polymer that exists in a water-soluble state below its lower critical solution temperature (LCST) of 32°C. Above its LCST, which can be tuned closer to body temperature by varying its monomer makeup, it becomes hydrophobic. This leads to phase transformation to a gel state, or a change in architecture if bound to other molecules. In its hydrophobic state, PNIPAm can condense large DNA molecules and is small enough to enter cells. When cooled below its LCST, PNIPAm reverts to the solution state to release the DNA [29, 30]. PNIPAm has also been grafted with proven gene carriers such as PEI and chitosan to impart responsive properties and improve transfection [31-35].

Another class of thermo-sensitive polymers used for gene delivery is elastin-like polypeptides (ELPs). These are pentapeptide repeats Val-Pro-Gly-Xaa-Gly where Xaa specifies any amino acid residue except proline. These polymers exhibit an inverse phase transition with temperature, as well as controllable degradation [36]. In contrast to the conventional thermosensitive polymer PNIPAm, polyplexes generated with ELPs allow for hyperthermic DNA release instead of release upon cooling. This can be beneficial in certain cases, as hyperthermia is already an established targeted treatment for some diseases such as cancer. As synthetic polypeptides, ELPs can be produced by recombinant methods to control polydispersity and expressed as fusion proteins if additional domains are desired. Chen et al. used a recombinant diblock copolymer consisting of cationic oligolysine (VGK_8G) and an ELP block with 60 repeat units of

VPGXG, where X is Val, Ala, and Gly in a 5:2:3 ratio for hyperthermic gene delivery [37]. While these and other novel thermo-responsive polymeric gene carriers, such as the diblock copolymer methoxy PEG-co-poly(ε-caprolactone) (mPEG-PCL) [38] are being explored and developed, temperature-sensitive gene delivery vectors have obvious drawbacks in that a temperature gradient must be applied in a site-specific and non-invasive manner for the technology to be attractive to physicians and patients. The sol-gel transition must also be sharp since the strong temperature buffering capacity in vivo would dampen any thermal gradient. These challenges hinder clinical translation, and currently limit the technology primarily to the realm of in vitro studies.

2.2.3.4 Light-Sensitive Polymers

Light is a physical stimulus that can be very convenient, depending on the application and target tissue. It is an appropriate stimulus for targets located near the surface of the body, as near-infrared (NIR) light between 750 nm and 1000 nm in wavelength penetrates the skin without damaging cells or tissues. This so-called "water window" is useful due to the lack of absorption from water or biological chromophores. Handwerger et al. designed a novel photolabile monomer for gene delivery. P25M consists of three domains, a cationic domain of 25 kDa PEI to bind DNA, a polymerizable methacrylamide moiety for crosslinking DNA within the polyplex, and a photolabile nitrobenzyl domain for triggered release by 365nm light [39]. Gel retardation demonstrated that P25M condensed DNA at a charge ratio of 3:4, and light scattering

showed the polymer forms polyplexes of < 500 nm diameter. This work demonstrates the feasibility of light-responsive polymeric gene carriers for the spatial, temporal, and metered delivery of DNA. Few other light-responsive polymers have been developed for gene delivery applications, but some have shown promise in the delivery of non-nucleic acid cargo [40-42].

2.2.4 Inclusion of Enzymes and Inhibitors

Polyplex systems need not be limited to simple pairs of polymer and DNA. Other molecules such as proteins, enzymes, and chemicals can also be included into the polyplex to enhance DNA protection or facilitate release. In a study of DNA-gelatin nanospheres for gene delivery, Truong et al. observed incomplete protection of complexed DNA from nuclease digestion. In an attempt to increase the protection of DNA, they co-encapsulated inhibitors of DNase I [43]. The inclusion of sodium iodoacetate and aurintricarboxylic acid each showed minor improvements in DNA protection, but the benefits did not translate to any improvement in transfection levels.

A pair of more recent studies examined the use of chitosanase to promote the dissociation of chitosan-based polyplexes [44, 45]. In the first report, the enzyme was pre-delivered to cells prior to transfection. The authors observed that radiolabeled chitosan polyplexes were able to penetrate cells twice as efficiently as commercial lipid transfection reagents, but the resultant transgene expression was far lower. However, upon pre-delivery of chitosanase via osmotic lysis, cells transfected with chitosan

polyplexes containing a LacZ reporter gene expressed twice as much β-galactosidase activity as those transfected with lipid reagents. In the subsequent report, the chitosanase gene was co-transfected along with the gene of interest since pre-delivery via osmotic lysis is impractical in vivo. The rationale was that once the chitosanase gene was processed, it would start a positive-feedback cascade leading to the degradation of all the chitosan and efficient release of DNA. In four different cell lines, the authors found that β-galactosidase and green fluorescent protein expression levels were similar between lipid-mediated transfections and chitosan polyplex transfections using the chitosanase construct. Expression levels with an inactive mutant of the chitosanase gene were identical to those with no chitosanase gene at all, barely above the levels achieved by naked DNA. Similar techniques have been used to neutralize the threat of binding and sequestration of nanoparticles by extracellular matrix (ECM) components. The functionalization of nanoparticles with collagenase resulted in the localized degradation of matrix molecules and a less tortuous path leading to the cell membrane that increased the rate of polyplex transport [46].

2.3 Imaging Techniques and Engineering Models to Evaluate the Protection and Release of DNA from Polyplexes

Traditionally, fluorescence microscopy has been the method of choice to image molecules involved in gene delivery. Fluorescently labeled carriers and DNA can be followed from the extracellular compartment, through the cell, and into the nucleus. However, co-localization of fluorescent signals and imaging at discrete time-points can

only give so much information about a carrier's function and fate. Recent advancements have vastly improved the precision with which engineers can observe the details of polyplex trafficking and dissociation. Technologies such as time-lapse microscopy, multiple particle tracking, fluorescence correlation spectroscopy, quantum dot labeling, and fluorescence energy resonance transfer (FRET) now allow much finer details of nonviral transfection to be observed.

2.3.1 Determination of Dissociation Status by Fluorescence Microscopy

While single fluorescent markers affixed to polyplexes allow their subcellular localization to be determined, no information is gained about their integrity or dissociation status. Packaged nucleic acid cargo must be released at the appropriate time and place to ensure processing. One method used to follow the intracellular unpacking fate of polyplexes is colocalization of two different fluorescent markers, one attached to the polymer and one to the DNA [47]. These approaches are limited by the need for the polymer and DNA to diffuse sufficiently far enough from each other to detect their distinct signals, thereby lacking the sensitivity and spatial resolution to determine when and where the precise onset of dissociation occurs. It is conceivable that the fluorescently labeled molecules could be co-localized without actually being associated. Another fluorescent assay used to study the unpacking of polyplexes and DNA release uses the fluorophore YOYO-1. The fluorescent emission signal of the YOYO dye is three orders of magnitude higher when bound to DNA than when it is unbound in solution. When the

YOYO-labeled DNA is complexed with polymer and the dye molecules are pulled near one another, they interact with one another to cause a self-quenching effect that decreases the emission signal [48]. Thus, the YOYO signal is high only when bound to free DNA, and can be used to probe the dissociation status of polyplexes. However, this technique is better suited for bulk measurements than single-particle tracking due to the lack of a clear binary signal indicating binding or release for each polyplex.

2.3.2 Förster Resonance Energy Transfer

Another technique used to study the time-dependent intermolecular interactions of polyplexes is fluorescence resonance energy transfer (FRET). In FRET, a fluorescent donor label has an emission spectral peak that overlaps the excitation peak of an appropriately chosen acceptor label. When energy is applied at the excitation frequency of the donor, the donor fluorophore emits energy at an appropriate wavelength to excite the acceptor by non-radiative dipole-dipole interactions [49, 50]. The acceptor then emits at its own emission wavelength (Figure 5). The result is that the acceptor will only emit if it is close enough to be excited by a donor. The efficiency of FRET falls off relative to the sixth power of the distance separating the donor-acceptor pair, with appreciable acceptor emission only occurring when the two fluorophores are less than ten nanometers apart [51]. This property makes FRET pairs ideal to probe the dissociation kinetics of polyplexes with high sensitivity and resolve distances below the diffraction limit of conventional microscopy.

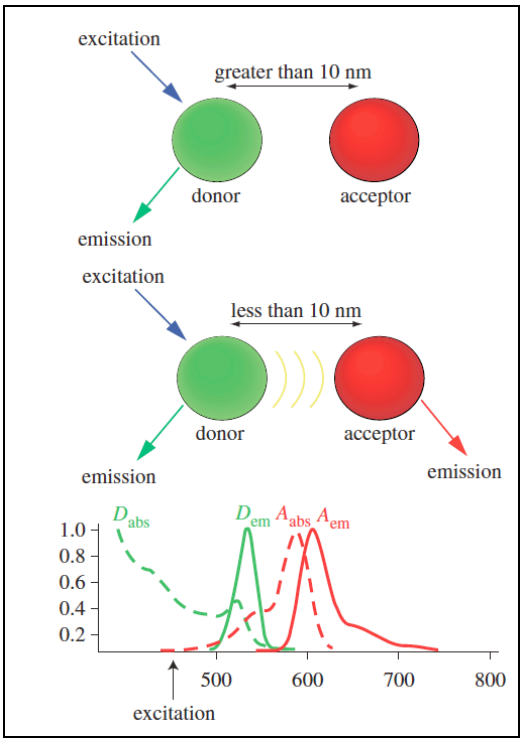

Figure 5: Förster Resonance Energy Transfer
When a FRET donor and acceptor are less than 10 nm apart, energy transfer takes place. Otherwise, the acceptor is not excited and does not emit. When a quantum dot acceptor is excited, it emits at a wavelength that overlaps the acceptor absorbance spectra, but not the acceptor emission spectra.

Traditionally, FRET pairs consist of commercially available organic fluorophores. Itaka et al. employed plasmid DNA doubly labeled with fluorescien and X-rhodamine as a FRET pair to determine the serum stability of poly(L-lysine) (PLL) polyplexes in physiological media. They observed that the fluorescence spectra of the labeled DNA changed drastically upon complexation and condensation with polymer [52, 53]. In a later study, the same group used a fluorescein and Cy5 FRET pair to probe the uptake and release of polyplexes derived from linear (22 kDa) and branched (25 kDa) PEI [53]. They found that linear PEI promoted fast uptake and unpacking, whereas branched PEI

resulted in retarded release of DNA as indicated by the FRET signal. Their results correlated well with measures of transfection efficiency using each carrier. In another report, PEI-DNA polyplexes were labeled with Alexa Fluor 488 and rhodamine as a FRET pair and used to study the effect of substrate stiffness on polyplex uptake and dissociation [54]. FRET is quickly gaining popularity in the field as its utility becomes apparent.

However, traditional organic fluorophores are not without shortcomings, as most of them have narrow excitation and broad emission spectra. If the emission spectrum of the donor overlaps that of the acceptor, crosstalk will occur and contaminate the FRET output signal. Another drawback to the use of organic fluorophores in FRET is their susceptibility to photobleaching, which often renders their use incompatible with time-lapse and real-time polyplex tracking studies. One proposed solution to address the issues with organic fluorophores is the use of semiconducting nanocrystals called quantum dots (QD's) as efficient FRET donors [55, 56]. They are characterized by broad absorption, narrow emission spectra, and high photostability, which help minimize complications typical of conventional FRET such as spectral crosstalk and direct acceptor excitation [55]. A QD-FRET system allows the tracking of a single polyplex over an extended period of time in a living cell via confocal microscopy with a high signal-to-noise ratio. Chen and Ho et al. used such a QD-FRET system to elucidate the intracellular fate of polyplexes derived from three different polymers [57,

58]. Analysis of confocal microscopy images taken in live cells allowed them to construct a three-compartment kinetic model describing the subcellular localization and dissociation status of the three different polyplexes in either the cytosol, endocytic vesicles, or the nucleus at various times. Their results reveal how unpacking kinetics can correlate with transfection efficiency, a mechanistic insight that could lead to the rational design of better gene carriers.

A recent refinement of this technique is to apply a two-step or relay QD-FRET approach to also monitor DNA degradation at the same time [59]. In this case, plasmid DNA, double-labeled with QD (525 nm emission) and nucleic acid dyes were complexed with Cy5-labeled polymeric gene carriers. The QD donor drives energy transfer stepwise through the intermediate nucleic acid dye to the final acceptor Cy5. At least three distinct states of DNA condensation and integrity (complexed and intact, unpacked and intact, and unpacked and degraded) were distinguished in a single-particle manner and within cells by quantitative ratiometric analysis of energy transfer efficiencies. This novel two-step QD-FRET method allows for more detailed assessment of the onset of DNA release and degradation simultaneously.

2.3.3 Fluorescence Correlation Spectroscopy

Another means of detecting the dissociation of polyplexes in the cell is termed fluorescence correlation spectroscopy (FCS), whereby the colocalization of the fluorescent signals is tracked not only spatially, but also temporally in the excitation

volume of a confocal microscope [60, 61]. The concentration of labeled molecules is kept low, so that each contributes significantly to the detected signal. The detection volume is also very small (~ femtoliters), so that only a few fluorophores are detected at a given time. Then, the diffusion of fluorescent molecules in and out of the detection volume leads to fluorescent fluctuations that provide information about the molecules. When associated, the tagged molecules move in and out of the fixed excitation volume simultaneously. When dissociated, they move independently. Based on the measured kinetic properties of the labeled molecules, their diffusion coefficients can be calculated to determine if they are bound or free. This approach is convenient and powerful, but does have limitations. It relies on the differences in the diffusive properties of the complexed or dissociated molecules, which are likely to be affected by associations with other intracellular charged species, limiting sensitivity and precision. Lucas et al. employed FCS by transfecting cells with polyplexes consisting of rhodamine green labeled nucleotides and either high molecular weight poly-DMAEMA or low molecular weight PLL labeled with Cy5 to determine if the polyplexes dissociated before or after reaching the nucleus [62].

Image correlation spectroscopy (ICS) is an analogous technique also used to track polyplex behavior intracellularly over time. Again, polyplexes are conjugated with fluorophores and excited by a laser under a confocal microscope. However, now the image of the entire cell is used instead of a smaller fixed focal volume. The fluorescent

intensities at each pixel are used to calculate autocorrelation functions, gaining insight into the transport and aggregation behavior of polyplexes once internalized. Using ICS, Kulkarni et al. found that for short intervals (< 10 s), polyplexes tend to move along distinct paths that perhaps implicate microtubules in polyplex transport [63]. For longer intervals, the motion was much more Brownian, indicative of passive transport.

Sometimes, it is advantageous to employ more than one imaging technique in combination to answer specific questions pertaining to DNA protection and release. One example is the combination of FRET and FCS to probe the stability of DNA delivered intracellularly [64]. Remaut et al. delivered oligonucleotides bearing a rhodamine green and a Cy5 fluorophore on its 3′ and 5′ termini, respectively. Using the two labels as a FRET pair, the authors performed dual-color FCS to monitor the red-to-green acceptor-to-donor fluorescence ratio. They were able to study the degradation of the delivered DNA at very low concentrations in cytoplasmic extract and living cells by both methods simultaneously. Degradation of the DNA was indicated by the disappearance of the FRET signal, as well as the red-to-green emission ratio and diffusion times calculated from the autocorrelation curves. They estimated that the cytoplasmic turnover time for an unmodified 40-mer oligonucleotide was between 2 and 10 minutes, underscoring the necessity of DNA protection until it is delivered to its final destination.

2.4 Unpacking in Extracellular Space

The intracellular barriers to nonviral gene delivery are better understood than those encountered by polyplexes prior to reaching the cell surface. It is unfortunate that the consideration and characterization of these extracellular barriers is often neglected. Exposure of polyplexes to serum or proteoglycans often decreases their transfection efficiency by causing aggregation or premature DNA release [65-67]. Just as charged species inside the cell, such as chromosomal DNA and cytoplasmic RNA can cause the release of DNA via competitive ion exchange, charged molecules found in the extracellular compartment and on the cell surface can also influence the release process. Aggregation outside the cell results both in premature unpacking, as well as the formation of larger conglomerates of nanoparticles that hinder uptake. PEGylation, the addition of polyethylene glycol units, is a common modification made to polymers to increase their salt and serum stability. However, studies have shown that the addition of PEG may actually result in a less stable ionic complex outside the cell and decreased transfection efficiencies [65, 68-72]. The hydrophilic PEG chains may induce swelling of the polyplexes and can lead to either premature release of DNA in the extracellular compartment or increased access to nucleases that can degrade DNA before it reaches the cell.

DNA delivered via polyplex is very susceptible to sequestration and degradation by a variety of processes before it ever reaches a target cell. To overcome these

challenges, accurate in vitro models must be developed to recapitulate the extracellular barriers found in vivo for rational carrier design. This is a formidable challenge, as the relevant barriers vary greatly with the route of administration. One route may require the balance of protection versus release to be skewed far toward one extreme, while another demands the reverse. For example, it is known that injection of naked DNA results in substantial transgene expression in skeletal muscle [73, 74]. However, DNA delivered orally needs to survive the acid and enzymes found in the stomach and gut [75]. It follows that carriers for intramuscular injections should be labile and unpack rapidly, whereas carriers for oral delivery must form tight complexes with DNA to provide maximum protection until they reach their target. Other routes of administration require more intermediate properties. The different demands typical of different routes of delivery complicate the considerations in designing systems to model extracellular barriers.

The study and evaluation of most new gene carriers currently takes place primarily in monolayer cell culture systems. Such two-dimensional environments generally fail to accurately mimic the extracellular environment polyplexes will encounter in vivo. When nanoparticles are added to the culture dish, they interact with the cell monolayer from the apical side. In two-dimensional (2-D) culture systems, the amount of extracellular matrix secreted by cells is lower on the apical side than the basolateral surfaces [76, 77]. So, polyplexes delivered to the culture medium have a

relatively unimpeded path, where the reality of the situation in vivo includes a far more tortuous path through the small pores of the ECM. Furthermore, the molecular constituents of the ECM are neither neutral nor inert. For example, proteoglycans are negatively charged under physiological conditions. They can interact with polyplexes possessing positive zeta potentials, sequestering or disrupting them prior to their ever reaching a target cell [65, 78]. As a result, some groups are looking at three-dimensional (3-D) tissue culture systems that more accurately portray the conditions found in vivo in terms of the structure, volume, and composition of the extracellular domain. More accurate models could result in more reliable assessments of gene carrier efficiencies in vitro, bridging the gap in success that often exists between cell culture experiments and animal studies.

The sophistication of these 3-D models ranges from simple hydrogels of crosslinked ECM molecules to multicellular spheroids, multilayer cell cultures, and ex vivo tissue models [79]. A model as basic as a hydrogel of crosslinked ECM molecules, such as collagen or Matrigel, can offer a great deal of insight into the transport properties and dynamic stability of polyplexes in the extracellular domain. The effects of polymer modification or functionalization on polyplex behavior outside the cell can be studied, as well as the shape and size restrictions imposed on polyplexes by the ECM pore sizes [80, 81]. Hydrogel models have been used to demonstrate that aggregation and premature dissociation of polyplexes by charged ECM components does indeed

take place [82]. If desired, cells can be added to the hydrogel to look beyond transport, at the effect of ECM on uptake and transfection. More sophisticated hydrogel systems can be perfused to more accurately mimic the situation in vivo where fluids flow and influence nanoparticle transport [83]. Hydrogels also allow real-time nanoparticle imaging in situ without any significant processing required.

A more complex 3-D model of spherical cell clusters that secrete their own ECM is called the multicellular spheroid [84-87]. As perhaps the smallest approximation of native tissues, multicellular spheroids are a convenient means of probing polyplex transport and stability in the intact spheroid, and subsequently in the constituent cells upon enzymatic disruption [88]. They can be grown to reach various sizes, up to a few millimeters in diameter. They produce ECM in a 3-D manner similar to native biological tissues, with a composition more like native tissues than hydrogels made of only a few components [89]. Small spheroids consist entirely of healthy cells that can be used to study polyplex distribution and transport in normal tissues. Larger spheroids more closely resemble tumor tissue, with distinct proliferating, quiescent, and necrotic regions. Multicellular spheroids, as with hydrogels, can be used to study the effects of polyplex size, shape, charge, and functionalization on transport and transfection. Data collection is facile, often taking place in the form of confocal microscopy, immunohistochemistry, or flow cytometry of the dissociated spheroid cells. The use of multicellular spheroids is becoming more widespread as the need to evaluate gene

carriers in 3-D systems becomes more apparent.

Multilayer cell cultures are another useful tool for studying the transport and stability of polyplexes. Using transwell type culture plates, one layer of cells can be cultured on a semi-permeable membrane insert. Beneath the membrane is a layer of culture medium covering a second layer of cells. Multilayer systems are especially useful for modeling scenarios in which polyplexes must pass through a layer of cells prior to reaching their target cells. Such situations are encountered in extravasation through the vascular endothelium after systemic administration of polyplexes, as well as in the escape from the gut through the intestinal epithelium in oral gene delivery. Similar barriers are found in the airway epithelium encountered by polyplexes delivered to the respiratory system. Multilayer transwell culture models have been developed to study each of these situations [90-93]. Additionally, each layer in the multilayer system is not confined to a single cell type. Co-cultures can be seeded on either layer to more accurately mimic the situation in vivo. For example, the intestinal epithelium contains mucus-secreting goblet cells and M-cells of the immune system that continually shuttle particulate contents of the intestinal lumen to their basolateral side via transcytosis. The presence of mucus and transcytotic activity could significantly alter the transport characteristics of polyplexes involved in oral gene delivery, so the inclusion of these cell types in co-culture multilayer transwell models could provide valuable information [94-96].

The final category of common 3-D models is ex vivo tissue cultures. By using tissue directly from an animal or patient, preservation of the native ECM structure and composition, cell organization, and cell phenotypes is possible. Such models have a higher likelihood of predicting in vivo efficacy accurately. Ex vivo cultures of a wide range of tissue types have been successful: liver, cartilage, airway epithelium [97], lung [98], and intestine [99]. Imaging, histology, and most other standard assays are feasible with ex vivo tissue cultures. The drawbacks of using tissue explants for the evaluation of gene carriers include the cost and ethics associated with the use of primary tissues, as well as the relative difficulty of maintaining the architecture and phenotype of entire tissues compared to more basic cell layers and spheroids. However, they still may provide the most accurate information about transfection capabilities short of testing in animal models.

2.5 Cell-Specific Design Requirements

A final consideration in carrier design is the potential differences in the desired protection and release characteristics of polyplexes when introduced to different cell types. The transfection efficiency of a gene carrier can vary by orders of magnitude depending on the cell type being transfected. One can envisage that metabolically active cells favor a tilt towards protection whereas slowly proliferating cells might favor more rapid unpacking. The proliferation rate of target cells can play a major role in whether or not polyplexes gain access to the nucleus where some unpacking has been shown to take

place. During each iteration of the cell cycle, the nuclear envelope is broken down and reformed. While the nuclear envelope becomes discontinuous during mitosis, polyplexes or DNA may diffuse into what will become the nucleus of the daughter cells and eventually be transcribed. In a non-dividing cell, they may have been unable to penetrate the nucleus. This is often the case with primary cells and cells of the immune system that proliferate more slowly than transformed cell lines, accounting for the lower transfectability of the former.

Furthermore, cells internalize polyplexes through a variety of uptake pathways, including clathrin-mediated endocytosis, calveolin-mediated endocytosis, clathrin- and calveolin-independent endocytosis, macropinocytosis, and phagocytosis [100, 101]. The route ultimately taken likely depends on the target cell type, as well as polyplex size and vector physiochemical properties. To maximize efficacy, the anticipated internalization pathway should be considered during the vector design process. Another difference between cell types is the amount and composition of extracellular matrix they secrete. Secretion of a large volume of ECM with small pore sizes will certainly diminish the ability of polyplexes to reach and transfect cells. Other cell types pose unique challenges, such as the macrophage. Macrophages are a key component in inflammatory reactions and the foreign body response. They also function as antigen-presenting cells and participate in B and T lymphocyte development. Thus, they are desirable targets for gene delivery. Unfortunately, macrophages are very active in phagocytosis and

degradation of particulate matter they consume [102]. Polyplexes internalized by macrophages rarely escape the phagocytic/endocytic pathway and are usually degraded. However, these same challenges sometimes offer unique opportunities to hijack cellular processes to enhance gene delivery. Acid-labile carriers are being developed to respond to the acidic environments typical of macrophage phagosomes [103]. This is one example of the special rational design considerations that will be necessary to efficiently transfect troublesome cell types.

2.6 Conclusions on Carrier Design and Selection

Computational models and experimental evidence have shown that inadequate protection and inefficient release of DNA from polymeric vectors are both serious obstructions to successful gene delivery. A thorough understanding of the properties and processes that contribute to the protection and release of DNA in polyplex-mediated gene delivery systems is indispensable to the rational design of future vectors. Phenomenological comparisons of vectors based on readouts of reporter genes offer only a glimpse into the complex systems involved in transfection of cells and transport through tissues. The rate-limiting barriers are undoubtedly multifactorial, so a systematic engineering approach is the only way to gain an understanding of why, how, where, and when one carrier is superior to another.

Researchers have now begun to study and isolate each step, and each molecule, of the nonviral gene delivery process. The accumulation of knowledge from both the life

sciences and physical sciences has made such an interdisciplinary approach to the problem possible. When changing polymer properties such as the molecular weight and charge density is insufficient to provide optimal protection and release, some polymers can be made to respond to environmental or applied stimuli. Changes in temperature, light, pH, and redox potential can be harnessed to trigger a switch from a protective complex to one favoring release. Ternary polyplexes can be formed by the inclusion of enzymes or genes meant to help relax the ECM to facilitate extracellular transport or degrade the polymeric carrier intracellularly to allow DNA release.

Fortunately, the developmental pace for imaging technologies and engineering models is accelerating. Fluorescence imaging techniques have advanced from the colocalization of fluorescently labeled DNA and polymer to much more sophisticated technologies such as quantum dot mediated FRET, fluorescence correlation spectroscopy, and non-fluorescence techniques like MRI. Furthermore, these techniques are often combined with three-dimensional models that can recapitulate native tissues with high fidelity. It is at the interface between materials science, imaging, and biology that nonviral gene delivery will make progress towards meaningful clinical translation. While the task remains daunting, successful nonviral gene therapy is crucial to realizing the potential of genetic medicine. As future therapeutics will increasingly rely on nucleic acids such as DNA, antisense oligonucleotides, therapeutic RNA, and siRNA, the rewards for this line of investigation will continue to multiply.

2.7 QD-FRET Nanosensors

The rational design of improved carriers depends on a quantitative, mechanistic understanding of the rate-limiting barriers to efficient intracellular delivery. Separation of the nucleic acid from the carrier is one of the barriers, which may be analyzed by Förster resonance energy transfer (FRET), a mechanism used to detect interactions between fluorescently labeled molecules. When applied to the molecular components of polymer or lipid-based nanocomplexes, FRET provides information on their complexation status, uptake, release, and degradation. Recently, the design of FRET systems incorporating quantum dots as energy donors has led to improved signal stability allowing prolonged measurements, as well as increased sensitivity enabling direct detection and the potential for multiplexing. The union of quantum dots and FRET is providing new insights into the mechanisms of nonviral nucleic acid delivery through convergent characterization of delivery barriers, and has the potential to accelerate the design of improved carriers to realize the potential of nucleic acid therapeutics and gene medicine.

2.7.1 Role of QD-FRET in Nonviral Gene Delivery

Delivery of gene-loaded nanocomplexes into cells has emerged as an essential tool in modern therapeutics and biomedical research. Compared with viral vectors, the main advantages of nonviral gene carriers are diminished immunogenicity, ease of scale-up, and tremendous potential for optimization. Their primary weakness, however,

has been poor transfection efficiency. The putative barriers associated with the low efficiency of nonviral vectors are illustrated in Figure 6: (i) cellular binding and uptake, (ii) endosomal escape, (iii) cytosolic transit to the nucleus and unpacking, (iv) nuclear entry, and (v) transcriptional processing.

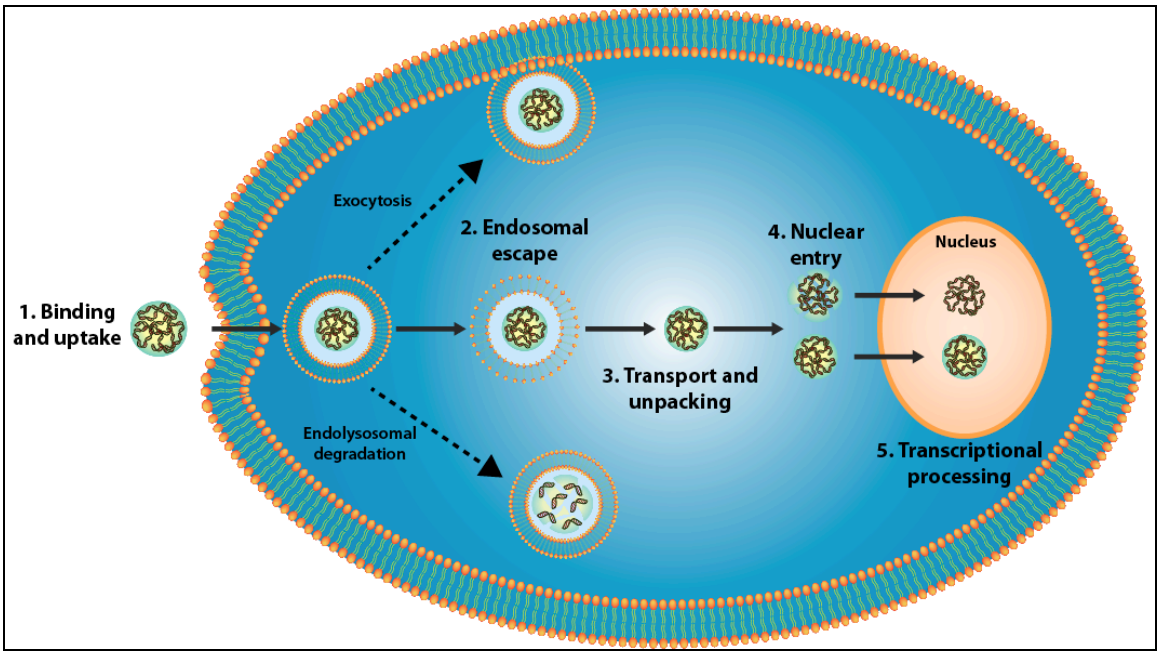

Figure 6. Intracellular Transport and Release
The putative barriers contributing to the low transfection efficiency typically achieved by nonviral delivery systems are illustrated. Additional processes such as exocytosis and endolysosomal degradation may also contribute to diminished transfection. Unpacking may occur in any of the subcellular compartments, while it is also possible for intact complexes to enter the nucleus.

Quantitative intracellular trafficking studies enable the identification of these rate-limiting barriers, which can differ widely between delivery systems. Some carriers, especially those incorporating polyethylene glycol (PEG) for steric stabilization, are plagued by poor cellular uptake [104, 105]. Others lack sufficient buffering capability to

exploit the proton sponge effect for efficient endosomal escape [106]. Some types of nanoparticles reach the nucleus of target cells but still fail to mediate robust transgene expression [107]. With such disparate behavior among different types of nanocomplexes, the ability to track the delivery of nucleic acids within cells is crucial to understanding a carrier's unique strengths and limitations. However, measuring only the spatiotemporal trafficking activity of nanoparticles neglects other critical aspects of the complex process. To be effective, nucleic acids must be condensed and protected from enzymatic degradation en route to their destination, where they should be quickly released [108]. The dissociation status of the nanocomplex and payload integrity at each point are equally as important as their transport in ensuring that the therapeutic agent is delivered intact and available for processing. The ability to simultaneously detect subcellular location, nanocomplex stability, and payload integrity with increased precision would promote the establishment of more robust structure-function relationships and accelerate the rational design of improved gene carriers.

Fluorescence-based methods have been the techniques of choice to study the physicochemical properties and intracellular trafficking of nanocomplexes [109-111]. Interactions between a nucleic acid payload and its polymer or lipid carrier can be probed using fluorescently labeled molecular components and followed from the extracellular domain to the cytoplasm or nucleus under physiological conditions [47, 62, 109, 112]. Colocalization of their signals provides some indirect information about their

interactions [113]. However, detection of dissociation and release is limited by the need to resolve distinct signals from components that may not have achieved sufficient separation. Therefore, such detection methods do not offer the requisite sensitivity to precisely detect the onset of dissociation, or to differentiate between molecules that are interacting or simply adjacent. FRET has advantages over colocalization due to its unique ability to resolve molecular interactions beyond the diffraction limit of conventional microscopy [114]. When FRET occurs, a donor fluorophore excites an acceptor via a non-radiative dipole-dipole interaction if they are sufficiently close (within ~10nm). This so-called "molecular ruler" can be used to determine distances between labeled molecules inside cells, including gene carriers and nucleic acids. The ability to detect nanometer-scale separations of nanocomplex components makes FRET a more powerful tool than fluorescence colocalization for studying nanocomplex stability and dissociation.

Recently, some researchers have chosen to design FRET pairs that employ luminescent semiconducting nanocrystals called quantum dots (QDs) as energy donors. Conventional fluorophores suffer from chemical and photodegradation, photobleaching, and broad spectra. Conversely, QDs possess resistance to bleaching and chemical degradation, broad absorption spectra, tunable narrow emission spectra, and large energy separation between excitation and emission [115]. The increased stability of QDs makes the imaging of FRET signals over extended periods of time possible.

Furthermore, the ability to tune emissions and excite multiple QDs at a single wavelength creates the potential for multiplexing [116]. The first reports proposing the use of QDs in biological sensing applications generated significant excitement [117, 118]. In 2006, the specific benefits of FRET incorporating QDs (QD-FRET) for the study of nonviral gene delivery were published [58]. Since then, several groups adapted and refined the technique to study many aspects of nonviral nucleic acid delivery. In this section, we focus on the use of QD-FRET as a tool to investigate the intracellular fates of nanocomplexes used to deliver nucleic acids. We begin by detailing the rationale and appeal of the technique before exploring specific examples of its use and considerations when adopting QD-FRET to study nonviral nucleic acid delivery.

2.7.2 Why QD-FRET?

FRET is a process by which the energy of a donor chromophore is non-radiatively transferred to a nearby acceptor molecule via a dipole-dipole interaction, leading to a decrease in the donor emission and a concomitant increase in acceptor emission [49, 114]. A general expression of energy transfer efficiency, E, defined in Equation 1, accounts for the fraction of excitons transferred from the donor to acceptor, where k_T is the rate of nonradiative energy transfer, τ_D is the excited-state radiative lifetime, and r is the distance between the donor and acceptor.

$$E = \frac{k_T}{\tau_D^{-1} + k_T} = \frac{R_0^6}{R_0^6 + r^6} \qquad \text{Eq. (1)}$$

The Förster radius R_0, defined as where 50% of energy transfer occurs, is a function of the refractive index of the medium (n, typically ranges from 1.3 to 1.5), the unperturbed donor photoluminescence quantum yield (Q_D), the spectral integral from the overlap of donor emission and acceptor absorption ($J(\lambda)$, in units of $M^{-1}cm^{-1}nm^4$) and the relative orientation of the donor and acceptor dipoles ($\kappa^2 \sim 2/3$), as shown in Equation 2.

$$R_0 = 0.211[\kappa^2 n^{-4} Q_D J(\lambda)]^{1/6} \qquad \text{(in Å)} \qquad \text{Eq. (2)}$$

For most FRET pairs, R_0 is typically a few nanometers, enabling optical measurements of changes in donor-acceptor separation with angstrom resolution. Meanwhile, the sixth-power dependence of FRET efficiency on the donor-acceptor distance makes FRET well suited for probing conformational changes of molecules or detecting interactions between molecules.

Equation 2 illustrates that optimal FRET occurs when there is appreciable spectral overlap between the emission spectrum of the donor and the absorption spectrum of the acceptor, while the spectral overlap of the donor and acceptor emissions is minimized. Therefore, the broad absorption and emission spectra of organic

fluorophores used in FRET present significant challenges for reducing direct acceptor excitation (simultaneous excitation of energy acceptor and donor) and crosstalk (overlap of donor and acceptor emission spectra), as depicted in Figure 7. To cope with these concerns, some researchers are turning to QDs as energy donors for FRET applications in an attempt to overcome some of the limitations associated with conventional organic FRET pairs. Their benefits include diminished spectral crosstalk and direct acceptor excitation due to QDs unique photophysical properties: narrow size-tunable emissions, extremely high extinction coefficients over a broad absorption range, and enhanced photostability [119]. QDs have been preferentially adopted as energy donors rather than acceptors due to their relatively long radiative lifetime, broad excitation range, and high extinction coefficients [120]. Readers seeking a deeper discussion of the photophysics of QD-FRET for biological applications are referred to the excellent review by Medintz and Mattoussi [119].

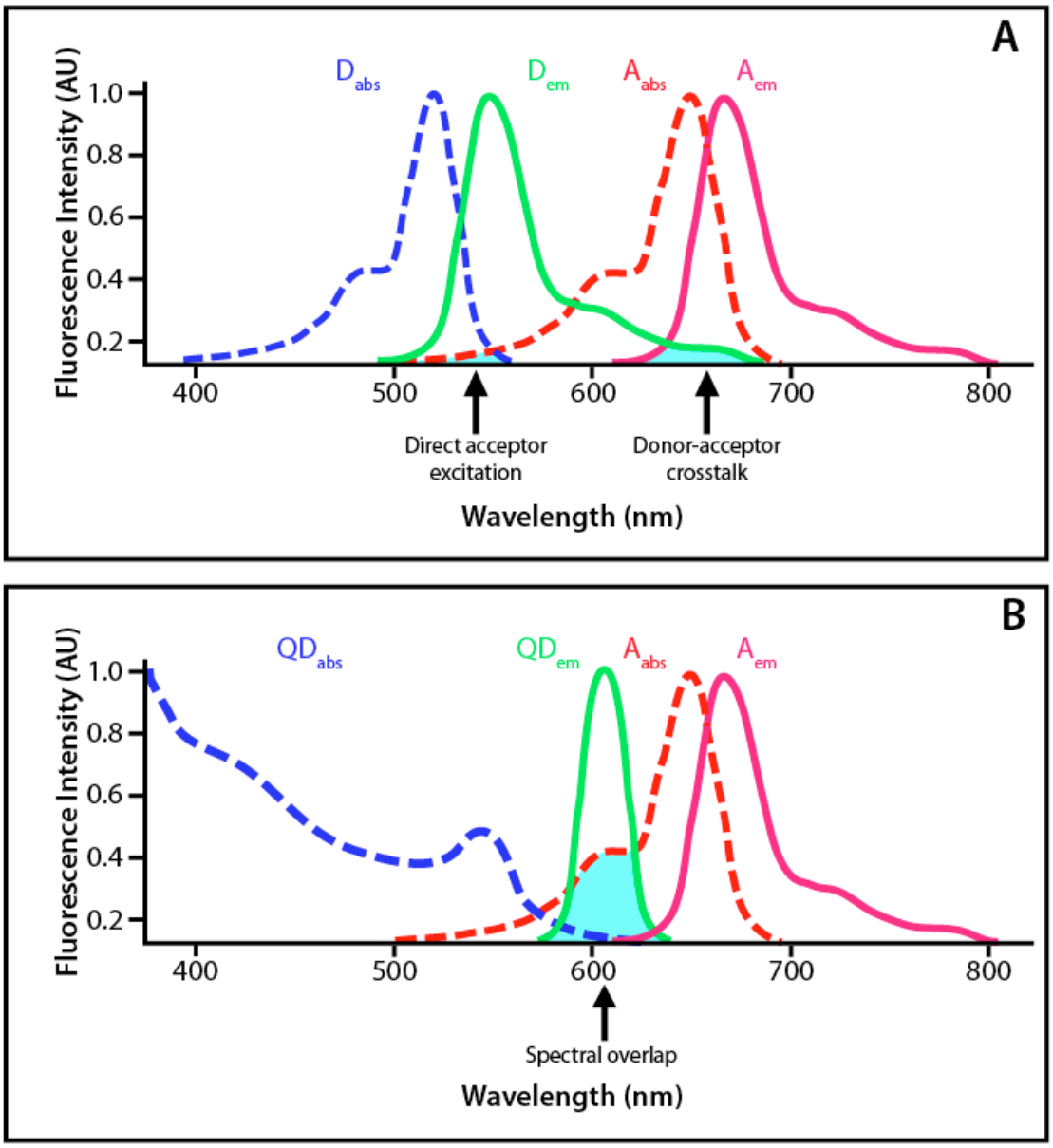

Figure 7. Quantum Dot-FRET
Absorption and emission spectra for (A) a conventional organic fluorophore-based FRET pair and (B) a QD-FRET pair with a QD energy donor. Direct acceptor excitation and donor-acceptor crosstalk are common problems with traditional organic fluorophores. Substituting QD donors avoids these concerns, while improving other properties such as a larger spectral overlap between donor emission and acceptor absorption.

2.7.3 QD-FRET as a Novel Strategy to Study Nonviral Delivery Barriers

Many nonviral systems depend on interactions such as electrostatic attraction and chain entanglement to condense and protect nucleic acids during delivery. Such interactions have been studied using FRET pairs of organic fluorophores either doubly labeled on DNA [52] or separately labeled on gene carriers and nucleic acids [121]. However, the former depends on stable coil-globule transition states of DNA and both require additional ratiometric analysis and disambiguation. Furthermore, the organic fluorophores used in conventional FRET are susceptible to photobleaching, limiting their utility in real-time studies of intracellular trafficking [114]. These weaknesses highlighted the need for an alternative.

The initial report of QD-FRET for the study of nonviral nucleic acid delivery described a sensitive and quantitative indicator of the stability and composition of chitosan-DNA nanocomplexes [58]. The authors labeled biotinylated plasmid DNA with streptavidin-decorated QDs, and conjugated the natural polysaccharide chitosan with Cy5 dye. The resulting high signal-to-noise ratio enabled digital detection of the formation and dissociation of single nanocomplexes using single molecule detection (Figure 8). They also used the frequencies of QD emission before and after nanocomplex disruption to estimate the number of plasmid copies contained within each particle (~30), which they validated with transmission electron microscopy. Cells readily internalized the QD-FRET nanocomplexes, and confocal microscopy revealed intact

particles in both the cytoplasmic and nuclear domains. The intracellular dissociation rate of the complexes was quantified, and the disappearance of QD-FRET emission showed that most particles unpacked within 48 hours.

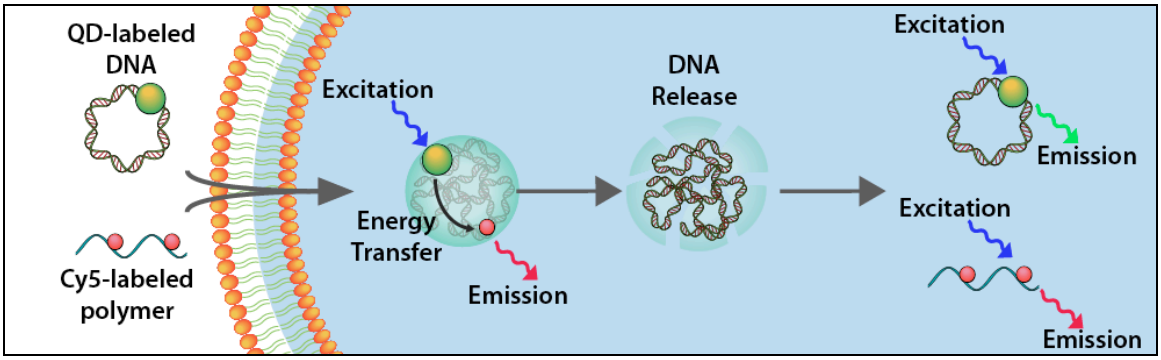

Figure 8. QD-FRET Detection of Intracellular Release.
When labeled molecular components are condensed into a nanocomplex, QD-FRET results in acceptor emission upon excitation of the donor. Once the complex unpacks in the cell, QD-FRET is abolished and donor emission regained.

Utilizing the ability to precisely detect DNA release, the same group developed a quantitative model to describe and predict distributions of free DNA throughout several subcellular compartments over time [122]. The average unpacking rate constants in the endosomal, cytoplasmic, and nuclear domains were recorded for chitosan, polyethylenimine (PEI), and poly(phosphoramidate) (PPA) nanocomplexes. The results were then correlated with transfection efficiency to further elucidate the contributions of nanocomplex stability and intracellular trafficking during gene transfer. The data revealed a compartmental dependence of unpacking between carriers, with PEI unpacking at equal rates in both endosomal and cytosolic compartments and PPA

unpacking preferentially in the cytosol. The results supported the conclusion that nanocomplexes must either escape the endosome quickly (PEI) or remain stable within them (PPA). If significant unpacking and degradation occurs within the endosome (chitosan), transfection efficiency may suffer. The calculated unpacking rate constants agreed with published computational models based on intracellular copy number, although release of DNA from PEI nanocomplexes occurred earlier than previously reported in studies using colocalization and conventional FRET [123-125].

The improved stability of the QD-FRET system allowed for direct measurement of nanocomplex stability over longer periods of time, and its inherent sensitivity led to the derivation of more robust quantitative models and the precise determination of the unpacking rate constants for three carriers. The technique has attracted the attention of delivery researchers as they seek high quality quantitative data in understanding the mechanisms of nucleic acid delivery and the design of nonviral systems. The field is gaining momentum as researchers continue to refine the technique and reports of interesting results from QD-FRET studies emerge with increasing frequency (Table 1).

Table 1: Reports of QD-FRET to Study Nonviral Delivery of Nucleic Acids

Payload and carrier	Mechanism detected	Detection approach	Significance of findings	Reference
pDNA Chitosan	Unpacking	Confocal microscopy, single molecule detection	First report of QD-FRET used to study unpacking of polymer-DNA nanocomplexes	[58]
pDNA PEI, PPA, Chitosan	Unpacking	Confocal microscopy	Kinetics of trafficking and unpacking correlated with transfection efficiency	[122]
pDNA PEI-PEG-TAT	Uptake, trafficking, unpacking	Confocal microscopy	Correlated transfection with faster uptake and diminished endosomal unpacking in multiple cell lines; used results to optimize carrier composition	[126]
pDNA Chitosan	Unpacking	Confocal microscopy	Higher M.W. chitosan unpacks faster at low pH and results in higher transfection efficiency	[127]
pDNA Liposome	Uptake, integrity	Confocal microscopy	Demonstrated intact QD-DNA complexes delivered to cytoplasm and perinuclear region by liposomes	[128]
pDNA DMAE-ss-PRX	Unpacking	Confocal microscopy	Showed that different carriers deliver DNA to different nuclear sub-domains	[129]
pDNA PEG-PPA	Unpacking	Confocal microscopy	Validated increased extracellular stability of crosslinked micelles, leading to increased transfection efficiency	[130]
pDNA DMAE-ss-PRX	Unpacking	Confocal microscopy	Showed that different carriers deliver DNA to different nuclear sub-domains	[129]
pDNA PEG-b-PPA Chitosan	Unpacking, degradation	Confocal microscopy, single molecule detection	Three distinct states of DNA condensation and integrity distinguished extra- and intracellularly	[131]
siRNA PEI	Uptake, unpacking	Confocal microscopy, flow cytometry	Adding Hph-1 to QD-PEI results in faster unpacking; QD-PEI silences better than PEI alone	[132]
siRNA QD-PMAL	Uptake, unpacking	Confocal microscopy	QDs coated with amphipol delivered siRNA efficiently while allowing intracellular tracking of integrity	[133]
ODN Liposome, PEI	Uptake, unpacking	Confocal microscopy, flow cytometry	ODN complexes formed with a polycation are internalized and unpacked more quickly than ODN-liposomes	[134]
pDNA PDEAEM copolymer	Unpacking	Spectrofluorometry	Demonstrated role of chloroquine in nanocomplex dissociation	[135]
pDNA Chitosan	Complexation	Fluorescence microscopy	Determined kinetics of nanocomplex self-assembly with millisecond resolution	[136]
Doxorubicin DNA aptamer, QD	Drug release	Confocal microscopy	Simultaneous detection of drug release, identification of cancer cells, and targeted cell killing; Demonstrates potential of QD-FRET in theranostics	[137]

2.7.4 Recent Applications of QD-FRET to Study Nonviral Delivery

2.7.4.1 QD-FRET for Delivery of Plasmid DNA

Plasmid DNA is the most commonly delivered nucleic acid, and it follows that QD-FRET has been most often applied in the study of its delivery. Ulasov et al. employed QD-FRET to study transfection by PEI-DNA nanocomplexes in multiple cell types, and used the results to derive new mathematical models to quantify intracellular trafficking [126]. They functionalized the particles with PEG and TAT peptide to modulate stability and cellular uptake. PEG incorporation conceals the surface charge of nanoparticles and results in prolonged residence in circulation following systemic delivery, and the incorporation of TAT-peptide enhances cellular penetration. The authors delivered complexes with different PEI:PEG and PEI:DNA ratios to cells and studied their trafficking via colocalization with fluorescently labeled plasma membranes, endolysosomal compartments, and nuclei. Relying on QD-FRET to detect particle integrity, they used experimental data to calculate the rates of 15 different aspects of the transfection process including unpacking and accumulation of DNA in the cytosolic, endolysosomal, and nuclear compartments. They observed that transfection efficiency was positively correlated with the rate of cellular uptake but negatively correlated with the rate of unpacking within the endosomes and lysosomes, and used these correlations to explain differences in transfection and establish the optimal component ratios in their carrier design to maximize efficiency.

For chitosan-based delivery systems, it is known that transfection depends heavily on polymer molecular weight, and overly tight binding is typically considered a critical barrier [138]. As chitosan possesses no stimulus-responsive degradative mechanism, DNA must be released in response to natural chemical changes in its surroundings. For instance, increasing ionic strength in the endosomal compartment may disrupt electrostatic interactions between DNA and the polycation. Another possibility is that hyperprotonation of the amine groups of chitosan may occur during endosomal acidification, leading to electrostatic repulsion, elongation, and disentanglement of polymer chains from DNA. This effect would be more pronounced with higher weight chitosan. Lee et al. observed this phenomenon using QD-FRET, and demonstrated that nanoparticles generated with higher molecular weight chitosan dissociate faster in acidic conditions similar to those found in the lysosome [127]. The result was reproduced in living cells, lending credence to the proposed mechanism by which high molecular weight chitosan mediates higher transfection levels than shorter polymer chains.

Some researchers choose to use intercalating DNA dyes as QD-FRET components. While the amount of dye must be tuned to optimize the signal-to-noise ratio, no chemical conjugation or separation steps are necessary. Intercalating dyes may also be a means to include more acceptors per donor than would otherwise be possible, increasing the overall FRET efficiency. In one such case, a lipid-based transfection

reagent was used to deliver QD donors conjugated to DNA labeled with the BOBO-3 intercalating dye as the acceptor [128]. Four hours after transfection, QD-FRET signal was detected throughout the cytoplasm and perinuclear region, indicating the presence of intact complexes in those regions. Although the QDs and DNA were stably conjugated, differences in QD-FRET signal were detected between condensed particles and those that were released. As the signal dissipated, the authors measured both trafficking and unpacking kinetics. The application of QD-FRET in a lipid-based delivery system and use of DNA intercalating acceptors are the most novel and interesting features of these studies.

QD-FRET has also been incorporated into more complex delivery systems. Harashima's group has engineered a lipid based tetra-lamellar multifunctional envelope-type nano device (T-MEND) containing a polycation-DNA core encapsulated by inner nuclear membrane and outer endosome fusogenic envelopes that facilitate nuclear entry and endosomal escape, respectively [129]. T-MEND particles were formed with QD-labeled DNA and their synthetic polymer, a biocleavable polyrotaxane modified with dimethylaminoethyl-modified α–cyclodextrin and a disulfide-linked PEG chain (DMAE-ss-PRX), labeled with rhodamine energy acceptors. Using QD-FRET they found that modulation of the supra-molecular structure of DMAE-ss-PRX caused a shift in decondensation to regions of euchromatin in the nucleus. This was the first report of directed unpacking to a specific nuclear sub-domain using a polymeric carrier. Using

low molecular weight polymer resulted in equal delivery to regions of hetero- and euchromatin, but unpacking occurred preferentially in regions of heterochromatin. Particles containing higher molecular weight polymer delivered more DNA to the nucleus, with more than 70% deposited to euchromatin regions. The authors hypothesized that the shorter polymer generates a weakly associated core that is easily disrupted by the high concentration of cationic histones contained in the heterochromatin adjacent to the nuclear membrane. More stable cores may reach the euchromatin regions intact, where activity of the nuclear transcriptional machinery may encourage their dissociation. Deposition of free DNA into transcriptionally active euchromatin regions increases transgene expression levels. Using QD-FRET the authors quantified three states of complex dissociation and intranuclear disposition, elucidating a mechanism that accounts for the different efficiencies of two carriers.

Characterization and optimization of custom delivery systems have proven to be valuable applications for QD-FRET. Jiang et al. designed micellar DNA nanocomplexes with a PEG-b-PPA polymer for targeted delivery to the liver [130]. Micelles made with high molecular weight PPA blocks exhibited instability in physiological salt solutions [131]. Taking advantage of this rapid mode of unpacking, they added bioreducible crosslinkers to enhance stability prior to reaching the cytoplasm. The crosslinked micelles remained stable in serum and ionic solutions, but degraded in a similar manner to non-crosslinked analogs in the presence of salt following crosslink reduction in the

cytoplasm. This dual sensitivity provided stability in the extracellular and endocytic compartments, while enabling rapid cytosolic release of DNA. As expected, the custom carrier mediated higher and more prolonged transfection levels than non-crosslinked analogs. The authors used QD-FRET to study the intracellular behavior of crosslinked and non-crosslinked carriers by measuring distributions of intact and unpacked micelles in the cytosol, endolysosomal, and nuclear compartments. The dual-sensitive micelles unpacked much more slowly, and tended to release their payload in the cytoplasm and nucleus. They yielded higher transfection levels, improved extracellular stability, and more sustained gene expression. In this case, quantitative QD-FRET studies elucidated the mechanism by which enhanced extracellular micelle stability results in improved performance.

2.7.4.2 QD-FRET for Alternative Nucleic Acid Payloads

In addition to plasmid DNA, delivery of other nucleic acids is also attractive for both clinical and research applications. Small interfering RNA (siRNA) delivered intracellularly triggers RNA interference (RNAi) and leads to the specific knockdown of expression of the target gene. While efficient uptake, subcellular trafficking, and cytoplasmic release remain necessary, delivery of siRNA does not require nuclear entry or transcription. To study siRNA delivery and the effect of carrier functionalization with cell penetrating peptides, Lee et al. designed a QD-FRET pair by attaching QDs to PEI and Cy5 to siRNA [132]. Instead of using image analysis to quantify nanocomplex

disassembly, the authors instead opted for a high-throughput approach using flow cytometry. They measured the kinetics of endocytic and non-endocytic uptake, intracellular trafficking, and dissociation of nanocomplexes with and without the cell penetrating peptide (CPP) Hph-1. Detection of QD-FRET intensity by flow cytometry showed that QD-PEI-CPP complexes were both internalized and unpacked faster than those composed of non-functionalized QD-PEI. Both types ultimately unpacked almost completely within five hours. The difference in early-stage behavior was attributed to the need for QD-PEI complexes to escape endosomes before unpacking, and there was no difference in gene silencing after 24 hours. Interestingly, QD-PEI complexes mediated more gene silencing than unconjugated PEI, which the authors attributed to altered physical properties that increased endocytic uptake. In this case, QD-FRET coupled with flow cytometry enabled high-throughput quantification of dissociation kinetics. However, confocal fluorescence microscopy techniques and image analysis were needed to determine the subcellular compartment in which dissociation occurred.

Another group used QD-FRET to study complexes formed with QDs modified to bind and deliver siRNA [133]. Qi et al. conjugated poly(maleic anhydride-*alt*-1-decene) modified with dimethylamino propylamine to custom synthesized QDs. The resulting carriers were small (~ 12 nm), water-soluble particles with a positive zeta potential that could bind, protect, and efficiently deliver siRNA into cells. Binding of FITC-labeled siRNA was detected by the quenching of FITC signal by FRET following addition of

sufficient red-emitting QDs serving as acceptors. The nanocomplexes remained colloidally stable and mediated robust gene silencing in both serum-free and complete culture media. QD emission, along with the absence of FITC signal, allowed tracking of the binding and uptake of intact complexes. Appearance of FITC signal after 1.5 hours indicated the onset of siRNA release. After 5 hours, FITC-labeled free siRNA was observed distributed throughout the cytoplasm. By functionalizing QDs with an amphipathic brush, the authors generated a novel QD-based siRNA delivery system with integrated imaging capabilities. As QDs are further developed as carriers themselves, QD-FRET promises to play an even greater role in the design and use of such delivery systems.

Another payload of interest is oligodeoxynucleotides (ODN). Antisense ODN delivered to the cytoplasm of cells can inhibit expression of a specific gene by binding its complimentary mRNA transcript to block ribosomal access and hasten its degradation. QD-FRET has been used to study and compare the uptake and intracellular fate of ODN delivered by either lipoplex or polyplex [134]. Incorporation of QD-FRET pairs did not affect the performance of the ODN in either case. PEI-ODN nanocomplexes were internalized more readily during the first hour of transfection, likely due to a more positive zeta potential than the lipoplexes. The intracellular QD-FRET signals from both carrier types equilibrated by the end of the four-hour transfection period, and some unpacking was observed as early as four hours post-transfection. Polymer-ODN

nanocomplexes demonstrated a much higher rate of dissociation than lipoplexes, and unpacking of nearly all complexes of both types was observed by 48 hours post-transfection. Furthermore, the presence of intracellular QD-FRET signal in cells incubated with liposomes indicates that the complexes are internalized via endocytosis rather than membrane fusion, which would result in immediate dissociation and elimination of FRET. In this case, despite the differences in uptake and unpacking rates, ODN-mediated inhibition of gene expression was similar for both delivery systems.

2.7.4.3 QD-FRET for Mechanistic Studies

In addition to its utility in the study of nanoparticle trafficking and identification of intracellular barriers to delivery, QD-FRET is also applicable to the more fundamental, mechanistic studies associated with the design phase of nonviral carrier systems. Specifically, QD-FRET has been used in cell-free systems to scrutinize nanocomplex self-assembly, composition, and stability. A thorough understanding of these processes and properties combined with precise quantitative data will accelerate the evolution of improved carriers.

An interesting quenching phenomenon discovered between QDs and the pentablock copolymer, poly(diethylaminoethylmethacrylate) (PDEAEM)/Pluronic F127 allowed Zhang et al. to study the effects of chloroquine on complex stability and DNA release in a cell free assay [135]. Chloroquine is a lysosomotropic agent known to enhance transfection in many systems, and may participate in the dissociation of DNA

from polymer carriers. The emission of cysteine coated QDs was quenched via FRET by both plasmid DNA and pentablock copolymer, but not by pre-formed polymer-DNA nanocomplexes. Reductions in QD emission in the presence of complexes thus indicated dissociation and the release of freed components. Addition of chloroquine resulted in quenching that varied linearly with the concentration of chloroquine added. This result revealed the contribution of chloroquine to complex destabilization and demonstrated the feasibility of using QD-FRET to measure induced dissociation in a well-defined, cell-free setting

In an attempt to understand the poorly understood process of nanocomplex self-assembly, Ho et al. combined QD-FRET with microfluidic technology to monitor polymer-DNA complexation with millisecond resolution [136]. By generating complexes on a microfluidic chip, they were able to eliminate many of the forces involved with typical bulk mixing to isolate the assembly process. Solutions of Cy5-labeled chitosan and QD-DNA were introduced into microchannels under laminar flow conditions, and self-assembly occurred at the channel interface. The band of QD-FRET-mediated Cy5 signal grew wider and brighter with distance as the complexes nucleated, matured, and diffused outward, creating a spatial signal pattern that was subsequently transformed to determine the kinetic parameters of self-assembly. The authors described two distinct stages of the assembly process: a primary stage where assembly was determined to be diffusion-limited, and a secondary diffusion-reaction limited stage. QD-FRET provided

a sensitive and quantitative indication of the onset and progression of molecular interactions throughout the self-assembly process. Such a system could be used to screen the chemical properties of carriers that affect DNA condensation, nanocomplex size and structure, and ultimately their efficiency. The same group also used single molecule detection to compare the rates of QD emission before and after nanocomplex disruption to determine the number of plasmid copies within each nanoparticle [58]. The single particle analysis of the nanocomplex facilitates understanding of the physicochemical basis for its biological performance.

2.7.4.4 Two-Step QD-FRET

The narrow emission spectra and broad absorption windows of QDs make them a natural choice for multiplexed applications, allowing the simultaneous detection of two or more processes. Instead of investigating each delivery barrier independently, Chen et al. recently proposed an integrated approach to monitor DNA release and degradation simultaneously with two-step QD-FRET [131]. Their system is based on three-fluorophores and two parallel energy transfers (Figure 9). Three distinct states of DNA could be distinguished through quantitative ratiometric analysis of FRET efficiencies: (I) When double-labeled plasmid DNA (QD/nuclear dye (ND)-DNA) is condensed in stable nanocomplexes, the QD donor drives energy transfer through the ND (E_{12}) which acts as a relay to Cy5 (E_{23}) conjugated on the polymeric gene carrier. For stable nanocomplexes, both the ND and Cy5 are 'on', or actively exhibiting FRET-

mediated emission. (II) When the nanocomplex begins to unpack and release intact DNA, only the ND is 'on' through E_{12} while Cy5 is 'off' due to the loss of E_{23}. (III) When free DNA is degraded, both ND and Cy5 are 'off' due to the loss of both E_{12} and E_{23}. The system was developed with two different carrier systems: quickly dissociating PEG-b-PPA and more stable chitosan, and resolved mechanistic differences between them. Chitosan protects DNA more effectively, but its slow release ultimately limits its efficacy relative to PEG-b-PPA. This novel two-step QD-FRET method allows for detailed assessment of the onset of DNA release and degradation simultaneously, and is only possible due to the narrow emission spectra of the QD donor. An organic donor fluorophore would likely have resulted in significant levels of direct second acceptor excitation, which may bias the analysis. Given the heterogeneity of nanocomplexes and intracellular microenvironments, the single-particle resolution makes two-step QD-FRET particularly powerful in understanding the critical barriers to gene delivery.

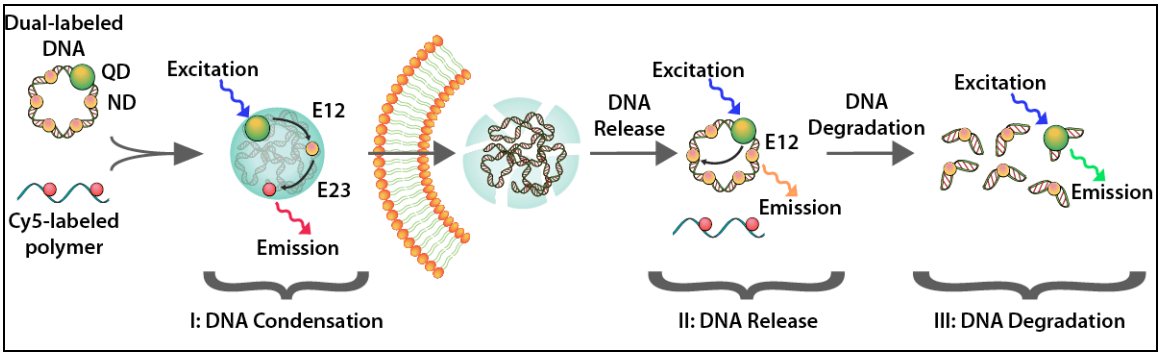

Figure 9. Two-Step QD-FRET
Two-step QD-FRET enables the simultaneous detection of nanocomplex unpacking and nucleic acid degradation using a three-fluorophore system (1: QD, 2: nuclear dye (ND), and 3: Cy5) through two parallel energy transfer processes (E_{12} and E_{23}). Under excitation of the QD donor, three distinct states of DNA could be distinguished: (I) When condensed within intact nanocomplexes, the QD donor drives energy transfer through the ND (E_{12}) which acts as a relay to the carrier-bound acceptor (E_{23}), resulting in emission from Cy5. (II) When the nanocomplex is unpacked only the ND is 'on' through E_{12} while Cy5 is 'off' due to the loss of E_{23}. Emission from the ND, through E_{12}, suggests that DNA remains intact. (III) When free DNA is degraded, both ND and Cy5 are 'off' due to the loss of both E_{12} and E_{23}, leaving only emission from the QD donor.

Similarly, another group used two-step QD-FRET to monitor the delivery of the chemotherapeutic drug doxorubicin by a QD-RNA carrier [137]. They conjugated QDs to RNA aptamers, loaded with intercalated doxorubicin and targeting the prostate specific membrane antigen. In the intact complex, both QD donor and doxorubicin acceptor fluorescence were quenched, the QD being quenched by doxorubicin and doxorubicin in turn by intercalation with the aptamer. Drug release resulted in recovery of both QD and doxorubicin fluorescence, which were then used to detect cancer cells that internalized the targeted nanocomplexes. The complexes used in this study killed

antigen-expressing cancer cells with high selectivity, demonstrating that QD-FRET has potential in combined therapeutic and diagnostic applications.

2.7.5 Selection of QD-FRET Pairs and Practical Concerns

To maximize the benefits of QD-FRET in the study of nonviral nucleic acid delivery, a researcher planning to adopt the technique should give some thought to the relevant practical considerations when designing the system. Adoption of QD-FRET has likely been slowed by the perceived complexity of the chemical modification process and potential effect on the bioactivity of nucleic acids that arises from the size and surface properties of conjugated QDs. One group did report a decrease in DNA bioactivity after conjugation, likely due to a combination of random incorporation of biotin sites into coding regions and steric hindrance of the transcriptional machinery [58]. However, other groups have demonstrated high expression levels with QD-labeled DNA [139], and total retention of nucleic acid bioactivity is often not crucial in mechanistic studies.

Determination of the ideal labeling frequency requires some optimization. Less than one QD per plasmid DNA molecule on average would provide sufficiently high sensitivity, given that each complex typically consists of multiple plasmids. Such a configuration would also guarantee minimum interference to complexation as well as false positives from excess free QDs. Similar principles apply to the labeling of gene carriers, although multiple organic fluorophore acceptors are typically required. The

optimization involves the number of fluorophores per molecule, acceptor to donor ratio (which could also be tuned by adjusting the carrier to payload ratio), and balance between reasonable energy transfer efficiency and unaltered expression. When reduced bioactivity is a problem, one alternative is to use mixtures of labeled and unlabeled reagents. An additional consideration unique to the use of intercalating dyes for intracellular studies is that nuclear staining may occur, reducing the detectable fluorescence from nanocomplexes or released nucleic acids. Some QDs are large, so the physical properties of labeled and naïve particles should be compared before moving forward. Cell-free characterization of the QD-FRET signal and nanocomplex formation is strongly recommended before moving to intracellular studies. QDs are poorly suited as acceptors in QD-FRET, due to their broad excitation windows and long exciton lifetimes. The cytotoxicity of labeled complexes should also be evaluated to avoid unexpected complications.

To date, most published QD-FRET pairs have been comprised of commercially available fluorophores. The optical characteristics of the pairs described here have been summarized in Table 2. Theoretically speaking, QD-FRET pairs are chosen for their substantial spectral overlap $J(\lambda)$. Practically, however, detection sensitivity is also determined by the optical capabilities available to the user, including the excitation source, filter combinations, and spectral response of the detector. While cellular imaging reveals the spatial distribution of complexes at given time points, flow cytometry-based

detection enables the rapid screening of a range of experimental conditions. A combination of the two techniques would supply a more complete picture of where and when nanocomplexes unpack. While a more exhaustive discussion of detection techniques, modes of analysis, and methods of determining QD-FRET are beyond the our scope, we refer interested readers to a comprehensive review on FRET imaging [50].

Table 2: Optical Parameters of QD-FRET Pairs Used to Study Nucleic Acid Delivery

Fluorophores /QDFRET Pair	Emission (nm)	Extinction coefficient ($M^{-1}cm^{-1}$)	Quantum Yield	Spectral Overlap, J(l) ($M^{-1}cm^{-1}nm^4$)	Förster Radius, R_0 (Å)	Ref
Cy3	570	$1.5x10^5$ (Ex: 552nm)	0.15			
Cy5	670	$2.5x10^5$ (Ex: 650nm)	0.28			
Texas Red	614	$8.5x10^4$ (Ex: 596nm)	N.A.			
Rhodamine	573	$1.29x10^5$ (Ex: 560nm)	N.A.			
AlexaFluor647	668	$2.37x10^5$ (Ex: 633nm)	0.33			
BOBO3	605	$1.48x10^5$ (Ex: 570nm)	0.39			
Adirondack Green QD	525	$1.3x10^5$ (Ex: 488nm)	0.4			
Qdot545	545	$2.9x10^5$ (Ex: 488nm)	0.4			
Qdot605	603	$11x10^5$ (Ex: 488nm)	0.4			
Qdot625	621	$27x10^5$ (Ex: 488nm)	0.4			
Qdot525-Cy3				$7.02x10^{15}$	59.19	[131]
Qdot525-BOBO3				$4.44x10^{15}$	52.26	[128, 131]
Adirondack Green QD - Texas Red				$1.17x10^{15}$	43.92	[127]
Qdot545-Rhodamine				$8.07x10^{15}$	60.58	[129]
Qdot605-Cy5				$1.24x10^{16}$	65.09	[58, 122, 130, 134, 136]
Qdot605-AlexaFluor647				$1.11x10^{16}$	63.89	[126]
Qdot625-Cy5				$2.13x10^{16}$	71.24	[132]

* Remarks: These values were estimated according to Eq. (2) for the FRET pairs used in the studies reviewed here. Orientation factor (κ^2) and refraction index (n) were assumed to be 2/3 and 1.4, respectively. Other parameters were obtained from the manufacturers when possible, or adopted from: (i) Invitrogen: http://www.invitrogen.com/, (ii) Fluorophores Database: http://fluorophores.mgfb.at/, and (iii) Pubspectra: http://home.earthlink.net/~pubspectra/

2.7.6 Future Perspectives for QD-FRET

Nonviral delivery of nucleic acids represents a potentially safe and effective treatment option for many diseases. However, success to date has been hindered by poor transfection efficiency. Elucidation of the rate-limiting barriers in nonviral gene transfer will help the engineering of more efficient carriers. QD-FRET has been a valuable addition to the arsenal of tools used to quantify the formation, composition, unpacking, and degradation of nucleic acid nanocomplexes. The unique optical properties of QDs result in improved sensitivity, increased precision, and ultimately the ability to derive more robust structure-function relationships. The versatility of QD-FRET enables not only studies of specific subcellular behavior with confocal microscopy, but also multiplexing and high-throughput analysis using flow cytometry.

Quantum dots encounter some criticism for potentially interfering with biological entities due to their larger size compared to organic fluorophores [140]. The challenges to QD-based assays are retention of bioactivity and functionality, although QD-conjugation has been shown to have minimal effects in many cases. Furthermore, the additional mass of larger QD may alter the diffusivity of biomolecules, or disrupt the movement of biomolecules. However, the ongoing improvement of QD synthesis yields fluorophores with reduced size but undiminished brightness, emission, and photostability. These QDs promise to facilitate future QD-FRET studies with reduced concerns about interference.

The utility of QD-FRET in understanding nucleic acid delivery will continue to expand. QDs are already used in a number of in vivo applications [141], and can be tuned to operate in the near infrared range required for tissue penetration. This would open the door for the development of QD-FRET theranostics [142], as the field transitions from the molecular to the integrative level. As QD synthesis is further refined so that multiple QDs can be excited at a single wavelength and emit in distinct spectral ranges, the frequency of multicolor applications and multiplexing should increase. This will lead to even more detailed information, as multiple processes are monitored simultaneously. QD-FRET will continue to offer prolonged, sensitive, and real-time imaging of the nonviral nucleic acid delivery process, and should help the field move away from trial-and-error approaches and redouble its effort toward the rational design of effective systems.

2.8 Traditional Methods of Nanocomplex Assembly

It is understood that the cellular uptake, transfection efficiency, circulatory residence time, and toxicity of nanoparticles all depend to some degree on physical attributes such as size, shape, and charge. However, little attention has been paid to the manufacturing process of polymer-nucleic acid nanocomplexes, and how it may affect these properties. The assembly of nanocomplexes by charge neutralization is a rapid, highly energetic thermodynamic process. To quantify the kinetics of the complexation reaction, Ho et al. studied parallel laminar streams of fluorescently labeled chitosan

polymer and plasmid DNA on a microfluidic T-junction chip. Using the FRET signal that occurred as complexes formed at the stream interface, the reaction was determined to occur within milliseconds [136]. This result matched that of an earlier study using polyamidoamine dendrimer carriers [143]. Currently, the vast majority of nanocomplex assembly is accomplished by bulk mixing methods. These involve pipetting a solution of polycation into a nucleic acid solution and either shaking, inverting, pipetting up and down, or more commonly vortex mixing. While convenient, bulk mixing is poorly suited to produce uniform particles, given the fast reaction kinetics involved. Bulk mixing introduces significant variability into the preparation and often yields metastable products of non-equilibrium composition [5]. The final properties and composition of the product depend on how the polyelectrolytes initially encounter one another, which is determined by the chaotic mixing. Irreproducibility is rampant, as slight perturbations of mixing protocols are known to produce particles of differing qualities. The resulting heterogeneity is an impediment to the progress of nonviral gene delivery in multiple ways.

While complexation is impossible to control in a bulk setting where mixing takes much longer than milliseconds, a reduction of the reaction volume would reduce the time required to reach a fully mixed state. Calculations using a coarse-grain model and the estimated diffusivities of typical DNA and polymer reagents have been used to calculate that volumes in the picoliter range would be required to give complete mixing

within milliseconds [144], motivating our efforts to develop a system to generate picoliter droplets. However, we are not the only group to have become concerned with the problem of nanocomplex manufacturing. The heterogeneity resulting from bulk synthesis universally hinders advances in nonviral gene delivery with respect to rational carrier design, mechanistic understanding, and optimization. As the field has begun to consider nanoparticle assembly as an opportunity for innovation, several novel assembly techniques have emerged.

2.9 Recent Innovations in Nanocomplex Assembly

The need for greater control in the manufacturing of delivery systems has been recently identified as a critical unmet need the drug delivery field [145-147]. One technique to emerge as a result is the top-down nanoimprinting system called Particle Replication in Non-wetting Templates (PRINT). Pioneered by DeSimone, this approach offers the ability to produce precisely controlled particles with defined shape and size [146]. These particles have proven valuable in deconvoluting the effects of distinct properties on mechanisms such as cellular internalization and biodistribution. However, such top-down approaches would be difficult to adapt to suit the bottom-up self-assembly of polymer-nucleic acid nanocomplexes. The rapid reaction kinetics, aqueous conditions, and room temperature assembly instead favor microfluidic approaches.

A number of groups have explored the use of microfluidic systems to synthesize DNA nanocomplexes with both polymer and lipid carrier systems. Koh et al. formulated

Bcl-2 antisense oligonucleotide lipoplexes using a hydrodynamic focusing system, and demonstrated a more efficient knockdown of Bcl-2 expression than with the bulk-mixed controls [148]. The report attributed the effects to the smaller size, diminished polydispersity, and lower zeta potential of the lipoplexes made with microfluidics. The same group applied the same hydrodynamic focusing system to the production of PEI-DNA particles, and again reported enhanced performance relative to bulk-mixed controls in terms of cytotoxicity and transfection efficiency in NIH 3T3 fibroblasts and mouse embryonic stem cells [149]. When applied to chitosan-DNA particles, the hydrodynamic focusing platform gave similar improvements with respect to cytotoxicity, but only modest gains in transfection efficiency [136]. Hydrodynamic focusing may be suboptimal for polymer nanocomplex assembly; in this latter study the authors observed two distinct stages of particle formation – an initial period of rapid electrostatic binding in the millisecond range, followed by a second stage of nanocomplex flocculation caused by dispersion of the interface in the third dimension. This phenomenon led to a wider distribution in particle size. Another microfluidic approach, developed by Hsieh et al., was designed to produce lipoplexes within picoliter droplets [150]. This Picoliter Microfluidic Reactor and Incubator (PMRI) yielded more monodispersed lipoplexes that mediated more reproducible, though not always higher, levels of transfection. The microfluidics-assisted confinement (MAC) nanomanufacturing platform studied in this dissertation was modeled after this system,

and its adaptation and application to polymer-nucleic acid nanocomplexes could be even more effective. Unlike cationic lipids that are typically of low and uniform molecular weight, polycations are typically polydispersed, unless produced by recombinant methods, and thus even more susceptible to the deleterious effects of non-equilibrium mixing conditions.

Proof-of-principle studies with the MAC system were completed using two commercial transfection reagents and evaluated in HEK293 cells [144]. Synthesis of particles with Turbofect (poly(2-hydroxypropyleneimine)) and jetPEI (linear polyethylenimine, 20kD) and GFP-encoding plasmid DNA resulted in complexes that were smaller and more uniform in size, lower in zeta potential, less toxic, and more potent. While promising, these preliminary results do not prove the broad applicability of the technique, and do not demonstrate the benefits of MAC particles in more complex systems. Among the issues that still need to be addressed is the ability of MAC to improve particles loaded with different types of nucleic acids. Plasmid DNA remains of high interest in gene medicine, but messenger RNA as a payload obviates the requirement of delivery into the nucleus and more readily produces transgene expression in slowly dividing or post-mitotic cells. Finally, siRNA presents new options of therapeutic intervention via post-transcriptional gene silencing. However, substitution of the payload may not be trivial, as there is mounting evidence that polycations may interact differently with DNA than they do with RNA [151]. Double

stranded DNA has a longer persistence length than dsRNA, rendering it a stiffer molecule. Shorter nucleic acids may require more polycation to achieve condensation, due to a reduction in the effects of chain entanglement. Testing different types of nucleic acids and carriers will be necessary to demonstrate broad potential of MAC to control nanocomplex self-assembly. Products should be evaluated in terms of size, size distribution, zeta potential, payload protection efficiency, binding affinity between the polycations and nucleic acids, stability in the presence of competitors, aggregation behavior, amount of unreacted species, cytotoxicity, and transfection efficiency. Evaluation on these bases will give a strong justification to continue the development of MAC for applications in more complex and translationally relevant systems.

2.10 Alternative Microfluidic Approaches

Hydrodynamic focusing (HF) approaches may offer complementary benefits as compared to emulsion-based platforms such as MAC. HF operates using exclusively aqueous reagents, and may be more amenable to scale-up to increase throughput. However conventional 2-D HF, as described previously, suffers from dispersion of the reagents and products in the third dimension, resulting in diminished quality. Consequently, Huang et al. have developed a 3-D HF technology where the streams are also compressed in the third dimension [59]. The device is fabricated using soft lithography, and focuses the streams using a phenomenon called "microfluidic drifting". The input flow is first focused in the vertical direction while passing through a 90-

degree curve in a microfluidic channel. Around the curve, a pair of transverse secondary Dean vortices is induced. These vortices cause the sample stream to drift laterally to the opposite side of the channel. With proper flow control, the sample stream is compressed into a thin horizontal plane in the middle of the microchannel. Further focusing of the sample stream in the horizontal direction is achieved by injecting two orthogonal focusing sheath flows from both directions to form a 3-D focused sample stream at the center of the microfluidic channel. This method has shown promise as an alternative microfluidic nanomanufacturing platform with potential benefits primarily in scale-up and throughput, but it must be confirmed that the shear forces experienced by the polymer and nucleic acids do not compromise their activity and that polyplex quality is improved.

2.11 Clinical Needs in Neurodegenerative Disease

One of the most pressing unmet clinical needs, given the United States' aging population, is the rise in prevalence of intransigent neurodegenerative diseases. The cost to society, whether measured in dollars, disability, or deaths, is tremendous. Whether environmental, genetic, or idiopathic in origin, the root causes of neurodegenerative disease tend to be multifactorial. As such, they are difficult to prevent and treat, even with timely diagnoses. The Alzheimer's Association estimates that the costs of caring for people with Alzheimer's disease and other forms of dementia will increase from $203 billion this year to $1.2 trillion in 2050, while one in three seniors currently dies with

Alzheimer's or another form of dementia. The average post-diagnosis life expectancy is seven years [152]. The only drugs available for Alzheimer's patients are cholinesterase inhibitors and NMDA receptor antagonists, which only provide temporary effects in a subset of cases [153]. Parkinson's disease also exacts a heavy cost on society, affecting half a million Americans annually with a cost of $11 billion [154]. The treatment options for Parkinson's disease include L-DOPA, anticholinergics, MAO-B inhibitors, and deep brain electrical stimulation. Again, these options provide temporary relief of some symptoms, but inevitably lose effectiveness. While pharmaceutical intervention may slow the loss of neurons, the diseases continue to progress. Only cell replacement therapy has the potential to reverse the disease course once a patient's own cells are lost.

2.12 Current Approaches to Treatment

Patients with Alzheimer's or Parkinson's disease may see temporary improvements with pharmacologic intervention or deep brain stimulation, but the clinical benefits inevitably decline with the progressive loss of neuronal function. These diseases are characterized by the loss of neurons in the neocortex and hippocampus caused by an accumulation of amyloid plaques in the case of Alzheimer's, and by the loss of dopaminergic neurons in the substantia nigra in the case of Parkinson's. Cell replacement therapy has been proposed as a long-term solution [155, 156]. However, finding an appropriate cell source has been a challenge while safety and ethical concerns preclude the use of embryonic stem cells. Early clinical trials involving transplantation

of fetal dopaminergic neurons into the striatum of patients have shown survival and engraftment of the cells but inconsistent clinical outcome [156-161]. Advances in human embryonic stem cell (ESC) engineering offer a viable source of neurons since ESCs can undergo neurogenesis in vitro with the appropriate biochemical cues [162, 163]. However, the same ethical issue of fetus usage and concerns of teratoma formation hinder progress [164, 165]. The translation of therapies derived from induced pluripotent stem cells (iPSC) have also been slowed by concerns of teratogenic potential. It would be ideal to identify a source of cells, preferably autologous, that do not possess a differentiative or proliferative phenotype. If such cells could be generated in sufficient quantities, they could be grafted to achieve therapeutic effects, either by replacing the function of lost cells directly or supporting existing neurons by producing soluble factors (e.g. neurotrophins). Diffuse diseases such as Alzheimer's pose a targeting challenge, as compared to Parkinson's. However, ESC-derived cholinergic neurons implanted into Alzheimer's rodent models have given partial restoration of function [166, 167]. Parkinson's disease may represent a simpler scenario for cell replacement, as the disease is localized to a more defined region of the brain. As mentioned above, allogeneic grafting of dopaminergic neurons has shown some positive results. Induced pluripotent stem cells have also effected a restoration of motor function in animals following differentiation to dopaminergic neurons and implantation [168]. These studies

show that the potential of cell replacement therapy exists, if a safe, abundant, and effective source of cells can be identified.

2.13 Direct Conversion of Fibroblasts to Neurons

Recently, the reprogramming of adult somatic cells from one type to another was reported. In 2010, researchers found that expression of three genes encoding transcription factors (*Ascl1, Brn2, Myt1l: BAM factors*) delivered by lentivirus was sufficient to convert fibroblasts to functional neurons without going through complete de-differentiation to a pluripotent state. Neuronal transdifferentiation was first demonstrated by Wernig et al., where delivery of the BAM factors to mouse and human fibroblasts converted them into functional neurons with up to 20% efficiency, referred to as induced neuronal (iN) cells [6, 169]. The iN's were electrophysiologically active and formed functional synapses when cultured with primary neurons. This was the first report of the direct conversion of somatic cells from one type to another derived from a different germ layer. Such transdifferentiation brings the prospect of an ethical, practical, and safe neuronal cell therapy one step closer to reality. Subsequently, transcription factors have been identified to generate induced dopaminergic neurons that have been implanted to achieve a degree of phenotypic correction in animals [170-173]. Additional factor combinations are able to generate motor neurons [171]. These iNs are postmitotic and do not pass through a proliferative progenitor state [6, 174, 175], attributes making them an attractive cell source for cell-based therapy of CNS disorders

such as epilepsy, stroke, Huntington disease, and Parkinson's disease. However, the unpredictable, potentially genotoxic, integration of viral DNA sequences into the genome of the converted cells renders them unsuitable for transplantation.

An important result of the published neuronal transdifferentiation studies is that the iN cell state is maintained even when exogenous transgene expression is discontinued [169]. Endogenous BAM factor gene expression continues to increase after the dox-inducible exogenous expression is shut down by doxycycline withdrawal. This suggests that analogous reprogramming is possible even with the transient nature of nonviral gene delivery. Prior to our report, all instances of neuronal transdifferentiation were achieved with viral delivery methods. In Chapter five, we show the generation of mouse and human fibroblasts expressing pan-neuronal markers by nonviral delivery of the BAM factors. The nonviral transdifferentiation efficiency was initially low, but we also show that there exists room for improvement through optimization of the delivery protocol and the incorporation of topographical cues.

3. Gene Carrier Selection, Synthesis, and Optimization

Some of the material in Chapter 3 is included in:

Comparative study of nanoparticle-mediated transfection in different GI epithelium co-culture models. Loo Y, Grigsby CL, Yamanaka YJ, Chellappan, MK, Jiang X, Mao HQ, Leong KW. 2012. J Cont Rel. 160(1):48-56

Nonviral nucleic acid delivery is feasible and attractive. However, some polymeric gene carriers can be too stable for efficient intracellular dissociation from their nucleic acid payloads. A challenging nonviral gene delivery barrier is the efficient release of intact DNA into the cytoplasm or nucleus of a target cell. The natural polysaccharide chitosan has been used for oral gene delivery in mice, achieving phenotypic correction in multiple disease models [75, 176]. However, quantitative intracellular trafficking studies have shown that the chitosan system used in those studies is limited by overly stable binding of nucleic acids. We made efforts to improve the transfection capabilities of chitosan by adjusting physical properties such as molecular weight, degree of deacetylation, and the addition of ternary components. Additionally, we investigated another class of stimulus-responsive synthetic polymers as an alternative carrier system with improved dissociation characteristics. Unlike natural polymers, bioreducible linear poly(amido amine)s (SS-PAAs) can be designed

from the bottom up to meet the manifold requirements of nonviral gene delivery, and they can be engineered to possess the competing functionalities of DNA protection and efficient release. We studied SS-PAAs functionalized with either 4-amino-1-butanol (ABOL) or a combination of histamine and 3-(dimethylamino)-1-propylamine (HIS/DMPA). Coupling these functionalities that control buffer capacity for endosomal escape and charge density for DNA binding with the bioreducibility of the backbone results in a gene carrier with advantageous properties. Cytotoxicity (IC_{50} = 160-190 μg/mL) is an order of magnitude lower than 25 kDa branched PEI, and transfection in cell monolayers is 30-fold higher than Lipofectamine 2000 and 100-fold higher than 390 kDa, 83.5% deacetylated chitosan. The high transfection and low toxicity of SS-PAAs allows for the delivery of multiple doses to sustain robust transgene expression for prolonged periods of time, a requirement of many current applications.

3.1 Introduction

Chitosan is a naturally-sourced polysaccharide derived from the partial deacetylation of chitin, primarily from crustacean and insect shells. It consists of repeating units of glucosamine and N-acetyl-glucosamine, the proportions of which determine the degree of deacetylation of the polymer. Positively charged chitosan will bind to cell membranes, decrease the trans-epithelial electrical resistance (TEER) of cell monolayers, and increase paracellular permeability [177-181]. The per os mechanism of action includes interactions with the tight junction proteins occludin and ZO-1, re-

distribution of F-actin, and slight de-stabilization of the plasma membrane [182-184]. It is generally considered non-toxic and biodegradable, with an oral LD_{50} in mice of over 16 g/kg [185]. The safety of chitosan, its ability to prolong residence time in the gastrointestinal tract through mucoadhesion [186], and its ability to enhance absorption by increasing cellular permeability have all been major factors contributing to its widespread evaluation as a component of oral dosage forms. It has also been investigated as a gene carrier in recent years [14, 75, 187-196]. The bioavailability of delivered DNA can be improved via protection from serum nucleases by the polymer matrix, and there is little release of bound DNA until the nanoparticle is sequestered into the endolysosomal pathway. The nanoparticles can also be lyophilized without loss of bioactivity, so that chitosan polyplexes can be handled more like conventional pharmaceutical formulations in terms of production, reproducibility, and storage.

However, recent quantitative studies on the intracellular trafficking and unpacking kinetics of chitosan nanoparticles for gene delivery have revealed that a rate-limiting barrier is the efficient release of DNA into the cell [57]. Chen et al. labeled both chitosan and PEI and their nucleic acid payloads with QD-FRET components to detect discrete changes in intracellular polyplex stability. The uptake and unpacking of polyplexes was captured over time with confocal microscopy, and the data used to construct a three compartment first-order kinetic model of intracellular nucleic acid release. The photostability of the QD-FRET system enabled monitoring the distributions

of intact and unpacked particles for up to 72 hours. At two hours post-transfection, over 80% of PEI nanoparticles had unpacked, whereas only about half of chitosan particles had released their payload. PEI also resulted in an earlier shift toward nuclear plasmid translocation, perhaps encouraged by faster release of free plasmid in the cytoplasmic compartment. The unpacking time constant for chitosan was more than twice as large as that of PEI, adversely affecting its transfection capabilities. We first attempted to address this inefficiency through substitution of the 390 kDa, 83.5% deacetylated chitosan with shorter polymer chains bearing different degrees of deacetylation. The rationale was that shorter chains and/or a reduction in charge density may result in a slight relaxation of binding and accelerated intracellular release, while maintaining adequate levels of protection. In a parallel attempt to modulate the binding stability of chitosan polyplexes, we added the ternary component poly(γ-glutamic acid) (PGA) as a biodegradable anionic modulator of binding. It has been reported that addition of such ternary anionic components can increase transfection efficiency, but using nucleic acids themselves can be undesirable due to premature enzymatic degradation [197]. PGA is a water soluble, non-toxic, naturally-occurring peptide that has been tested in the oral nanoparticulate delivery of insulin and other drugs [176]. Despite the reported ability of PGA to improve transfection with low molecular weight chitosan [198], neither modulation of chitosan physical properties nor systematic incorporation of PGA was sufficient to effect

adequate enhancement of transfection. As a result, we shifted our focus to a class of synthetic, bioresponsive polymeric gene carriers.

Bioreducible poly(amido amine)s (SS-PAAs) are a class of synthetic peptidomimetic cationic polymers that has been tested for gene delivery [199]. The rationale of including SS-PAAs as gene carriers in this study comes from the desire to overcome the barrier of releasing nucleic acids from nanoparticles, and from in vitro studies showing that they are as efficient as PEI but much less toxic [22]. The disulfide links in the polymer backbone allow for rapid degradation once a SS-PAA polyplex reaches the reducing environment of the cytoplasm, facilitating efficient unpacking and release of the payload. The ease of chemical functionalization of these polymers during their synthesis allows for the incorporation of side chains that can yield a variety of characteristics. We studied SS-PAAs functionalized with either 4-amino-1-butanol (ABOL) or a mix of histamine and 3-(dimethylamino)-1-propylamine (HIS/DMPA). Coupling these functionalities that control buffer capacity for endosomal escape and charge density for DNA binding with the bioreducibility of the backbone results in a gene carrier with desirable properties. We show that SS-PAAs can form polyplexes of appropriate size and charge, dissociate readily upon challenge with typical intracellular concentrations of reducing agents, and transfect cells efficiently. We demonstrate their ability to achieve modest levels of transfection in vivo, and show that their favorable

cytotoxicity profiles allow for repeated doses to be delivered in order to sustain high transgene expression levels.

3.2 Methods

3.2.1 Polymer Synthesis

High molecular weight chitosans of 390,000 Daltons and 83.5% deacetylation, 209,000 Daltons and 86.9% deacetylation, and 350,000 Daltons and 77.3% deacetylation were gifts from Vanson Chemicals (Redmond, WA). Chitosans were dissolved at 1% in 1% acetic acid overnight, then filtered through filter paper under vacuum and precipitated with NaOH. They were then collected by centrifugation at 6k RPM for 20 minutes, washed four times with purified water, and lyophilized for storage. PGA (20,000 Daltons) was purchased from Vedan (Taichung, Taiwan). Poly(CBA-HIS/DMPA) was a gift from Prof. Johan Engbersen (Univ. of Twente, Netherlands). Poly(CBA-ABOL) was synthesized by Michael-type polyaddition of 3.67 g N,N-cystaminebisacrylamide (CBA) (Polysciences, Warrington, PA) and 1.26 g 4-amino-1-butanol (ABOL) (Sigma-Aldrich, Saint Louis, MO) as described by Lin et al [22]. The reaction product was purified by dialysis (3.5 kDa cutoff) in acidified deionized water (pH 4) and then lyophilized. The polymer was collected in its HCl-salt form (1.63 g, 33% yield). Polymer products were validated by Matrix Assisted Laser Desorption/Ionization (MALDI) mass spectrometry and ^{1}H NMR prior to use.

3.2.2 Cell Culture and Transfections

For all cell culture experiments, 20,000 cells cm^{-2} cells were seeded 24 hours prior to transfection in TCPS plates (BD, Franklin Lakes, NJ) and cultured at 37 °C and 5% CO_2 in the appropriate complete growth media recommended by the supplier. The cell types studied were human embryonic kidney HEK293 (ATCC, Manassas, VA), human hepatocellular carcinoma HepG2 (ATCC), human colon carcinoma (Caco-2) (ATCC), and normal human dermal fibroblasts (NHDF) (Millipore). For transwell studies, Caco-2 cells were expanded to approximately 80% confluence, harvested by trypsinization, then washed and resuspended in culture medium. $3x10^5$ cells were then seeded onto the upper chamber of a transwell (6.5mm diameter, 3.0 micron pore-size membrane) (Costar, Cambridge, MA). All transport experiments were performed using polyester (PE) transwell membranes. The cells were cultured for 14 days before validation of monolayer integrity by TEER analysis and subsequent use. All transfections were carried out at 37°C and 5% CO_2 in serum- and antibiotic-free OptiMEM (Invitrogen) unless otherwise specified, which was replaced with the appropriate complete growth medium 4 hours after the onset of transfection. Transfection efficiency and transgene expression were assayed at 24 hours post-transfection unless otherwise indicated. Luminescence measurements to quantify luciferase expression were performed using the SteadyGlo kit (Promega, Madison, WI) according to the manufacturer's protocol. For flow cytometric analysis, cells were trypsinized, resuspended in PBS, and analyzed on a

FACScan flow cytometer (Becton- Dickinson, Mountain View, CA) with gating such that the negative untransfected controls were one percent positive. At least 10,000 cells were analyzed per experimental condition.

3.2.3 Nanocomplex Preparation

Plasmids pDNA (pmaxGFP, Lonza, Switzerland), pLuc (VR1255 Luciferase, Vical, San Diego, CA) and pT7-EGFP-N1 (gift from David Boczkowski, Duke University) were propagated in *Escherichia coli* DH5α (Invitrogen, Carlsbad, CA) and purified with EndoFree Plasmid Mega and Maxi kits (Qiagen, Germantown, MD). Following linearization, in vitro transcription was performed on T7-EGFP-N1 with the mMESASGE mMACHINE T7 kit (Invitrogen) to generate mRNA encoding GFP. Chitosan nanoparticles were formed by adding 10 μg of pDNA or mRNA to 100 μL of 50 mM sodium sulfate and subsequently mixing with 100 μL of 0.02% chitosan solution under high-speed vortex mixing. When PGA was added to the formulation, 1% PGA dissolved in deionized water was used. The reactions were performed at 55°C. SS-PAA polyplexes were prepared by adding a complexation buffer solution (20 mM HEPES, 5 wt % glucose, pH 7.4) of polymer (844 μg mL^{-1} for DNA, 1125 μg mL^{-1} for RNA) to a complexation buffer solution of nucleic acid (75 μg mL^{-1}) followed immediately by 20 seconds of vortex mixing. Reaction sizes ranged from 5 to 15 μg of nucleic acid. Lipofectamine 2000 (Invitrogen) lipoplexes were prepared as per the manufacturer's

recommendations. The sizes and zeta-potentials of the nanoparticles were measured using a Zetasizer-3000 (Malvern Instruments, Southborough,MA).

3.2.4 Transepithelial Electrical Resistance Measurements

The transepithelial electrical resistance (TEER) across the intestinal epithelium is a measure of paracellular ion movement and indicator of monolayer integrity. A drop in TEER is interpreted as an increase in tight junction permeability. The TEER of each cellular insert was determined by means of a voltohmmeter – EVOM manufactured by World Precision Instruments (Sarasota, FL). All TEER studies were conducted after a 15-minute equilibration period at room temperature. Measurements were performed in triplicate and the mean value used for any subsequent calculations.

3.2.5 Transmission Electron Microscopy

Nanoparticles used for transmission electron microscopy (TEM) transport studies were synthesized using pGeneGrip Gold 10 nm colloidal gold-conjugated plasmid DNA (Genlantis, San Diego, CA). $9x10^6$ Caco-2 cells were seeded in 35mm tissue culture dishes and cultured for 16 days prior to transfection. Prior to transfection, the culture medium was changed to OptiMEM. A 6 μg DNA dose of nanoparticles was added for 4 hours at 37°C, then fixed in a 4% formaldehyde, 2% glutaraldehyde solution overnight at 4°C. The cells were post-fixed in 1% osmium tetroxide and stained en bloc with 0.5% uranyl acetate, then dehydrated with a graded series of ethanol. Samples were embedded in Polybed 812 resin, thin-sectioned, and picked up on 150 mesh copper

grids. After further staining with 1% uranyl acetate and 0.4% lead citrate, grids were examined on a FEI Tecnai G^2 Twin instrument under 80kV.

3.2.6 Animal Studies

Wistar rats (male, 200–250 g) were laparotomized under general anesthesia and the liver was isolated from the surrounding tissue. A 33 G needle was inserted into the common bile duct and a tie was used to secure the needle. Nanoparticles and naked DNA were administered at a dose of 20 μg of plasmid in 4 mL of 5% glucose medium into the common bile duct over 20 min (0.2 ml/min) using a syringe pump. A tie was then placed around the bile duct between the liver and the point of infusion to prevent back flow, and the needle was withdrawn. After 30 min, all ties were removed. If the needle hole in the bile duct required stitches to prevent leakage, 10-O nylon suture (Ethicon, Somerville, NJ, USA) was used. Luciferase expression was monitored non-invasively at 4, 24, and 72 h post-infusion with an IVIS Imaging System.

3.3 Results

3.3.1 Chitosan Transfections

Chitosan (Figure 10) of high molecular weight (390 kDa, C390) and 83.5% deacetylation has been used successfully in a variety of gene delivery applications despite its inherent disadvantages with respect to overly tight binding of DNA. We first examined the potential of high molecular weight chitosan to deliver mRNA more efficiently. Messenger RNA is a shorter molecule than plasmid DNA, diminishing the

contribution of chain entanglement to the complexation. Furthermore, its single stranded nature corresponds with a reduction in charge density that may also contribute to a relaxation of binding stability. To test whether these properties would translate to an increase in expression, we delivered chitosan-GFP pDNA and mRNA polyplexes to HepG2 cells and compared their expression after 48 hours with RT-PCR (Figure 11). Gel electrophoresis of the amplified RT-PCR product revealed that although mRNA delivery did yield a modest improvement in intracellular transcript levels at this time point, substitution of plasmid payloads with mRNA is insufficient to boost delivery to levels achievable with PEI and Lipofectamine 2000. Still, the result suggested that slight destabilization of high molecular weight chitosan polyplexes may promote increased transfection, so we next explored a variety of alternative methods to modulate the complexation of chitosan with nucleic acids.

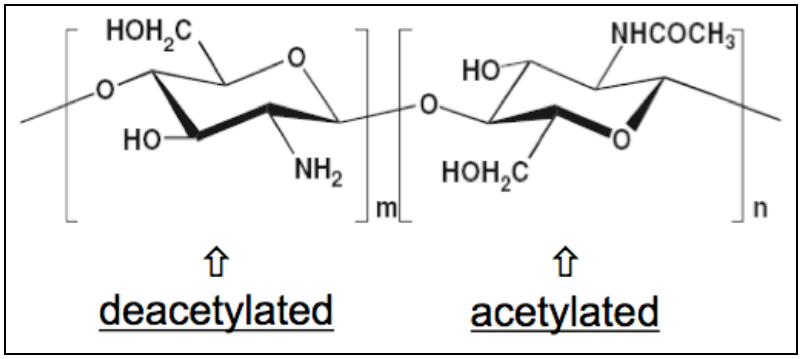

Figure 10. Chemical Structure of Chitosan
Chitosan is a naturally-sourced polysaccharide derived from the partial deacetylation of chitin, primarily from crustacean and insect shells. It consists of repeating units of glucosamine and N-acetyl-glucosamine, the proportions of which determine the degree of deacetylation of the polymer.

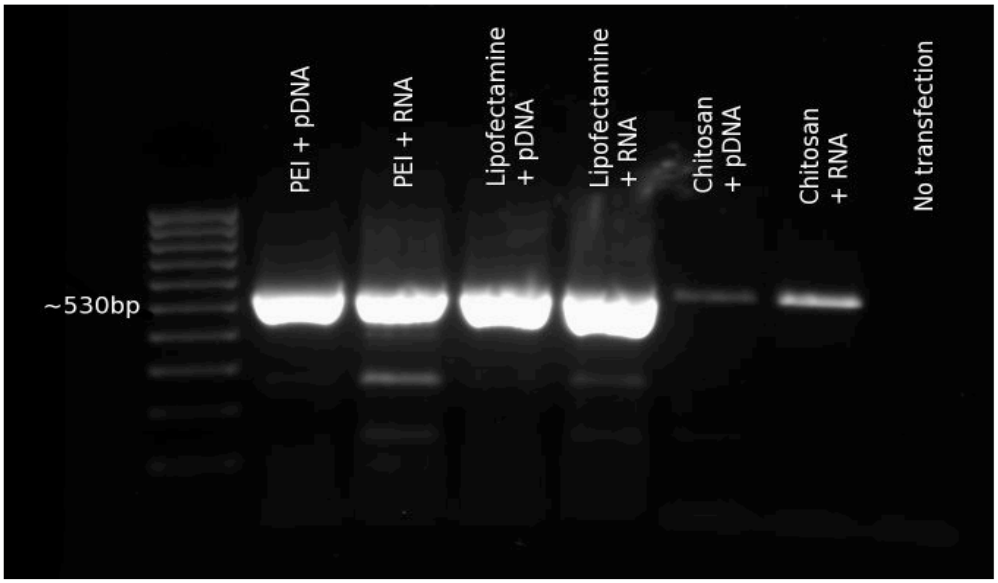

Figure 11. Delivery of Messenger RNA with Chitosan Polyplexes.
GFP transcript levels in HepG2 cells quantified by RT-PCR following delivery of mRNA with chitosan is slightly higher than levels mediated by pDNA.

3.3.2 Optimization of Chitosan Polyplex Formulation

Operating under the assumption that excessive binding stability of C390 hinders its ability to efficiently release nucleic acids within target cells, we next tested two additional high molecular weight chitosan formulations. C209 (209 kDa, 86.9% deacetylation) and C350 (350 kDa, 77.3% deacetylation) were evaluated for their ability to form nanocomplexes, protect nucleic acids, and transfect cells. To determine the appropriate formulation for each polymer, physical polyplex properties were analyzed over a range of N/P ratios. We determined that C209 formed the best particles at an N/P ratio of 5 (diameter ~ 120 nm, zeta potential ~ 14 mV), while C350 was unable to stably complex DNA at any point over the range tested (Figure 12).

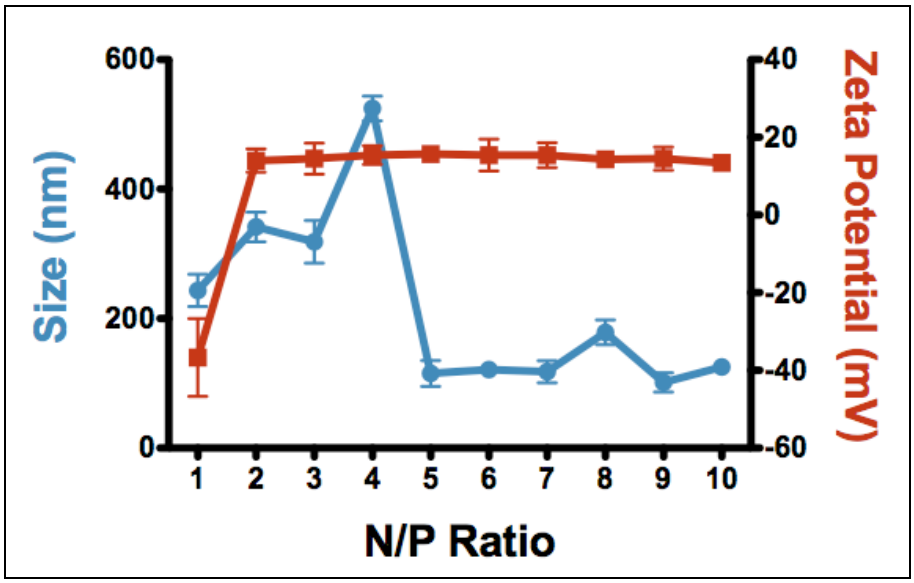

Figure 12. Size and Zeta Potential of C209 Polyplexes
Physical characterization of C209 polyplexes to determine the N/P ratio required to produce nanoparticles with the desired properties

We confirmed the complexation and protection of DNA using a gel retardation assay and DNase protection assay, respectively (Figure 13). In the gel retardation studies, the migration of free anionic nucleic acid is prevented upon complexation, condensation, and charge neutralization by cationic polymer. At N/P ratios greater than two, C209 completely prevented the migration of DNA. When the particles were incubated with DNase I prior to electrophoretic analysis, no smear was evident to indicate degradation of DNA. The DNA protection assay suggests that C209 is able to protect a payload from enzymatic degradation, even at low concentrations. Considering the corresponding polyplex size, zeta potential, and DNA protection ability, we selected an N/P ratio of five to use for the transfection analyses performed with C209.

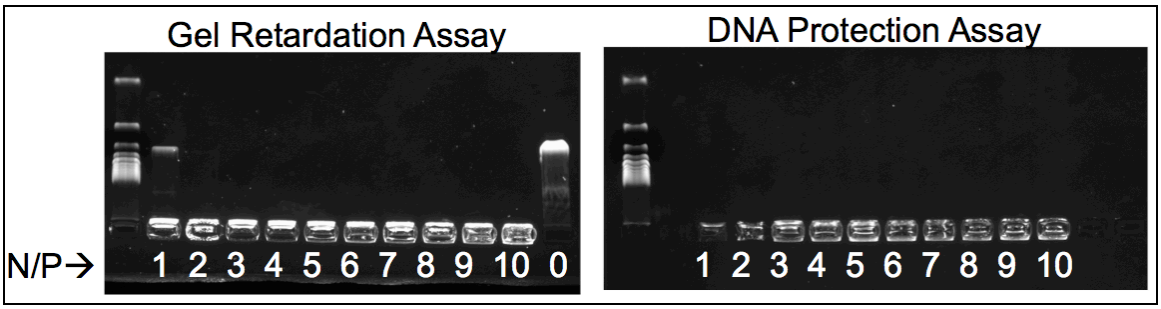

Figure 13. Characterization of C209 Polyplex Binding and Stability
Gel retardation and DNA protection assays show that an N/P ratio of 5 is sufficient for C209 to complex and protect nucleic acid payloads.

3.3.3 Quantification of Transfection Efficiency

Using this optimized C209 formulation, we tested the transfection capabilities of the polyplexes in HepG2 and HEK293 cells. Flow cytometric analysis of HepG2 cells transfected with GFP pDNA and mRNA matched well with previous RT-PCR results. Delivery of mRNA with C390 resulted in approximately twice as many GFP^+ cells than with pDNA (Figure 14). In both cases, C209 mediated lower transfection efficiency than C390. In the case of HEK293 cells, mRNA transfections were lower than pDNA, and C209 again performed poorly compared to C390 (Figure 15). The poor performance of mRNA particles in this cell line may be attributed to the higher metabolic activity and faster intracellular RNA turnover rate as compared to hepatocytes. To validate these results, we also measured gross transgene expression levels with a luciferase assay (Figure 16). Again, C209 underperformed relative to C390 in the delivery of the luciferase reporter plasmid to HEK293 cells. To confirm that cells readily internalize both C209 and C390 polyplexes, we delivered both types to mature monolayers of Caco-

2 cells to mimic delivery to the intestinal epithelium. The samples were treated with equal doses of polyplexes loaded with colloidal gold-functionalized plasmid DNA, and fixed following a four-hour transfection period. When visualized with transmission electron microscopy, nanocomplexes of both types were observed at similar concentrations within the intracellular compartment (Figure 17). With transfection efficiencies only slightly higher than background levels despite similarly high levels of cellular uptake, it was clear that simple carrier substitution among the available high molecular weight chitosans would be insufficient to increase transfection efficiencies to acceptable levels. Next, we elected instead to systematically modulate the binding stability of C390 polyplexes using the ternary anionic component PGA.

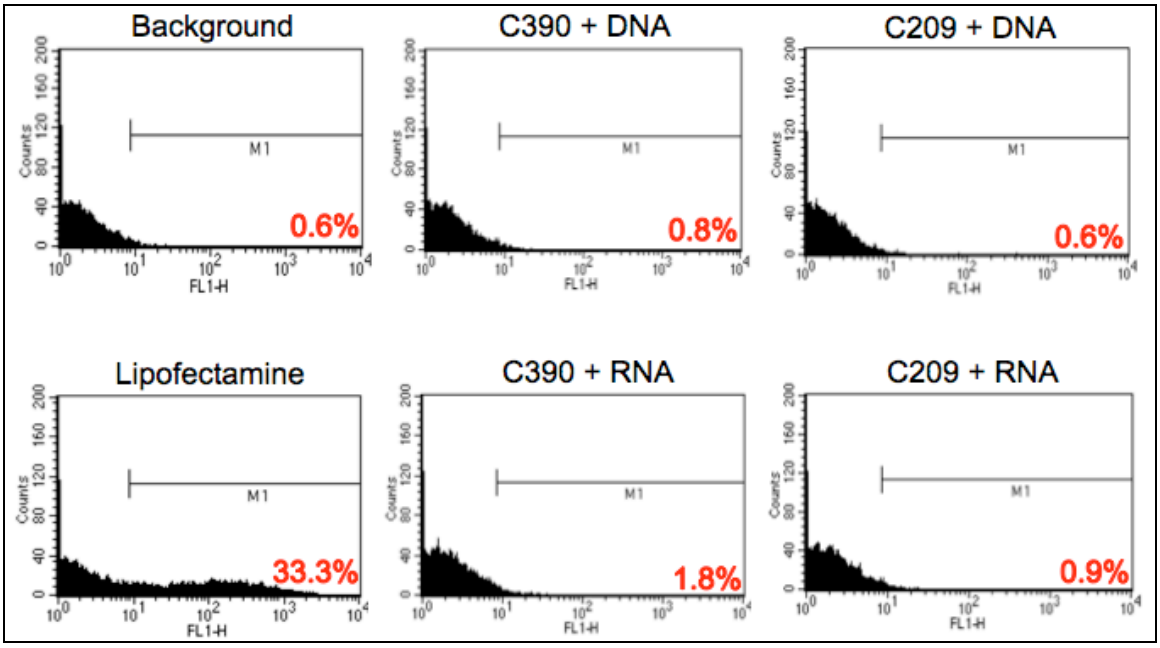

Figure 14. Flow Cytometric Quantification of GFP⁺ HepG2 Cells Following Transfection with Chitosan Polyplexes

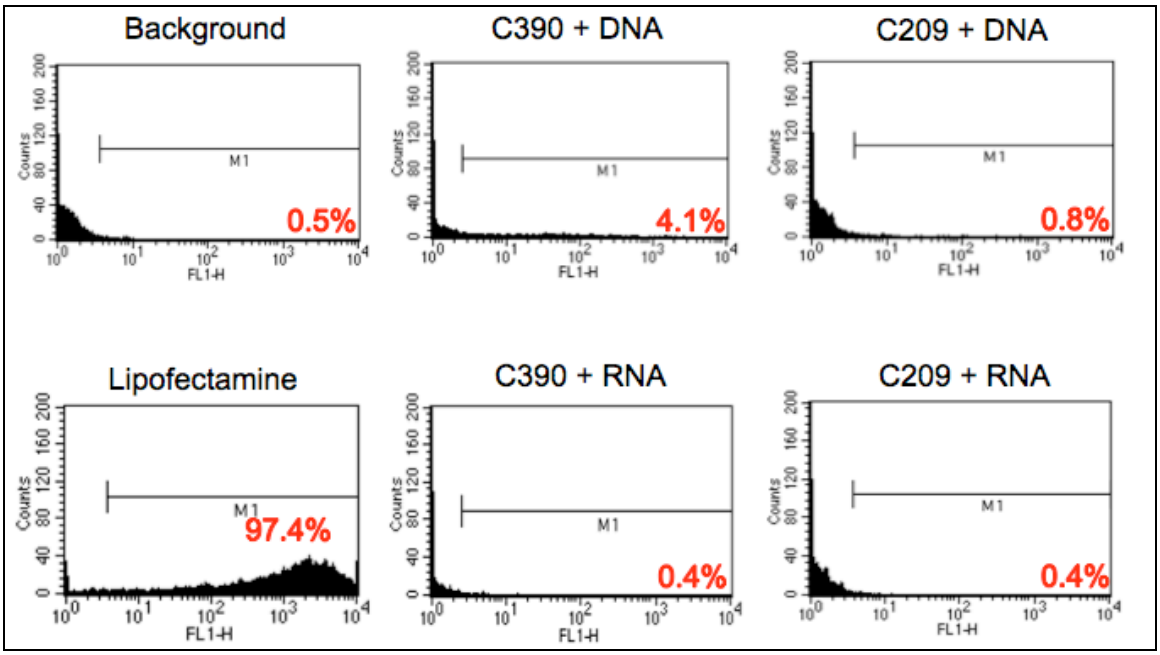

Figure 15. Flow Cytometric Quantification of GFP⁺ HEK293 Cells Following Transfection with Chitosan Polyplexes

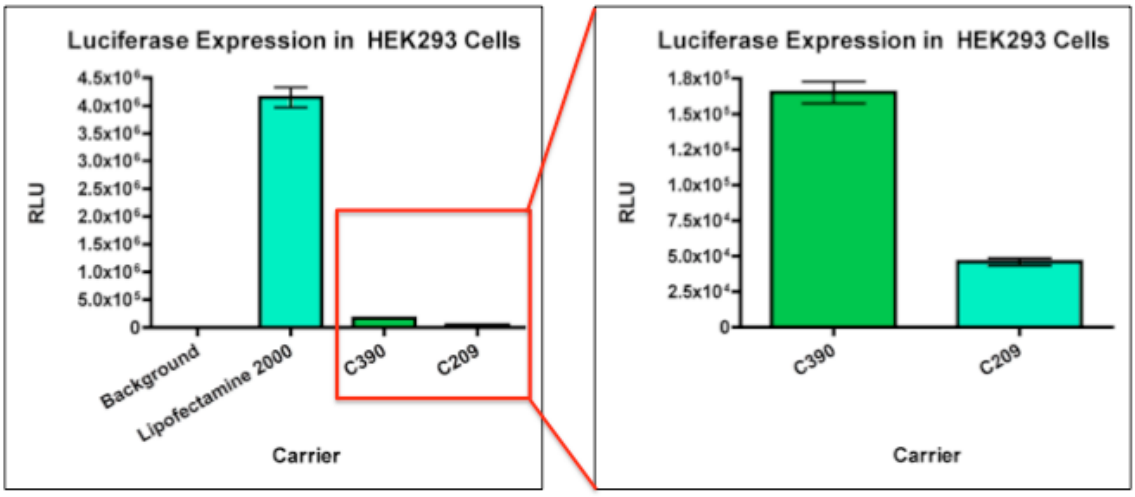

Figure 16. Quantification of Luciferase Transgene Expression in HEK293 Cells

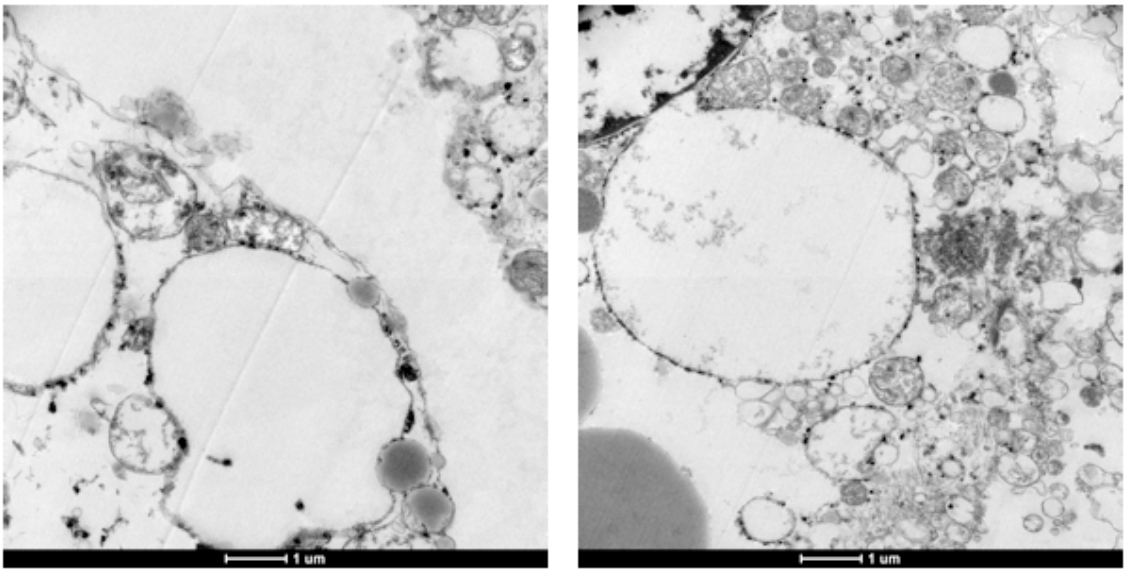

Figure 17. Transmission Electron Microscopy of Chitosan Polyplex Uptake
TEM images show cellular internalization of C209 (left) and C390 (right) polyplexes loaded with pDNA functionalized with colloidal gold for detection.

3.3.4 Systematic Modulation of Binding with PGA

PGA is a polyanionic, non-toxic peptide that has been used in oral drug delivery applications (Figure 18). It was chosen because it has been shown to compete with DNA for binding of chitosan, resulting in weakened chitosan-DNA interactions. The carboxylic (C) moieties on PGA compete with the phosphate (P) groups on nucleic acids for the amines (N) of chitosan. We added increasing amounts of PGA into the synthesis of C390 polyplexes to screen for increased transfection capabilities. The N/P/C ratio was varied from 3.2/1/0 to 3.2/1/4.2. Above the ratio 3.2/1/1.6, visible precipitation appeared in the tube during synthesis. This presumed flocculation caused by the slight excess of polyanion and more neutral polyplex zeta potentials ceased above ratio 3.2/1/4.2, at

which point the polyplexes possessed negative zeta potentials. C390-PGA polyplexes were loaded with pLuc and delivered to HEK293 cells. Luminescence detection at 48 hours after transfection was performed to quantify luciferase gene expression (Figure 19). Transfection was essentially absent at N/P/C conditions resulting in flocculation and precipitation. No amount of PGA addition resulted in an appreciable increase in luciferase transgene expression levels in HEK293 cells. Contrary to the success seen by others with the inclusion of PGA with low molecular weight chitosan to generate more efficient ternary polyplexes, the addition of PGA to high molecular weight chitosan polyplexes yields deleterious effects on their transfection capabilities. We concluded from these results that destabilization of C390-DNA polyplexes with PGA is insufficient to improve transfection efficiency beyond levels that are achievable with binary C390 formulations.

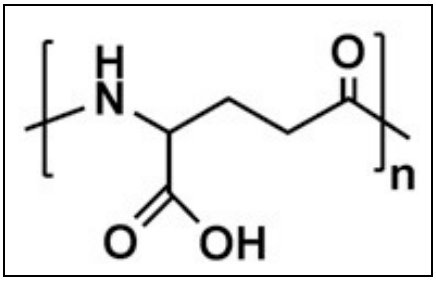

Figure 18. Chemical Structure of Poly(γ-Glutamic Acid)

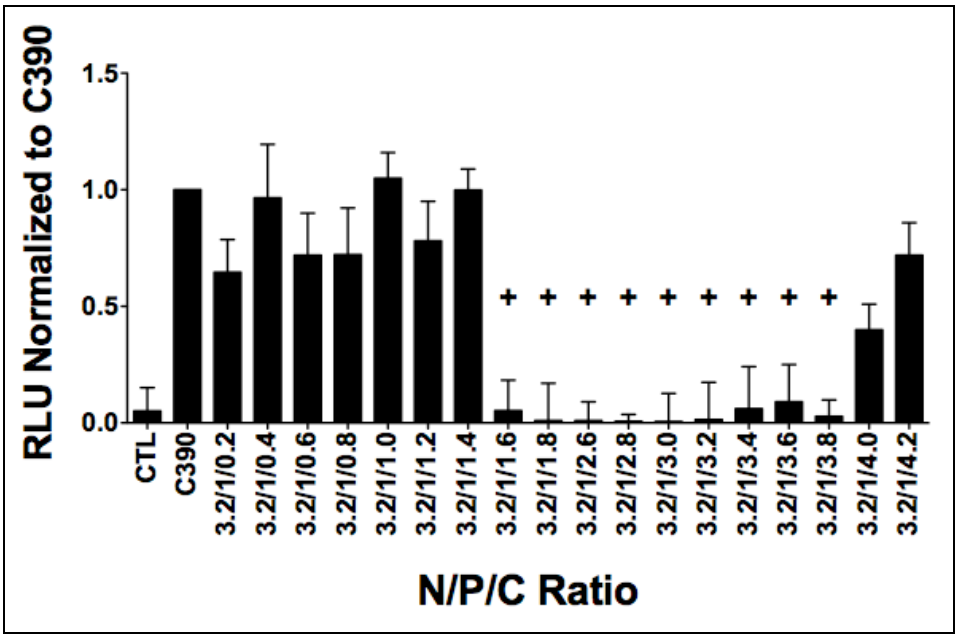

Figure 19. Quantification of Luciferase Transfections by C390 Polyplexes with Systematic Addition of PGA
Above the ratio 3.2/1/1.6, visible precipitation appeared in the tube during synthesis. This presumed flocculation caused by the slight excess of polyanion and more neutral polyplex zeta potentials ceased above ratio 3.2/1/4.2, at which point the polyplexes possessed negative zeta potentials. No amount of PGA addition resulted in an appreciable increase in luciferase transgene expression levels in HEK293 cells.

3.3.5 Selection and Characterization of SS-PAA Polyplexes

When adjustment of polymer properties and systematic addition of ternary destabilizing components proved inadequate to improve chitosan-mediated gene transfer by increasing the efficiency of nucleic acid release, we opted to test a new class of carriers with an incorporated bioresponsive release mechanism built in. We tested the linear bioreducible poly(amido amine)s (SS-PAAs) poly(CBA-ABOL) and poly(CBA-HIS70/DMPA30) (Figure 20). The side chain derived from 1-amino-4-butanol (ABOL) is slightly hydrophobic and increases interactions with cell and endocytic membranes.

Histamine (HIS) provides increased buffer capacity at low pH by virtue of its low basicity amino groups (pKa ~ 6.5) that are unprotonated at physiological pH, while dimethyl aminopropylamine (DMPA) adds high basicity amino groups (pKa ~ 8.0) that are protonated at physiological pH to provide positive charges to assist in nucleic acid binding.

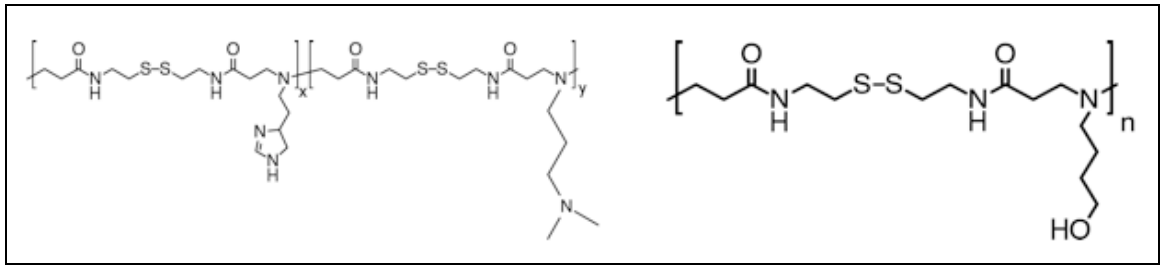

Figure 20. Chemical Structures of Poly(CBA-HIS/DMPA) and Poly(CBA-ABOL)

SS-PAAs showed good transfection capabilities and favorable toxicity profiles in preliminary screening, and are likely unhindered by inefficient release due to their engineered degradation mechanism. A salient feature of SS-PAAs is the disulfide bond present in their backbone, lending stability to the particles in the extracellular environment where glutathione concentrations are 2-20 μM, but facilitating rapid degradation and release in the reducing environment of the cytoplasm where glutathione species are present at 0.5-10 mM. Poly(CBA-ABOL) was synthesized by Michael addition of N,N-cystamine bisacrylamide with 4-amino-1-butanol, purified, and characterized by ^{1}H NMR and Matrix Assisted Laser Desorption/Ionization (MALDI)

mass spectrometry (Figure 21). The polymer to DNA mass ratio selected for use was determined by a systematic gel retardation study to determine the ratio necessary to fully condense DNA (Figure 22). In the same experiment, reductive release was verified by adding 2.5 mM dithiothreitol (DTT) to the particles. The mass ratios 48:1 and 60:1 were chosen for p(CBA-ABOL) DNA and RNA particles, respectively. The ratios 24:1 and 36:1 were chosen for p(CBA-HIS70/DMPA30). The presence of DMPA side chains increases the polymer charge density, thereby reducing the polymer mass required to achieve the same degree of complexation of SS-PAAs bearing neutral moieties.

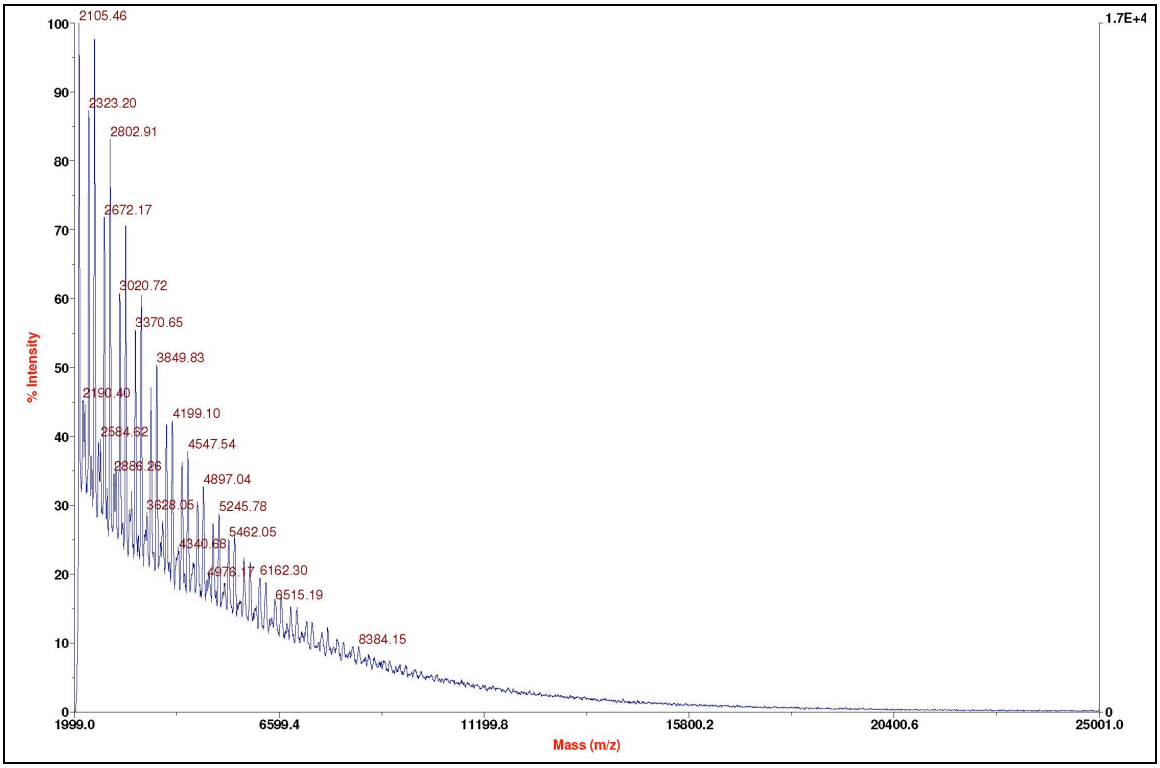

Figure 21. Matrix Assisted Laser Desorption/Ionization (MALDI) Mass Spectrometry of Poly(CBA-ABOL)
Peaks are separated by ~349.5 Daltons, the repeating mass unit of the polymer chain.

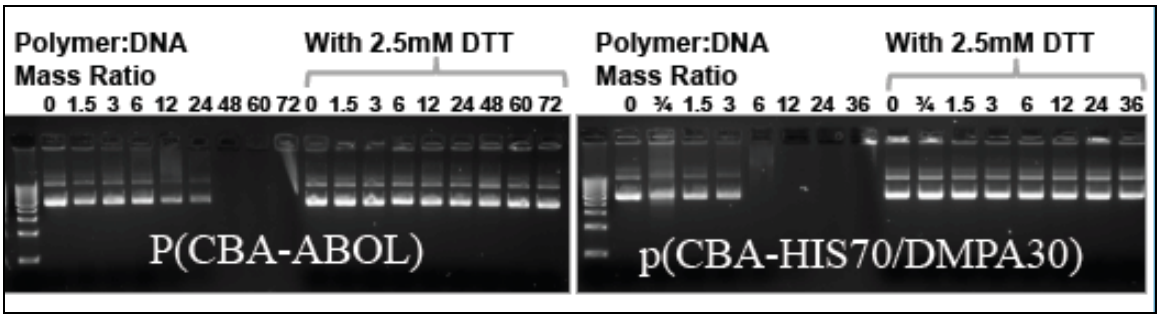

Figure 22. Gel Retardation and Reductive Release Assays for SS-PAA Polyplexes

3.3.6 Cytotoxicity and Transfection Efficiency of SS-PAA Polyplexes

In order to confirm the favorable cytotoxicity profile of the SS-PAA carriers, we conducted a dose escalation study to determine the IC_{50} of each polymer (Figure 23). Using the WST-1 colorimetric metabolic assay, we compared the concentrations at which fifty percent of cells were inhibited (IC_{50}) for each SS-PAA as well as 25 kDa PEI. We chose the Caco-2 and HepG2 cell types for their importance in the oral route of administration. In each case, the SS-PAAs were significantly less toxic than PEI, with IC_{50} values at least an order of magnitude higher. In comparison, reported IC_{50} values for Lipofectamine are approximately 6-10 μg/mL. We next assessed the transfection capabilities of the SS-PAA carriers in the same cell types. We delivered doses of GFP pDNA to cells in 24-well plates, then quantified transgene expression after 24 hours with fluorescence microscopy and flow cytometry (Figure 24). Poly(CBA-ABOL) gave 25 to 85 percent higher transfection levels than PEI with significantly less obvious cytotoxicity. To assess its potential for oral gene delivery, we applied p(CBA-ABOL) and chitosan

particles to the transwell cell culture system to simulate the transepithelial transport required by the oral route of administration. Administration of the particles did not damage the integrity of the epithelial monolayer, as indicated by the maintenance of pre-transfection TEER values following dosing (Figure 25). GFP expression was evident by fluorescence microscopy in both cell layers with p(CBA-ABOL) particles, however the increase in transfection in the basal HepG2 layer, relative to transfection with C390 polyplexes, determined by quantitative real-time RT-PCR was modest.

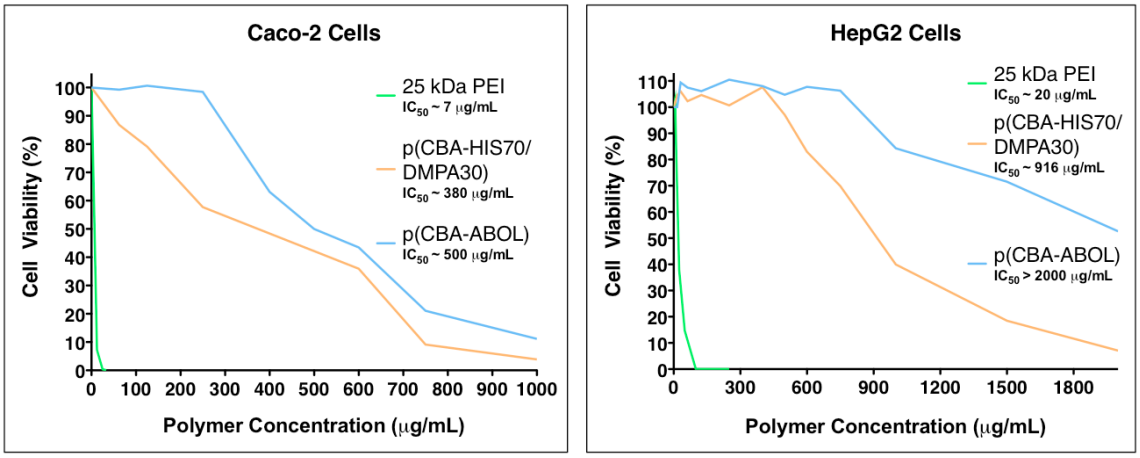

Figure 23. Cytotoxicity of SS-PAAs and PEI in Caco-2 and HepG2 Cells
SS-PAAs were significantly less toxic than PEI, with IC_{50} values at least an order of magnitude higher.

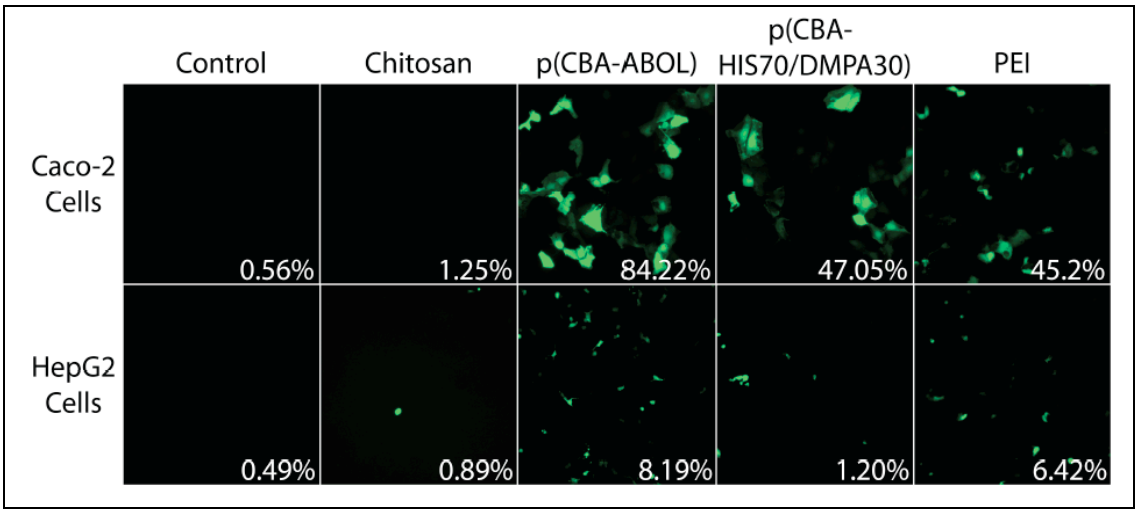

Figure 24. SS-PAA Transfection Efficiency in Caco-2 and HepG2 Cell Monolayers

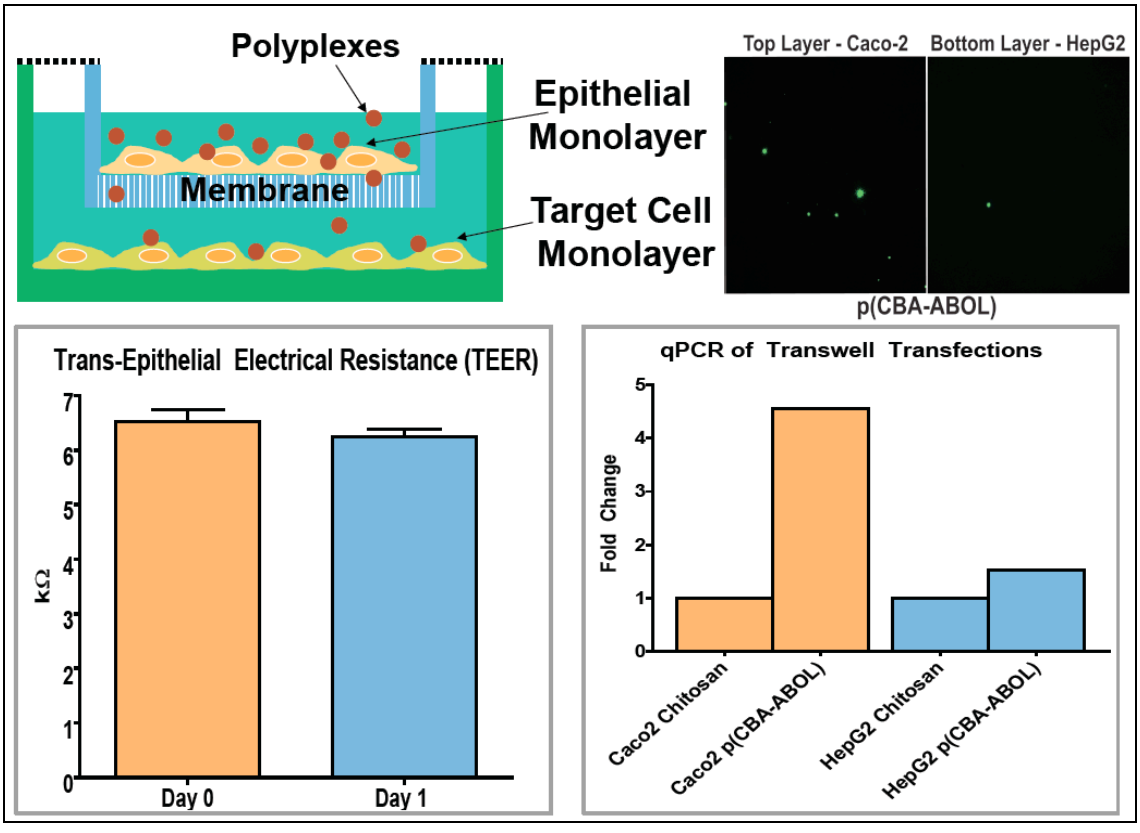

Figure 25. Transwell Transfections with p(CBA-ABOL) Polyplexes

As it did not appear that p(CBA-ABOL) polyplexes were ideally suited for the transepithelial transport and subsequent transfection of distal target cells required by oral administration, we tested them instead in an intrabiliary retrograde infusion model to determine if they could mediate gene transfer in the liver directly without having to cross a cellular barrier first. The liver is an important delivery target as it is the site of many diseases and proteins produced in the liver have easy access to circulatory system for systemic introduction. Under anesthesia, the livers of Wistar rats were isolated from the surrounding tissue, then a needle was inserted into the common bile duct and a tie was used to secure the needle. Nanoparticles and naked DNA were administered at a dose of 20 μg of minicircle luciferase plasmid in 4 mL of 5% glucose into the common bile duct over 20 min (0.2 ml/min) using a syringe pump. A tie was then placed around the bile duct between the liver and the point of infusion to prevent back flow, and the needle was withdrawn. After 30 min, all ties were removed. In these studies, a minicircle luciferase construct was utilized. Bacterial sequences integral to plasmid replication and amplification during the manufacturing process contain CpG motifs. These bacterial motifs cause gene silencing in mammalian cells [200], which can be overcome using a plasmid that only contains the elements essential to mammalian expression [201, 202]. During the plasmid amplification process, recombination is induced just prior to plasmid purification, producing a mammalian expression cassette minicircle and the bacterial amplification cassette, which is then degraded. In addition to diminished gene

silencing, the smaller plasmid also enables delivery of a higher effective transgene dose. Following dosing of the rats, luciferase expression was monitored non-invasively at 4, 24, and 72 hours post-infusion with an IVIS Imaging System. Imaging revealed that the animals given polyplexes showed significantly less transgene expression than the naked plasmid control at each time point (Figures 26 and 27). Expression was restricted to the liver and remained detectable up to the 72-hour time point.

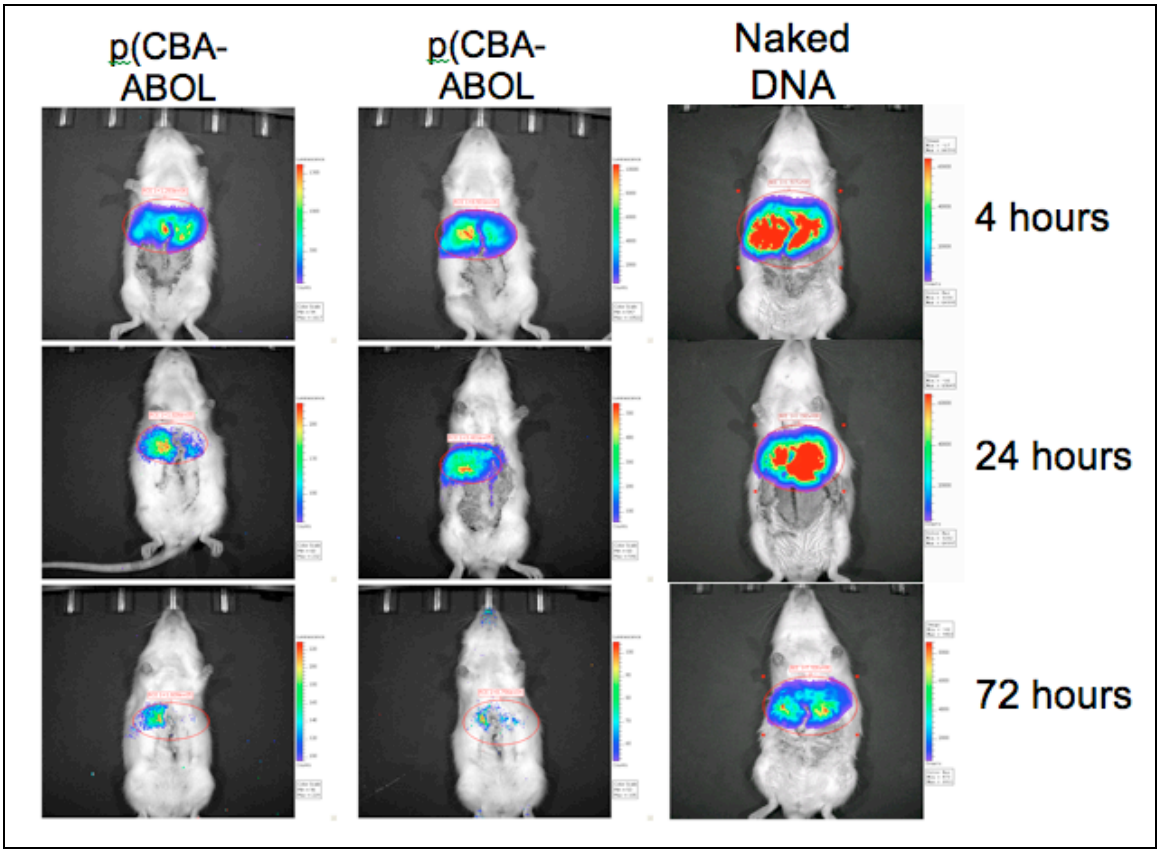

Figure 26. In Vivo Luciferase Imaging of Rats Following Retrograde Bile Duct Delivery of p(CBA-ABOL) Polyplexes or Naked Plasmid DNA
Animals given polyplexes showed significantly less transgene expression than the naked plasmid control at each time point. Expression was restricted to the liver and remained detectable up to the 72-hour time point.

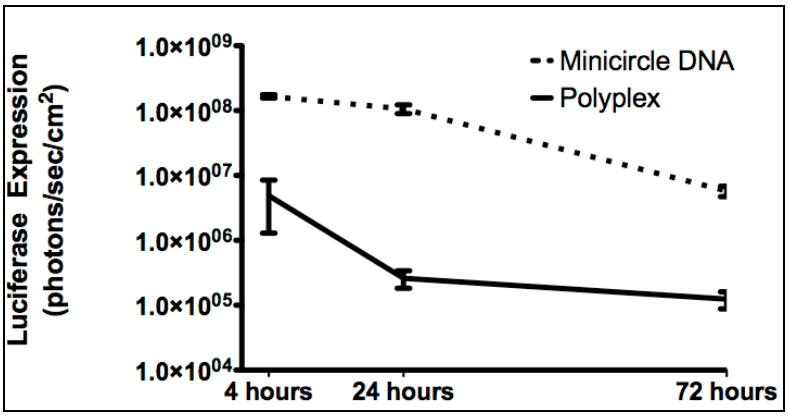

Figure 27. Quantification of In Vivo Luciferase Imaging Results

Having determined that SS-PAA polyplexes may not be best suited for in vivo gene delivery, we pivoted our efforts to exploit their potent in vitro transfection capabilities and favorable cytotoxicity toward the goal of cellular reprogramming. Many cellular reprogramming applications demand that genetic reprogramming factors be expressed at sustained high levels for periods of days to weeks. To confirm that p(CBA-ABOL) is capable of achieving this, we systematically determined the maximum tolerated dose and potential to deliver subsequent doses in adult NHDF cells in a 6-well plate format. Quantification of GFP transfection efficiency with flow cytometry showed that sustained, robust expression is achievable. The majority that became GFP^+ following a single dose remained positive at the twelve-day time point. Cells that received a second dose on day ten recovered, and in some cases exceeded, the fraction of GFP^+ cells generated by the first dose (Figure 28). This result demonstrates the feasibility of serial dosing with SS-PAAs to achieve sustained transgene expression levels.

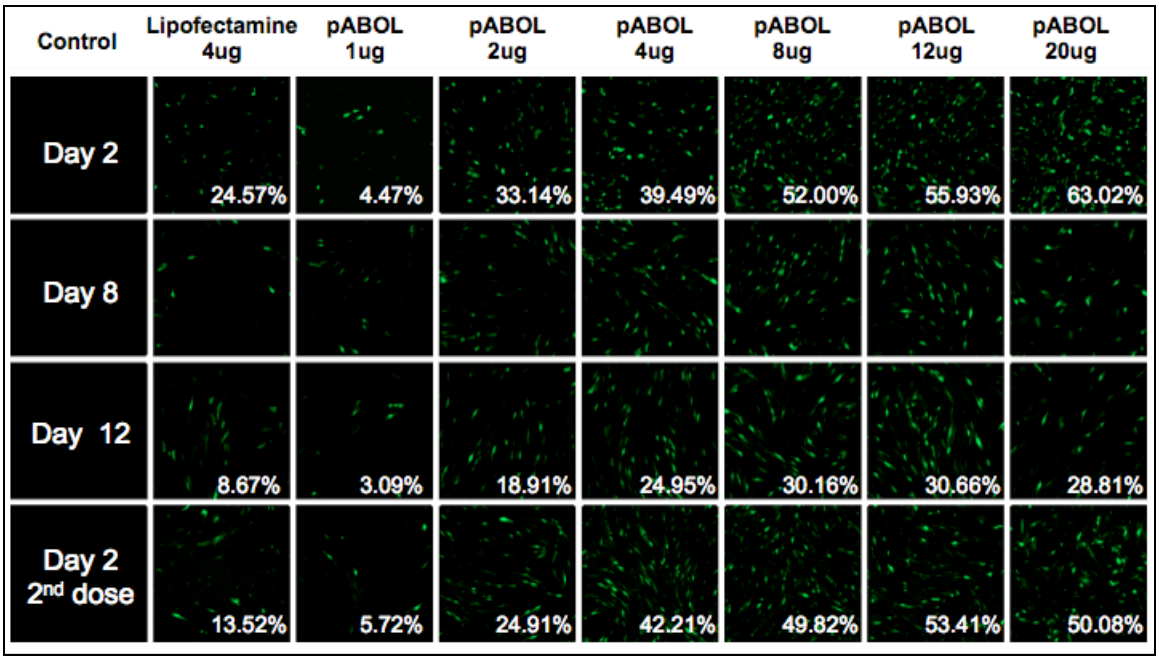

Figure 28. Serial Transfections with p(CBA-ABOL) Polyplexes
A single dose of pDNA p(CBA-ABOL) polyplexes gives prolonged transgene expression in NHDF cells, while a second dose at day ten boosts expression to levels similar to those observed following the initial dose.

3.4 Discussion

An ideal gene carrier would provide total protection of nucleic acid cargo from degradation prior to releasing it efficiently near or within the nucleus of target cells. While independent optimization of polymer properties, such as molecular weight and charge density, has proven largely inadequate in addressing this challenge, applying polymeric carriers that respond to biological cues to switch from a tight, protective complex to a relaxed interaction favoring release has shown promise. We first attempted to improve upon the modestly successful high molecular weight chitosan carrier system that has been used previously. However, efforts to solve the known issue of overly

stable binding through payload substitution, adjustment of molecular weight and charge density, and the addition of the ternary anionic component PGA all proved inadequate to significantly improve transfection levels. Despite attempts to optimize chitosan polyplex formulation, no appreciable enhancement was detected in any cell type or co-culture tested by fluorescence microscopy, luminescence quantification, flow cytometry, transmission electron microscopy, or quantitative RT-PCR.

We subsequently pivoted our efforts to an alternative carrier system - a bioreducible linear poly(amido amine) able to give sustained, robust transgene expression through serial dosing. Poly(CBA-ABOL) possesses an inherent degradative response mechanism to changes encountered in the redox environment while transitioning from the extracellular space to the cytoplasmic domain. It is designed to unpack efficiently within cells, and to break down to minimize associated sequelae. Following selection and synthesis of this promising carrier, we showed that it forms polyplexes of appropriate size and charge, dissociates readily upon challenge with intracellular concentrations of reducing agents, and transfects cells efficiently. We also demonstrated its ability to achieve modest levels of transfection in vivo, and show that its favorable cytotoxicity profiles allows for repeated dosing in order to sustain high transgene expression levels. The following two chapters describe efforts to optimize this carrier's formulation and application, to generate uniform, potent, and reproducible polyplexes that satisfy the contrary requirements of protection and efficient release.

4. Microfluidic Preparation of Polymer-Nucleic Acid Nanocomplexes Improves Nonviral Gene Transfer

Some of the material in Chapter 4 is included in:

1) Microfluidic preparation of polymer-nucleic acid nanocomplexes improves nonviral gene transfer. Grigsby CL, Ho YP, Lin C, Engbersen JFJ, Leong KW. 2013. Sci Rep. 3:3155

2) Tuning physical properties of nanocomplexes through microfluidics-assisted confinement. Ho YP, Grigsby CL, Zhao F, Leong KW. 2011. Nano Lett. 11(5):2178-82

As the designs of polymer systems used to deliver nucleic acids continue to evolve, it is becoming increasingly apparent that the basic bulk manufacturing techniques of the past will be insufficient to produce polymer-nucleic acid nanocomplexes that possess the uniformity, stability, and potency required for their successful clinical translation and widespread commercialization. Traditional bulk-prepared products are often physicochemically heterogeneous and may vary significantly from one batch to the next. Here we show that preparation of bioreducible nanocomplexes with an emulsion-based droplet microfluidic system produces significantly improved nanoparticles that are up to fifty percent smaller, more uniform, and are less prone to aggregation. The intracellular integrity of nanocomplexes prepared

with this microfluidic method is significantly prolonged, as detected using a high-throughput flow cytometric QD-FRET nanosensor system. These physical attributes conspire to consistently enhance the delivery of both plasmid DNA and messenger RNA payloads in stem cells, primary cells, and human cell lines. Innovation in processing is necessary to move the field toward the broader clinical implementation of safe and effective nonviral nucleic acid therapeutics, and preparation with droplet microfluidics nanomanufacturing represents a step forward in addressing the critical barrier of robust and reproducible nanocomplex production.

4.1 Introduction

Recent clinical trials hint at the therapeutic potential of gene therapy, but this potential remains stymied by the dearth of safe and efficient delivery systems [203-206]. While tremendous creativity and innovation in carrier design have produced very sophisticated polymeric gene delivery systems, nonviral methods remain prohibitively inefficient for most applications [207-210]. The circulatory residence time, cellular uptake, transfection efficiency, and toxicity of nanoparticles all depend to some extent on physicochemical attributes such as size, stability, shape, and charge [108, 211]. However, the physical aspects of polyplex production, and their role in determining these properties, have been largely overlooked.

The assembly of nanocomplexes by charge neutralization is a process that occurs in milliseconds [136, 143]. While preparation in bulk formats by pipetting, shaking, or

oscillatory mixing is convenient, these methods are poorly suited to reproducibly generate uniform particles given the kinetically determined nature of the formation process [5]. Irreproducibility is typical; slight perturbations of bulk mixing protocols often yield particles of varied properties. The poor quality of these polyplexes exacerbates the challenge of establishing precise structure-function relationships and precludes mechanistic understandings of the gene transfer process, as subpopulations of particles may be responsible for observed phenomena. The inability to manufacture nonviral delivery systems in a reproducible and scalable manner also hinders their clinical translation. As the field has begun to consider the physical control of nanoparticle assembly as an opportunity for innovation, several novel techniques have emerged [146, 147, 212]. Top-down nanoimprinting systems produce nanoparticles with defined shape and size that have proven valuable in deconvoluting the mechanistic effects of such characteristics. However, the rapid reaction kinetics, aqueous conditions, and temperature sensitivity of polyplex assembly favor microfluidic approaches, which have included both monophasic laminar flow systems and emulsion-based designs [136, 144, 148-150, 213]. The former suffer from flocculation at high concentrations, while the latter have been used successfully in production of both lipoplexes and polyplexes. Here, we have used an emulsion-based microfluidic system to confine the synthesis of polyplexes to picoliter sized water-in-oil droplets. This system for microfluidics assisted

confinement (MAC) enables the mixing of polyelectrolyte components to proceed more rapidly so that polyplexes are formed under equilibrium conditions.

For such a system to be broadly useful, it must perform well with different payloads and across multiple cell types. Plasmid DNA is the predominant payload in gene delivery, but messenger RNA eliminates the requirement of nuclear delivery and more easily produces transgene expression in some slowly dividing or post-mitotic cells. However, substitution of the payload may not be trivial, as there is mounting evidence that polycations interact differently with DNA than they do with RNA [151]. Double stranded DNA is a stiffer molecule with a longer persistence length than single-stranded messenger RNA, and shorter nucleic acids may diminish the effects of molecular chain entanglement. In line with our aim to establish the broad potential of MAC to control polyplex self-assembly, in this study we utilized a promising bioreducible linear poly(amido amine) gene carrier and hypothesized that DNA polyplexes prepared with MAC would be more homogeneous and more potent. Next, we tested whether the benefits of MAC preparation would also apply to complexes loaded with RNA payloads, and we probed particle potency in multiple translationally relevant and difficult-to-transfect target cell types. We evaluated the products in terms of size, polydispersity, zeta potential, binding stability, aggregation behavior, amount of unreacted polyion species, and transfection efficiency. Through the use of a QD-FRET based assay, we furthermore quantified the cellular uptake and intracellular unpacking

of MAC polyplexes in an attempt to correlate their performance with their ability to overcome these two specific rate-limiting barriers to delivery. This study helps bridge a void in the structure-function understanding of gene delivery by demonstrating how physical polyplex attributes dictated by their preparation can influence intracellular behavior and transfection efficiency. Together, the results of these studies demonstrate that nonviral gene delivery can be improved not only by chemical design and optimization, but also through innovation in processing and preparation techniques.

4.2 Methods

4.2.1 Polymer Synthesis and Labeling

Poly(CBA-ABOL) was synthesized by Michael-type polyaddition of 3.67 g N,N-cystaminebisacrylamide (CBA) (Polysciences, Warrington, PA) and 1.26 g 4-amino-1-butanol (ABOL) (Sigma-Aldrich, Saint Louis, MO) as described by Lin et al. [22]. The reaction product was purified by dialysis (3.5 kDa cutoff) in acidic deionized water (pH 4) and then lyophilized. The polymer was collected in its HCl-salt form (1.63 g, 33% yield). Due to the absence of primary amines on poly(CBA-ABOL) for conjugation of fluorescent labels, we also synthesized the copolymer poly(CBA-ABOL90/BDA10) by substituting 10% N-Boc-1,4-butanediamine (BDA) for 4-amino-1-butanol in the polymerization. Deprotection of the Boc-protected amino groups in the copolymers was performed in a mixture of methanol/trifluoroacetic acid (10 mL, 1/1, v/v) overnight prior to dialysis. The primary amines on the BDA side chains of the copolymer were then

functionalized with Cy5-NHS (Amersham Biosciences, Piscataway, NJ) fluorescent dye and purified again by dialysis. Labeled polymer was used at a 1:4 ratio with unlabeled p(CBA-ABOL) to maximize the efficiency of the QD-FRET sensor. The incorporation of fluorescent labels did not affect the size, zeta potential, or transfection efficiency of polyplexes. Polymer structures were validated by Matrix Assisted Laser Desorption Ionization (MALDI) mass spectrometry and ^{1}H NMR.

4.2.2 Nucleic Acid Production and Labeling

Plasmids pDNA (pmaxGFP, Lonza, Switzerland), pLuc (VR1255 Luciferase, Vical, San Diego, CA) and pT7-EGFP-N1 (gift from David Boczkowski, Duke University) were propagated in *Escherichia coli* DH5α (Invitrogen, Carlsbad, CA) and purified with EndoFree Plasmid Mega and Maxi kits (Qiagen, Germantown, MD). Following linearization, in vitro transcription was performed on T7-EGFP-N1 with the mMESASGE mMACHINE T7 kit (Invitrogen) to generate mRNA encoding GFP. To enable attachment of fluorescent labels, pDNA was biotinylated as described by the manufacturer (Label IT Biotin, Mirus Bio, Madison, WI) but scaled to have approximately one to two biotin labels per molecule, then purified from unreacted reagents by ethanol precipitation. Biotinylated samples were reacted with streptavidin-functionalized quantum dots (QDs, Qdot 605 ITK, Invitrogen) as described previously [58]. Nucleic acid was added in excess to QDs to ensure no unreacted QDs remained. The QDs were matched with the Cy5 used to label the polymer to comprise a quantum

dot Förster resonance energy transfer (QD-FRET) pair that was used to assess the intracellular binding status of polyplexes.

4.2.3 Fabrication and Operation of Microfluidic Devices

Cross-flow droplet generators were fabricated using conventional soft lithography [214, 215]. PDMS prepolymer was cast and cured on an SU-8 3025 (MicroChem, Newton, MA) master (Transparency mask, CAD/Art Services, Bandon, OR), which produced a channel height of approximately 35 μm. PDMS prepolymer (Sylgard 184 Silicone Elastomer Kit, Dow Corning, Midland, MI) was prepared in a 10:1 (base:curing agent) ratio and cured at 65°C for one hour. The cured PDMS was then excised, punched with through-holes to accept fluidic connections, and bonded to glass cover slips using a thin layer of spin-coated PDMS to create channels surrounded by PDMS on all sides. The fully assembled chips were then left in an oven at 95°C overnight to ensure complete bonding.

Prior to use, the microfluidic channels were flushed with the oil phase solution for 30 minutes to ensure wetting. To generate polyplexes, two syringe pumps (PHD2000, Harvard Apparatus, Holliston, MA) were used to infuse the oil/surfactant mix and aqueous reagents independently through syringe tubing adapters (Hamilton, Reno, NV). The oil phase consisted of FC-40 fluorocarbon oil (3M, St. Paul, MN) and 2% PEGylated fluorosurfactant (EA Surfactant RainDance Technologies, Lexington, MA or PicoSurf 1, Dolomite Microfluidics, Royston, UK). Flow rates were set at 7.5 μL min^{-1} for

the oil phase input and 2.5 μL min^{-1} for each of the three aqueous inputs. Water-in-oil droplets (~ 100 pL) were generated at the channel junction, where the polymer and nucleic acid solutions, separated by a buffer channel, were introduced to the continuous oil phase. Polyplexes self-assembled while confined to the droplets, while mixing of their components was enhanced by the inclusion of a serpentine channel segment [216]. MAC polyplexes were collected by breaking the droplets (Droplet Destabilizer, RainDance Technologies) and used directly from the aqueous supernatant for subsequent characterization or cellular investigation without any further purification. Bulk preparation was performed following published protocols [22]. Briefly, polyplexes were prepared by adding a complexation buffer solution (20mM HEPES, 5 wt % glucose, pH 7.4) of polymer (844 μg mL^{-1} for DNA, 1125 μg mL^{-1} for RNA) to a complexation buffer solution of nucleic acid (75 μg mL^{-1}) followed immediately by 20 seconds of vortex mixing. Reaction sizes ranged from 5 to 15 μg of nucleic acid. The presence of the reagents used for MAC droplet generation did not significantly affect the activity of bulk products. Identical reagent solutions and concentrations were introduced into the droplet generator to produce MAC polyplexes.

4.2.4 Nanocomplex Characterization

Polyplex sizes and zeta potentials were measured with a Zetasizer NanoZS-90 (Malvern Instruments, Southborough, MA). Polyplexes were assayed at a nucleic acid concentration of 15 μg mL^{-1} for size measurements. Measurements of five independent

samples were performed at 25°C using a 90° scattering angle. To assess aggregation kinetics, measurements were repeated at five-minute intervals over a four-hour period. Size is reported as the Z-average diameter, or intensity weighted mean hydrodynamic diameter. Zeta-potential measurements were performed on five independent samples at a final DNA concentration of 3 μg mL^{-1} using capillary flow cells (Malvern Instruments) in complexation buffer at pH 7.4 and at 25 ºC.

4.2.5 Cell Culture and Transfection

For all cell culture experiments, 20,000 cells cm^{-2} cells were seeded 24 hours prior to transfection in 12-well or 24-well TCPS plates (BD, Franklin Lakes, NJ) and cultured at 37°C and 5% CO_2 in the appropriate complete growth media recommended by the supplier. The cell types studied were human embryonic kidney HEK293 (ATCC, Manassas, VA), human hepatocellular carcinoma HepG2 (ATCC), primary mouse embryonic fibroblasts (PMEF) (Millipore, Manassas, VA), and human mesenchymal stem cells (hMSC) (ATCC). All transfections were carried out at 37°C and 5% CO_2 in serum- and antibiotic-free OptiMEM (Invitrogen), which was replaced with the appropriate complete growth medium 4 hours after the onset of transfection. Each transfection was performed in duplicate and quantified results represent three independent experiments. Transfection efficiency and transgene expression were assayed at 24 hours post-transfection. Luminescence measurements to quantify

luciferase expression were performed using the SteadyGlo kit (Promega, Madison, WI) according to the manufacturer's protocol.

4.2.6 Flow Cytometry

Flow cytometric analysis was performed using a FACSCanto II (BD Biosciences, Franklin Lakes, NJ) with at least 10,000 cells analyzed per sample. To quantify transfection efficiency 24 hours after transfection, cells were washed briefly with PBS without Ca^{2+} and Mg^{2+} (Mediatech, Washington, DC), and released from TCPS surfaces with 0.25% Trypsin-EDTA (Invitrogen). The trypsin was inactivated with serum-containing media and the cells were centrifuged at 4°C, resuspended in ice-cold PBS, centrifuged again, and resuspended in PBS containing 1% paraformaldehyde (PFA) (EMS, Hatfield, PA). The FSC/SSC was gated with untreated cells to exclude the dead cells or cell debris. Cells transfected with non-fluorescent pLuc plasmid served as negative controls for each equivalent pDNA or mRNA dose, with gating such that 1% of these cells were considered GFP^+.

Cellular uptake of polyplexes was evaluated in separate experiments using unlabeled poly(CBA-ABOL) polymer and QD-labeled pDNA. After predetermined post-transfection incubation periods at 37°C, cells were washed briefly with PBS without Ca^{2+} and Mg^{2+} and released from TCPS surfaces with 0.25% Trypsin-EDTA. The trypsin was inactivated with serum-containing media and the cells were centrifuged at 4°C, resuspended in ice-cold PBS, centrifuged again, and resuspended in PBS containing 4%

PFA and 2% glutaraldehyde for 15 minutes. The cells were washed with PBS, washed again with PBS containing heparin in PBS (20 units mL^{-1}) to remove membrane bound complexes, and then resuspended in PBS for analysis [217]. Timepoints represent the elapsed time from the start of transfection until the onset of trypsinization. The 405 nm laser served as the excitation source and the fluorescence emission was captured using the P10 channel (dichroric: 502LP, emission filter: 622/36 nm). To measure rates of intracellular unpacking, cells were transfected using 1:4 Cy5-labeled to unlabeled polymer complexed with QD-labeled pDNA. Samples were prepared using the same procedure described for the cellular uptake studies, however time zero was defined instead as the change from transfection medium back to growth medium for unpacking analyses. We examined the decay of the QD-FRET emission signal over time. Detection was accomplished by excitation with the 405 nm laser and 650LP emission filter. The fluorescence signals were compensated and gated with negative and single-color controls. FlowJo (v. 9.1, Tree Star, Ashland) and FACSDiva (BD) software were used to analyze the results.

4.2.7 Fluorescence Microscopy

Epifluorescent images were captured with an inverted fluorescence microscope (TE2000U, Nikon Instruments, Melville, NY) equipped with a 100-W mercury arc lamp (X-Cite 120 Fluor system, EXFO, Ontario, Canada) and a cooled CCD (CoolSnap HQ, Roper Scientific, Tucson, AZ). Monochrome emission from GFP was collected and

filtered through appropriate filters and dichroics. Image processing and analysis was performed with ImageJ (v1.43, http://rsb.info.nih.gov/ij).

4.2.8 Nanocomplex Stability and Free Polymer Measurements

Titrated volumes of PicoGreen or RiboGreen (Quant-iT, Invitrogren) reagent were added to polyplex solutions in a 96-well plate and incubated for 15 minutes before measuring the signal using a plate reader (BMG Labtech GmbH, Germany). To plot polyplex stability, the background fluorescence was subtracted and the measured fluorescence intensity was normalized to the signal in control samples containing no polymer. To quantify the amount of unreacted polymer remaining in solution following polyplex preparation, 10 μg of polyplexes were prepared using 4:1 p(CBA-ABOL) to Cy5-labeled p(CBA-ABOL90/BDA10) and centrifuged at 14,000 x g for 30 minutes to remove the particulate fraction. The supernatant was then collected, lyophilized then resuspended in 100 μL of complexation buffer. The suspensions were added to a 96-well plate and the Cy5 signal was quantified. Following subtraction of the background signal, the percentage of free polymer remaining was determined by a standard curve constructed with titrated polymer solutions.

4.2.9 Statistical Analysis

Results are reported as the mean ± S.E.M. as described for three or more independently performed experiments. Asterisks denote p-values < 0.05. Statistical

significance was determined using an unpaired t-test (Prism 5.0, GraphPad Software, La Jolla, CA). Two-tailed p-values are reported unless otherwise stated.

4.3 Results

4.3.1 Polyplex Preparation and Physical Characterization

We prepared polyplexes loaded with either plasmid DNA or messenger RNA using the bioreducible linear poly(amido amine) poly(CBA-ABOL) in bulk and MAC formats (Figure 29). We selected this gene carrier for its high efficiency, low toxicity, and ability to deliver multiple types of nucleic acids [218, 219]. Following a systematic optimization of binding characteristics, DNA and RNA polyplexes were synthesized exclusively at polymer:nucleic acid mass ratios of 45:1 and 60:1, respectively. In both cases, preparation with MAC resulted in the production of smaller and more monodispersed polyplexes. The Z-average diameters of MAC polyplexes were 40-50% smaller than those of bulk controls immediately following synthesis (Figure 30). The width of the size distribution was also significantly reduced, as evidenced by similar reductions in the polydispersity index (PDI). To quantify the propensity of the products to aggregate, we additionally measured changes in polyplex size at five-minute intervals over the course of a typical four-hour transfection period (Figure 30**)**. Bulk polyplexes began to aggregate immediately, and continued to grow in size throughout the period studied. In contrast, MAC polyplexes exhibited a much higher degree of colloidal stability and remained approximately unchanged in size throughout the measurement

period. The surface charge density of the polyplexes, represented by the zeta-potential, was also considered (Figure 30). MAC polyplexes exhibited lower zeta-potentials, suggesting more complete charge neutralization or the presence of a diminished polymer corona, either of which may contribute to improved colloidal stability by reducing charge imbalances and intraparticle heterogeneity [220]. The physical profiles of nanoparticles are important, as the putative rate-limiting barriers associated with the low efficiency of nonviral vectors include cellular binding and uptake, endosomal escape, cytosolic transport and unpacking, nuclear entry, and transcriptional processing. Physical particle properties determine the degree to which particles are able to overcome each of these barriers. Knowing that MAC preparation yields smaller, more monodispersed, and less positively charged DNA and RNA polyplexes, we next examined complex binding stability and the final disposition of the polymer component following the complexation reaction.

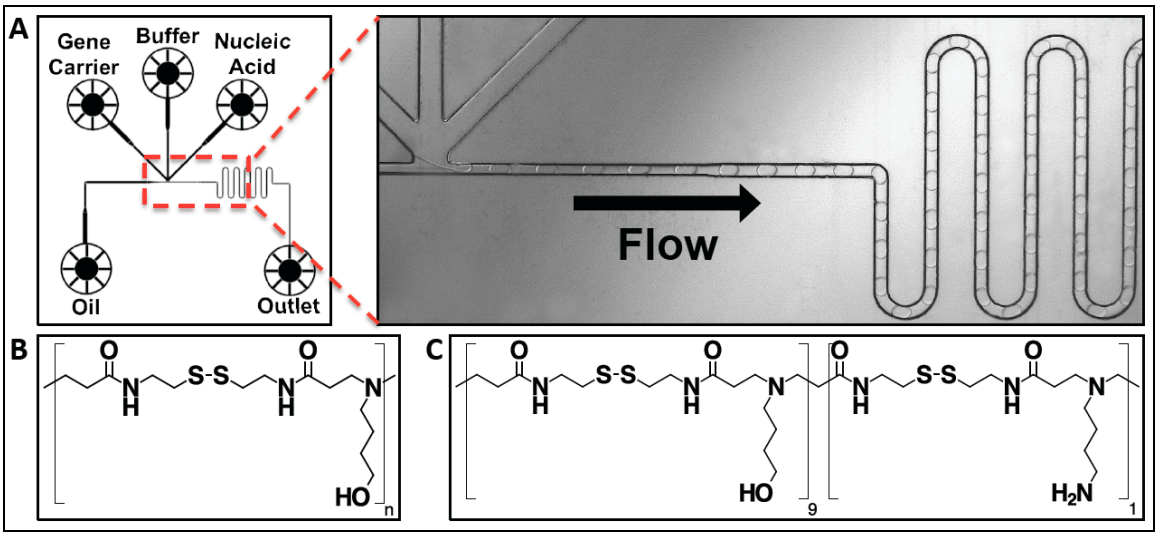

Figure 29. Design of Microfluidic Chip and Gene Carriers
A) A microfluidic cross-flow droplet generator chip is used to produce emulsified aqueous droplets containing the polymeric gene carrier and nucleic acids. While confined to these ~100 pL droplets, the polyions self-assemble into nanocomplexes. Following collection and disruption of the droplets, the polyplexes are collected and used directly. Channel dimensions are 50 μm (width) x 35 μm (height) B) Chemical structure of p(CBA-ABOL) C) Chemical structure of p(CBA-ABOL90/BDA10)

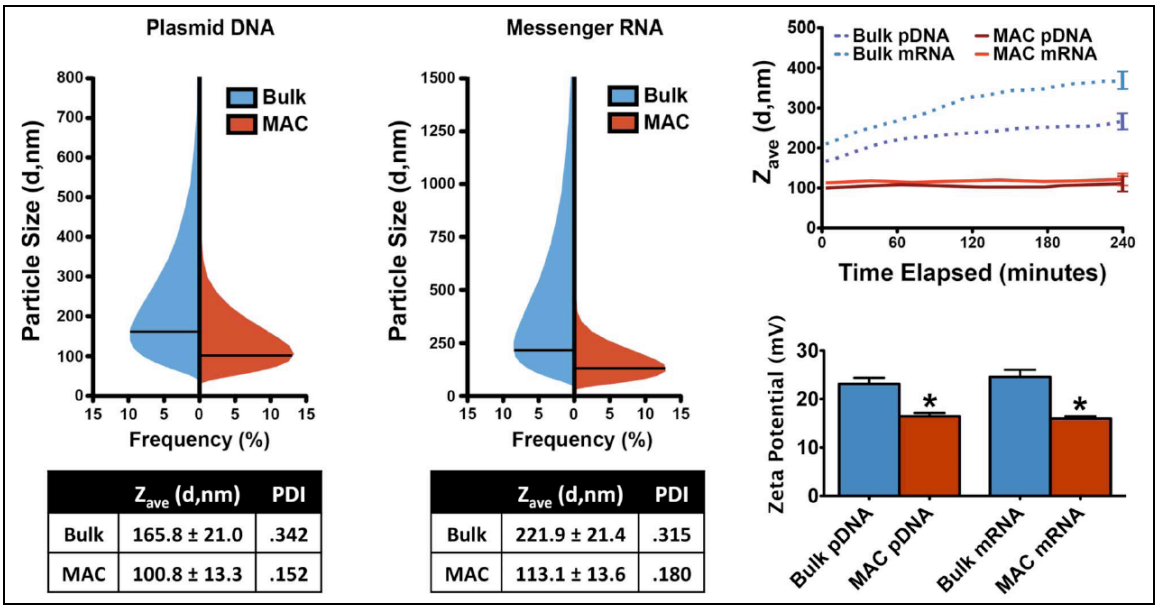

	Z_{ave} (d,nm)	PDI
Bulk	165.8 ± 21.0	.342
MAC	100.8 ± 13.3	.152

	Z_{ave} (d,nm)	PDI
Bulk	221.9 ± 21.4	.315
MAC	113.1 ± 13.6	.180

Figure 30. Size and Charge Characterization of Nanocomplexes
A) Size frequency distributions by intensity of polyplexes measured by dynamic light scattering immediately following preparation, with Z-average diameters indicated with black lines. Z-average diameter ± SEM and polydispersity indices are reported below for bulk and MAC preparations of both pDNA and mRNA polyplexes (n=5 each). B) Aggregation propensity shown as the Z-average diameter over time (n=5 each, measured at 5 minute intervals) C) Zeta potential for each type of polyplex, shown as mean ± SEM and analyzed with student's t-test (* $p < 0.05$) (n=5 each)

4.3.2 Analysis of Complexation and Binding

A common shortcoming of bulk preparation is the failure to exhaust the molecular reactants due to the rapid complexation under chaotic and heterogeneous conditions. This is problematic because excess unreacted polymer has been shown to contribute to polyplex aggregation and cytotoxicity during transfection [221]. To quantify the amount of unreacted polymer left in solution, we prepared 10 μg nucleic acid doses of polyplexes with p(CBA-ABOL) and Cy5-labeled p(CBA-ABOL90/BDA10)

in a 4:1 ratio. Following preparation, we removed the polyplexes by centrifugation. The supernatant was lyophilized, reconstituted in 100 μL complexation buffer, and transferred to a 96-well plate for quantification of the remaining excess polymer. MAC preparation significantly reduced the fraction of polymer left unreacted (Figure 31). To further probe the composition of MAC polyplexes, we then measured the binding stability between polymer and payload using a fluorescence-based binding assay. PicoGreen and RiboGreen are cationic dyes that fluoresce upon intercalation with DNA or RNA, respectively. When added in increasing concentrations to intact polyplexes, they compete with the gene carrier to bind nucleic acids. As complexes are disrupted by the competition and the shielding of the nucleic acids by the polymer is diminished, the fluorescent signal of the dye intensifies accordingly with little background signal from unbound reagent. Consequently, the increase in fluorescence indicates the level of decomplexation between nucleic acid and polymer. As seen in Figure 31, the MAC polyplexes remained comparatively more intact as increasing concentrations of competitor were introduced. At the maximum competitor concentrations, bulk controls were significantly disrupted while MAC polyplexes remained resistant. Such increased binding stability and resistance to competitive disruption may lead to better protection from premature degradation and a more sustained intracellular release of payload. However, this relationship depends on the gene carrier involved; some polymers bind nucleic acids too tightly to efficiently deliver them to the nucleus [57]. While this is less

likely to occur with bioreducible and biodegradable carriers such as the one used here, further analysis was necessary to demonstrate that increased complexation and tighter binding leads to improved activity.

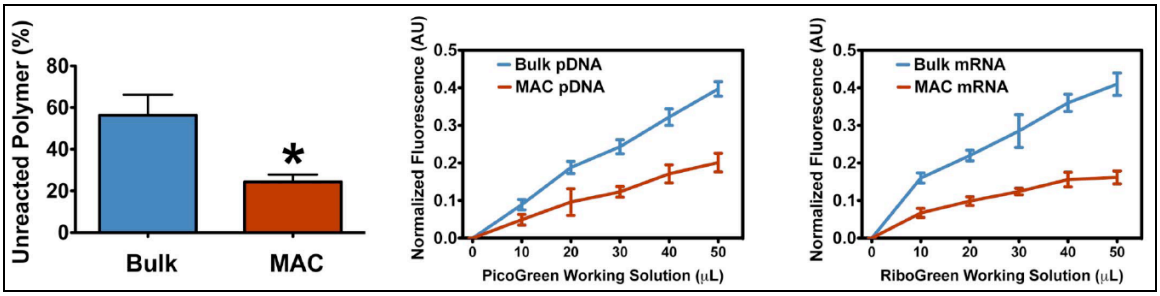

Figure 31: Unreacted Polymer and Binding Stability of Nanocomplexes
The amount of unreacted Cy5-labeled polymer remaining in the product from each method was quantified after removal of pDNA polyplexes by centrifugation. Binding stabilities of pDNA and mRNA polyplexes were measured using PicoGreen and RiboGreen competition assays, respectively. Fluorescence was corrected for background signal and normalized such that polymer-free controls = 1.0 arbitrary units (AU). Data is shown as mean ± SEM (n=3 each)

4.3.3 Cell Viability, Transfection Efficiency and Cellular Uptake

The most critical aspect of polyplex performance is transfection efficiency. We tested both DNA and RNA polyplexes in four cell types that spanned the most common target classes for gene delivery applications. Primary mouse embryonic fibroblast (PMEF) cells were selected for their prevalence in the cellular reprogramming and induced pluripotent stem cell fields. Human mesenchymal stem cells (hMSC) were included to represent primary human adult stem cells. HepG2 human hepatocellular carcinoma cells were tested due to their characteristic low transfectability and the importance of hepatocytes as a destination for gene delivery systems designed to target

the liver. Lastly, HEK293 human embryonic kidney cells were chosen to compare with the large body of prior work. At 24 hours following delivery to the four different cell types, the transfection efficiency polyplexes loaded with pDNA or mRNA encoding GFP was assessed with fluorescence microscopy and quantified by flow cytometry. In each case, transfection with MAC polyplexes resulted in a larger fraction of cells expressing the GFP reporter protein (Figure 32). The gains ranged from 6 to 31 percent more cells transfected, and were particularly significant in difficult-to-transfect cell types such as HepG2 and hMSC. Several different doses of polyplexes were delivered to HEK293 cells to verify that this result was not dose-dependent, and the improvement persisted across the range of doses (Figure 32). In some applications, the total level of transgene produced may be more important than the number of individual cells transfected. To measure gross transgene expression, doses of pDNA encoding luciferase were delivered to each of the four cell types. In each case, transfection with MAC polyplexes resulted in 1.9 to 6.8-fold higher total expression as quantified by luminescence detection (Figure 32).

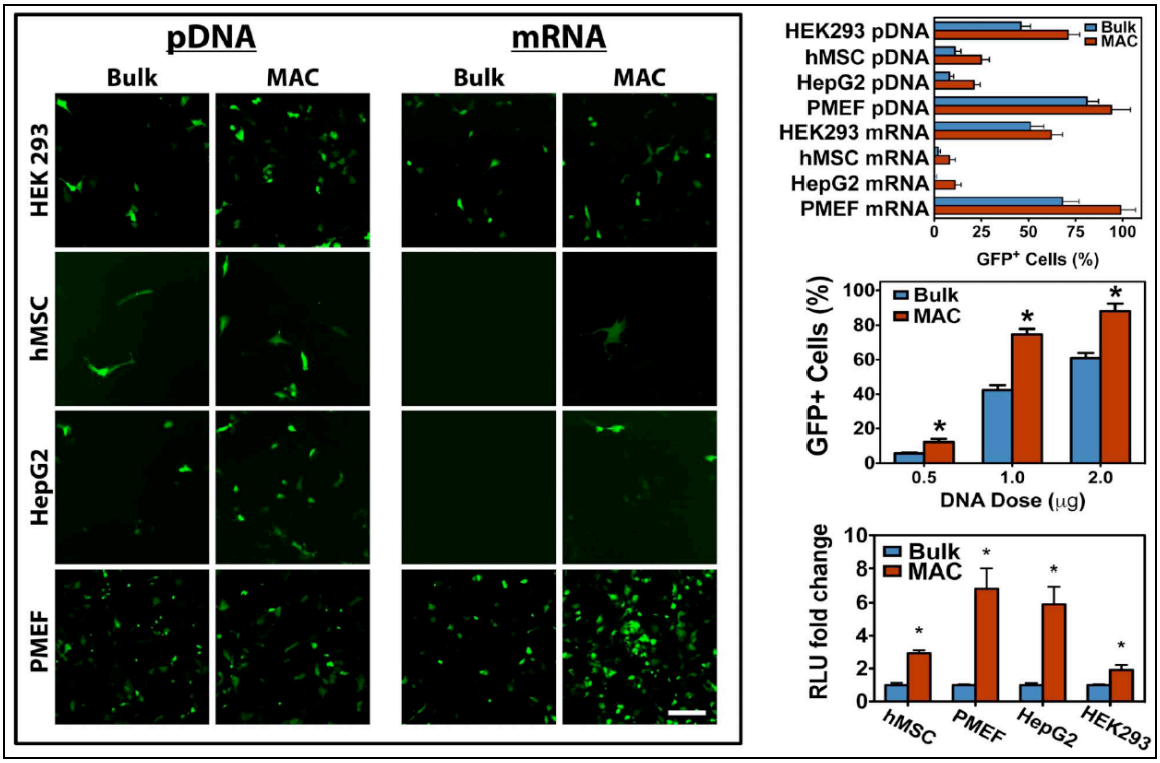

Figure 32. Transfection Efficiency in Multiple Cell Types
Fluorescence micrographs of four cell types transfected with bulk or MAC polyplexes loaded with either pDNA or mRNA encoding GFP are shown (scale bar = 50 μm), and the transfection efficiency quantified with flow cytometry ($p < 0.05$ in each case). Transfection efficiency in HEK293 cells across a range of doses confirms that the increased transfection by MAC polyplexes is not dose-dependent. Total transgene expression following transfection with pLuc DNA complexes is also improved.

To elucidate the mechanistic relationship between the physical attributes of MAC polyplexes and their improved performance, we focused on two of the primary rate-limiting barriers of nonviral gene delivery: cellular uptake and intracellular unpacking. Although the optimal dimensions of particles for cellular uptake remain a topic of debate, endocytosis is believed to be a size-dependent process [222]. It follows that the most straightforward means for MAC to improve transfection would be through an

increase in cellular uptake due to the smaller size of MAC polyplexes. We measured cellular uptake in a high-throughput manner using flow cytometric detection of internalized QD-labeled pDNA. Bulk and MAC polyplexes were delivered to HEK293 cells, which were fixed to arrest endocytosis at defined timepoints and washed with heparin to remove any remaining membrane-associated complexes. Flow cytometry was used to detect the percentage of cells containing the labeled plasmid at each point, as well as the mean fluorescence signal that correlates with the total mass of internalized plasmid. We observed no difference in uptake between bulk and MAC prepared polyplexes over the time course of a typical transfection period by either metric (Figure 33). While the size of MAC polyplexes is reduced, the difference may not be sufficient to alter the rates or modes of endocytosis. If increased uptake is not responsible for the functional benefits of MAC polyplexes, the improvements likely arise from a subsequent process.

4.3.4 Intracellular Behavior of Nanocomplexes

Next, we used QD-FRET detection to examine the intracellular decondensation rates of MAC polyplexes. FRET provides the unique ability to resolve molecular interactions beyond the diffraction limit of conventional microscopy. When FRET occurs, a donor fluorophore excites an acceptor via a nonradiative dipole–dipole interaction if they are sufficiently close (within ~10 nm). This so-called 'molecular ruler' can be used to determine distances between labeled molecules inside cells, including

gene carriers and nucleic acids [223]. Fluorescence colocalization methods do not offer the requisite sensitivity to precisely detect the onset of particle dissociation, to differentiate between molecules that are interacting or simply adjacent, or allow for high-throughput analysis. Furthermore, conventional fluorophores suffer from chemical and photodegradation, photobleaching and broad spectra. Conversely, semiconductor QDs possess broad absorption spectra, tunable narrow emission spectra, resistance to bleaching and chemical degradation, and large energy separation between excitation and emission eliminating the need for ratiometric disambiguation. In our case, excited QD donors transfer energy to Cy5 acceptors as long as polyplexes containing both constituents remain intact. When the complexes dissociate, the energy donors and acceptors become separated and the FRET-mediated Cy5 emission is lost, giving a precise digital indication of polyplex dissociation (Figure 33). It has been previously shown that QD-FRET labeling does not significantly alter the physical properties or bioactivity of polyplexes [57]. We again chose flow cytometric detection to acquire precise temporal data on the intracellular unpacking rates. It was assumed that at the first time point, most of the polyplexes would still be intact, with FRET-mediated emission signal deteriorating over time as polyplexes unpacked. The values at the first point were thus chosen to represent maximum complexation. Over 24 hours following transfection, MAC polyplexes remained intact much longer than the more quickly unpacked bulk samples (Figure 33). For example, by the six-hour time point, the QD-

FRET signal for bulk polyplexes had decayed to less than half of its maximum. Meanwhile, the MAC signal still exceeded 75 percent of its initial value. This prolonged intracellular stability may provide better payload protection prior to endosomal escape, as well as a more sustained release of the nucleic acid that may increase the chances of nucleic acids penetrating the nucleus during cell division. This flow cytometric population-level rate quantification shows that the increased extracellular stability of MAC polyplexes translates to the intracellular domain. This study therefore identifies a mechanistic relationship whereby controlling the physical assembly of nanocomplexes with MAC enables the modulation of polyplex properties to achieve improved nonviral gene transfer.

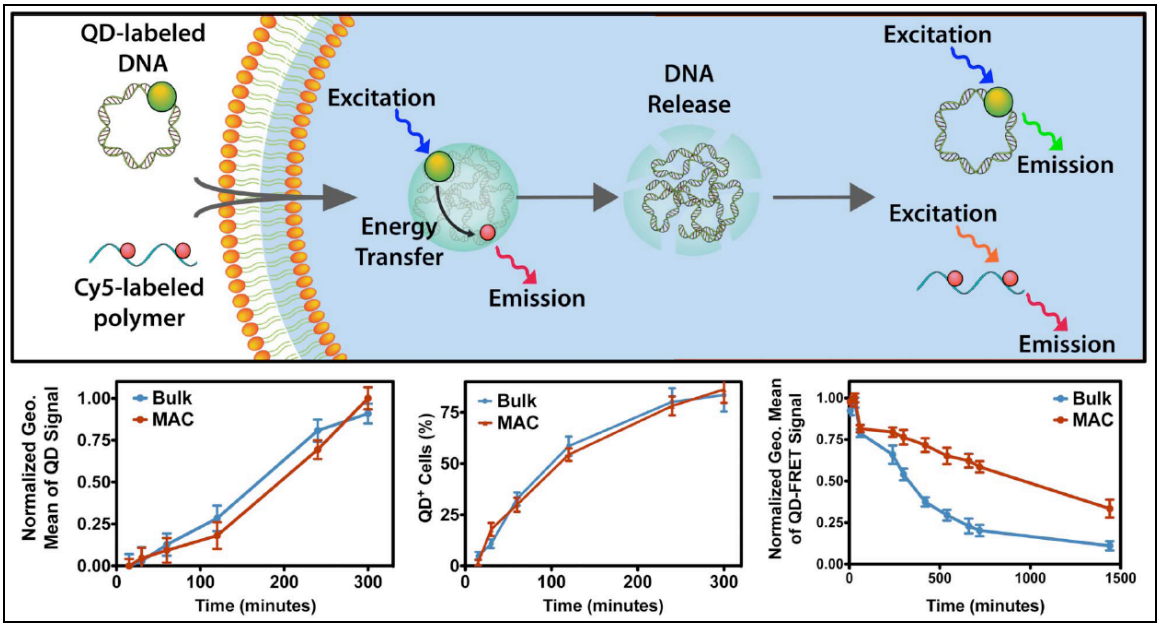

Figure 33. Cellular Internalization and Intracellular Unpacking
The labeling scheme used to detect uptake and unpacking using QD-FRET is shown. Biotinylated pDNA was labeled with QD energy donors, while the polymer was functionalized with the Cy5 QD-FRET acceptor. QD-FRET emission is detected while polyplexes are intact. Following unpacking, QD-FRET signal is lost and separate donor and acceptor emissions are recovered. Cellular internalization was quantified by measuring the fluorescence signal of QD-labeled pDNA in cells at different time points using flow cytometry. No significant difference was observed in the rates of uptake by cell number or normalized geometric mean fluorescence. Intracellular unpacking was quantified by measuring the QD-FRET signal in cells at different time points using flow cytometry. Bulk controls unpacked more rapidly than MAC polyplexes ($p < 0.05$ for all timepoints after 300 min).

4.4 Discussion

The development of safe and effective gene carriers is critical to the eventual success of nonviral gene therapy, and optimizing the assembly processes used to prepare polymer-nucleic acid nanocomplexes is one strategy to move toward this goal. We have reported the benefits of a microfluidic approach to better control the

preparation of polyplexes and to produce more uniform and more potent delivery systems. While polymer-DNA nanocomplexes have been synthesized by microfluidics, to our knowledge this is the first example of the production of polymer-RNA nanocomplexes with a droplet-based microfluidic nanomanufacturing approach, as well as the first time that QD-FRET has been used in combination with flow cytometry to quantify the intracellular unpacking of polymer-DNA nanocomplexes. We have demonstrated that MAC polyplexes exhibit significant and consistent decreases in size, zeta potential, and polydispersity relative to complexes synthesized by traditional bulk mixing. Both DNA- and RNA-loaded nanocomplexes exhibit increased colloidal and binding stability, as quantified by fluorescence-based competitive binding assays. Transfection was significantly improved in a broad range of cell types, in terms of both the number of cells transfected and gross transgene expression. We ascribed this improvement in part to a more gradual release of nucleic acids offered by MAC nanocomplexes, evidenced by the slower decline of intracellular QD-FRET emission. MAC preparation not only improves the biological performance of polyplexes, but may also help establish clearer structure-function relationships to guide future carrier design and advance nonviral gene therapy.

5. Nonviral Direct Conversion of Fibroblasts to Functional Neuronal Cells

Some of the material in Chapter 5 is included in:

Nonviral direct conversion of mouse embryonic fibroblasts to neuronal cells. Adler AF*, Grigsby CL*, Kulangara K, Wang H, Yasuda R, Leong KW. 2012. Mol Ther Nuc Acids. 1:e32

In the first example of direct cellular reprogramming, where differentiated cells are transdifferentiated into another cell type without going through an intermediate proliferative stem cell-like stage, the conversion of fibroblasts into functional induced neuronal cells (iNs) was achieved. Subsequent reports of direct conversion into clinically relevant neuronal subtypes have further validated the potential of autologous cell therapies for the treatment of neurodegenerative disorders. So far, all published neuronal reprogramming protocols rely on lentiviral gene delivery, which diminishes their utility and potentially precludes clinical translation. Instead, we delivered plasmids encoding neuronal transcription factors (Brn2, Ascl1, Myt1l) non-virally to fibroblasts with p(CBA-ABOL) polyplexes. The low toxicity and high transfection efficiency of this system enabled us to adopt a serial dosing protocol capable of sustaining high transgene expression levels throughout the reprogramming process. Consecutive 0.25 – 1.0 μg cm^{-2} doses of reprogramming factors delivered at 48-hour intervals to mouse and human

fibroblasts produced Tuj1$^+$ (neuron-specific class III beta-tubulin) cells, a subset of which expressed MAP2 (microtubule-associated protein 2), tau, and synaptophysin. A synapsin-RFP reporter helped identify more-mature, electrophysiologically active cells, with nearly all patch-clamped RFP$^+$ cells firing action potentials. Some non-virally-induced neuronal cells (NiNs) were recorded firing multiple and spontaneous action potentials. Once the feasibility of the nonviral protocol was established, we proceeded to apply p(CBA-ABOL) polyplexes prepared by microfluidic nanomanufacturing to maximize the conversion efficiency. Finally, we screened an array of substrate topographies for positive influence on nonviral neuronal reprogramming, and identified a subset of features that promote conversion more readily than unpatterned culture surfaces. This chapter demonstrates the feasibility of nonviral direct neuronal cellular reprogramming, as well as its optimization through the application of microfluidic polyplex nanomanufacturing and incorporation of substrate topography. This nonviral cellular reprogramming method, along with its specific refinements developed here, may also be amenable to other direct transdifferentiation processes.

5.1 Introduction

Neurodegenerative diseases include such recalcitrant disorders as Alzheimer's disease (AD), Parkinson's disease (PD), Huntington's disease, and amyotrophic lateral sclerosis (ALS). Despite decades of research, these conditions remain incurable and very difficult to manage [224, 225]; AD remains the sixth leading cause of death in the United

States. They are characterized by extensive cell death - loss of neurons in the neocortex and hippocampus in the case of Alzheimer's, and loss of dopaminergic (DA) neurons in the substantia nigra in the case of Parkinson's. In AD and PD, cell replacement therapy has been proposed as a more promising long-term alternative to pharmacologic intervention and deep brain electrical stimulation, which lose efficacy as the diseases progress [155]. However, identification of an appropriate therapeutic cell source has proven challenging. Although allogeneic transplantation of DA neurons from fetal ventral mesencephalic tissue into the striatum of PD patients has shown some clinical benefits [157-160], the effects are modest and results are mixed across several trials [156, 161]. Ethical concerns about the derivation of cells from fetal tissues, and low yields of DA neurons present additional challenges. Embryonic stem cells (ESCs) can be differentiated into functional neuronal cells in sufficient quantities [164], but safety and ethical issues remain. Induced pluripotent stem cells (iPSCs) [226] sidestep the ethical issues of ESCs, differentiate into DA neurons, and produce phenotypic recovery in an animal model of PD [168], but the risk of teratogenesis remains largely unmitigated.

In 2010, Wernig et al. succeeded in using three neuronal transcription factors (TFs) - Brn2, Ascl1, and Myt1l (BAM factors) - to convert mouse fibroblasts directly into functional neuronal cells [6], referred to as induced neuronal cells (iNs). Human cells were converted subsequently with the addition of NeuroD1 [227]. These iNs generate action potentials and form synapses when co-cultured with primary cortical neurons or

glia. Since the first reports, additional transcription factors that generate induced functional human dopaminergic neuronal cells (iDAs) [171, 172, 228-230], and cholinergic motor neuronal cells (iMNs) [231] have been identified. The direct conversion of fibroblasts from patients with familial Alzheimer's disease [232], hepatocytes [233], astrocytes [230], as well as from cells infected with lentiviral miRNA and transcription factor cocktails [234, 235], into functional neuronal cells has also been published. Lineage-tracing experiments confirm that iNs are not generated from, and do not transition through, an intermediate proliferative state [231, 233].

So far, neuronal transdifferentiation has only been accomplished via lentiviral gene delivery of the reprogramming factors. Virally-generated iNs are important tools for neuronal disease recapitulation, drug development, and studying the biology of transdifferentiation. However, potential genotoxic sequence integration into the host genome impedes the clinical translation of lentiviral iNs [236], and creates a demand for alternative methods to generate them. A critical finding of viral neuronal reprogramming studies is that the epigenetic program of the source cells is silenced in favor of a stable iN state [233], which persists even after exogenous gene expression is discontinued. Endogenous neuronal TFs become activated and continue to be expressed even after a relatively brief pulse of doxycycline-inducible ectopic transgene expression is terminated by dox withdrawal [171, 228]. This fact, along with the prior success of

nonviral iPSC generation [237-241], suggested that neuronal reprogramming could be accomplished with a nonviral gene delivery strategy.

The conversion efficiency is a critical parameter given the need to generate a sufficient quantity of cells for potential transplantation, as neurons are non-proliferative and cannot be expanded once induced. In order to convert the greatest number of fibroblasts to induced neurons, the reprogramming factors should be co-expressed at high levels in as many source cells as possible for long enough to induce terminal transdifferentiation. It follows that application of polyplexes that induce higher levels of transgene expression, along with greater transfection efficiency, would have the capacity to improve the conversion rate. As the microfluidic nanomanufactured p(CBA-ABOL) polyplexes described in the previous chapters possess these qualities, we tested their potential to improve nonviral neuronal transdifferentiation. Furthermore, the incorporation of micro- and nanotopographical cues into the cell culture substrate has been suggested as another means to enhance nonviral transfection efficiency, while certain substrate topographies have also been reported to induce hMSCs to express neuronal markers in the absence of neural inductive factors, as well as promote neuronal differentiation of mNPCs and hESCs [242-245]. So, we also made efforts to study the effects of substrate topography on nonviral neuronal transdifferentiation. We performed reprogramming on arrays of micro- nano- and hierarchical topographies to screen for influence on the efficiencies of both transfection and reprogramming. While substrate

topography did not exert significant influence on transfection levels with the p(CBA-ABOL) system, a subset of patterns studied did significantly increase the efficiency of neuronal reprogramming. The convergent optimization of reprogramming factor delivery and physical environmental cues in the form of substrate topography is a step toward establishing a viable platform for future cell replacement therapy for the treatment of neurodegenerative diseases.

5.2 Methods

5.2.1 Molecular Cloning and Plasmid Purification

The reporter vectors pmax-GFP (3486 bp, Amaxa, Cologne, Germany) and VR1255C (6413 bp, Vical, San Diego, CA), which respectively express GFP and luciferase under control of the CMV promoter, were used for measurement of transfection efficiency. Pmax-Brn2 (4154 bp), pmax-Ascl1 (3497 bp), and pmax-Myt1l (6359 bp), which express the mouse transcription factors Brn2, Ascl1, and Myt1l, respectively, under control of the CMV promoter, were generated by first excising the GFP coding sequence from pmax-GFP with SacI digestion, blunting by DNA polymerase I Klenow fragment, NheI-HF digestion (NEB, Ipswich, MA), and gel extraction (QIAquick Gel Extraction Kit, QIAGEN, Hilden, Germany). Then, Brn2, Ascl1, and Myt1l inserts were prepared by digestion of the lentiviral vectors Tet-O-FUW-Brn2 (Addgene 27151), Tet-O-FUW-Ascl1 (Addgene 27150), and Tet-O-FUW-Myt1l (Addgene 27152) with EcoRV and NheI-HF (NEB) and gel extraction, and were subsequently ligated into the empty pmax

vector with T4 DNA ligase (NEB). When used together, these three plasmids are abbreviated as pmax-BAM. pUNO1-mAscl1 (3892 bp, InvivoGen, San Diego, CA) and pUNO1-mMyt1lb (6744 bp, InvivoGen), expressing mouse Ascl1 and Myt1l under control of the EF1α/HTLV promoter, were used in conjunction with pmax-Brn2, and when used together are abbreviated as pUNO-AM/pmax-B. pUNO-Brn2 was generated by first replicating the Brn2 cassette from pmax-Brn2 via PCR (left primer: CAAATGACCGGTCACCATGGCGACCGC, right primer: CTCCCCCTGAACCTGAAAC). Primers were designed to introduce an AgeI restriction enzyme site at the 5′ end of the amplicon. To improve cloning efficiency, the PCR product was subcloned into a TOPO-ligase conjugated vector and expanded in E. coli following transformation, colony PCR, and gel extraction. After purification (Plasmid Mini-Prep, Qiagen), the intermediate plasmid and pUNO-Ascl1 were digested with HpaI and AgeI enzymes, then separated by agarose gel electrophoresis, extracted, and purified by ethanol precipitation. The Brn2 insert was ligated into the pUNO-Ascl1 backbone, transformed into E. coli, selected by colony PCR, expanded and purified (Plasmid Mini-Prep, Qiagen), and validated by sequencing, immunocytochemistry, and Western blot. Plasmids used for transfections were propagated in *Escherichia coli* DH5α (Invitrogen, Carlsbad, CA) and purified with EndoFree Plasmid Mega and Maxi kits (QIAGEN). Plasmid DNA concentrations were quantified by measurement of absorbance at 260 nm with a NanoDrop ND-1000 Spectrophotometer (Thermo Scientific, Waltham, MA).

5.2.2 Production and Purification of Lentiviral Synapsin Reporter

Stbl3 bacteria (Invitrogen) were transformed with pLV-hSyn-RFP [246] (Addgene 22909) according to the manufacturer's protocol. Plasmid DNA was propagated and purified using the EndoFree Maxiprep kit (QIAGEN). For the lentiviral production, HEK293T cells were seeded in 75 cm^2 dishes, cultured in DMEM (Invitrogen) containing 10% Premium Select FBS (Altanta Biologicals, Lawrenceville, GA) and 1% penicillin-streptomycin (Invitrogen), and were transfected by the calcium phosphate technique with the following plasmids: 16.9 μg of pMD2.G (Addgene plasmid 12259) 31.3 μg of psPAX2 (Addgene plasmid 12260) and 48.2 μg of pLV-hSyn-RFP. The medium was changed after 14 hours. Seventy-two hours after transfection, the medium was collected in 50 mL tubes, centrifuged, and filtered through a 0.45 μm filter to remove cell and membrane debris. The supernatant was then concentrated to 100x in Amicon Ultra centrifugal filter tubes, (Millipore, Billerica, MA) and the concentrated virus was stored at -80°C. PMEFs in 2 cm^2 wells were infected with 1 μL of 100x viral concentrate in PMEF medium 5 days before patch clamping.

5.2.3 Poly(CBA-ABOL) Synthesis and Bulk Polyplex Formation

Poly(CBA-ABOL) was synthesized by Michael polyaddition of 3.67 g N,N-cystaminebisacrylamide (CBA) (Polysciences, Warrington, PA) and 1.26 g 4-amino-1-butanol (ABOL) (Sigma-Aldrich, Saint Louis, MO) as described by Lin et al [22]. The reaction product was purified by dialysis (3.5 kDa cutoff) in acidic deionized water (pH

4) and then lyophilized. The polymer was collected in its HCl-salt form (1.63 g, 33% yield), and its structure validated by ^{1}H NMR (in D_2O) on a Varian Mercury 300 MHz NMR Spectrometer. p(CBA-ABOL)/DNA nanocomplexes (polyplexes) were synthesized at a polymer:DNA mass ratio of 45:1, which was selected based on a preliminary optimization of GFP expression in PMEFs. Polyplexes were prepared by adding a HEPES buffer solution (20 mM HEPES, 5 wt % glucose, pH 7.4) of p(CBA-ABOL) (900 μg/mL) to a HEPES buffer solution (20 mM HEPES, 5 wt % glucose, pH 7.4) of plasmid DNA (75 μg/mL), followed immediately by vortexing for 20 seconds. Reaction sizes ranged from 5 to 15 μg of plasmid DNA.

5.2.4 Fabrication and Operation of Microfluidic Devices

Cross-flow droplet generators were fabricated using conventional soft lithography [214, 215]. PDMS prepolymer was cast and cured on an SU-8 3025 (MicroChem, Newton, MA) master (Transparency mask, CAD/Art Services, Bandon, OR), which produced a channel height of approximately 35 μm. PDMS prepolymer (Sylgard 184 Silicone Elastomer Kit, Dow Corning, Midland, MI) was prepared in a 10:1 (base:curing agent) ratio and cured at 65°C for one hour. The cured PDMS was then excised, punched with through-holes to accept fluidic connections, and bonded to glass cover slips using a thin layer of spin-coated PDMS to create channels surrounded by PDMS on all sides. The fully assembled chips were then left in an oven at 95°C overnight to assure complete bonding.

Prior to use, the microfluidic channels were flushed with the oil phase solution for 30 minutes to ensure wetting. To generate polyplexes, two syringe pumps (PHD2000, Harvard Apparatus, Holliston, MA) were used to infuse the oil/surfactant mix and aqueous reagents independently through syringe tubing adapters (Hamilton, Reno, NV). The oil phase consisted of FC-40 fluorocarbon oil (3M, St. Paul, MN) and 2% PEGylated fluorosurfactant (EA Surfactant RainDance Technologies, Lexington, MA or PicoSurf 1, Dolomite Microfluidics, Royston, UK). Flow rates were set at 7.5 μL min^{-1} for the oil phase input and 2.5 μL min^{-1} for each of the three aqueous inputs. Water-in-oil droplets (~ 100 pL) were generated at the channel junction, where the polymer and nucleic acid solutions, separated by a buffer channel, were introduced to the continuous oil phase. Polyplexes self-assembled while confined to the droplets, while mixing of their components was enhanced by the inclusion of a serpentine channel segment [216]. MAC polyplexes were collected by breaking the droplets (Droplet Destabilizer, RainDance Technologies) and used directly from the aqueous supernatant for subsequent characterization or cellular investigation without any further purification.

5.2.5 Preparation of Multi-Architecture (MARC) Chip Arrays

Multi-architecture (MARC) chips were a gift from Prof. Evelyn Yim (National University of Singapore). Prior to seeding cells, chips were sterilized for one hour with 75% ethanol and ultraviolet irradiation. Chips were dried for 30 minutes in a 70°C oven, then air-plasma treated for two minutes (Harrick Expanded Plasma Cleaner). They were

then placed in a 6-well plate and coated with 100 μL of fibronectin (Sigma) in sterile water (50 μg/mL) in a 37°C incubator for one hour. Chips were next washed with PBS, and 50,000 cells seeded in a bubble on top, taking care to cover the array while preventing the cell solution from reaching the edges of the chip. After 30 minutes to allow for cell attachment, the culture well was filled with additional culture medium to cover the chip.

5.2.6 Cell Culture and Transfection

40,000 cells (80,000 cells) passage six (eight) PMEF-HLs (Millipore, Billerica, MA) or 40,000 passage two PMEFs (ATCC) were seeded per well in 24-well TCPS plates (BD, Franklin Lakes, NJ) at 37°C and 5% CO_2 in complete PMEF medium: Dulbecco's Modified Eagle's Medium with 4.5 g/L glucose (GIBCO 11960-044) (Invitrogen), 10% Premium Select FBS (Atlanta Biologicals), 25 μg mL^{-1} gentamicin (Invitrogen), and 1x GlutaMAX, non-essential amino acids, sodium pyruvate, and β-mercaptoethanol (Invitrogen). In the case of electrophysiology and some immunofluorochemistry experiments, 12 mm BD BioCoat poly-D-lysine/laminin-coated glass coverslips were placed in the bottom of TCPS wells prior to cell seeding. Twenty-four hours after seeding, PMEFs were transfected with either: reporter plasmids for flow cytometry, or pmax-BAM, pUNO-AM/pmax-B, or pUNO-BAM plasmid cocktails for induced neuronal transdifferentiation. BAM factor plasmids were delivered at an equimolar ratio in all cases. A 2:1 ratio of Lipofectamine 2000 (Invitrogen) volume (μL) to DNA mass

(μg) was used for flow cytometry experiments, in accordance with the manufacturer's protocol. All transfections were carried out in serum- and antibiotic-free OptiMEM (Invitrogen). OptiMEM was replaced with complete PMEF medium four hours after the onset of transfection. Forty-eight hours after the final transfection was completed, PMEF medium was replaced with N3 neural induction medium containing: DMEM/F-12 (Invitrogen), 25 μg mL^{-1} bovine insulin (Gemini Bio-Products, West Sacramento, CA), 50 μg mL^{-1} human apo-transferrin, 30 nM sodium selenite, 20 nM progesterone, 100 μM putrescine (Sigma-Aldrich), 10 ng mL^{-1} human bFGF2 (Stemgent, Cambridge, MA), and 25 μg mL^{-1} gentamicin (Invitrogen).

5.2.7 Viability Assay

The quantification of PMEF viability following transfection was duplexed with flow cytomety experiments. Twenty-four hours after the onset of the final transfection with pmax-GFP, cells were incubated for four hours with fresh PMEF medium containing alamarBlue (Invitrogen) in accordance with the manufacturer's protocol. Metabolic reduction of alamarBlue was monitored at 570 nm/590 nm excitation/emission using a BMG Labtech FLUOStar Optima plate reader (Ortenberg, Germany). AlamarBlue-containing medium was then removed, and the cells were prepared for flow cytometry.

5.2.8 Flow Cytometry

Twenty-four hours after completion of the final transfection with pmax-GFP, PMEFs were washed briefly with PBS without Ca^{2+} and Mg^{2+} (Mediatech, Washington, DC), and released from TCPS surfaces with 0.25% Trypsin-EDTA (Invitrogen). The trypsin was inactivated with serum-containing medium and the cells were centrifuged at 4°C, resuspended in ice-cold PBS, centrifuged again, and resuspended in PBS containing 1% PFA (EMS, Hatfield, PA). Cells were then filtered through 40 μm nylon cell strainers (BD) and analyzed with a BD FACSCanto II flow cytometer. PMEFs transfected with the non-fluorescent VR1255C plasmid served as negative controls for each equivalent pmax-GFP dose, with gating such that 1% of these cells were considered GFP^+. The recorded median fluorescent intensities of GFP^+ cells (MFI_{GFP}) were linearized according to an assumption of ideal logarithmic amplifier behavior, and normalized by the median fluorescent intensity of negative control cells (MFI_{NC}) to calculate the reported % MFI change: $100\%*(MFI_{GFP} - MFI_{NC})/MFI_{NC}$.

5.2.9 Real-time RT-PCR

Comparative C_T real-time RT-PCR was performed in 20 μL reactions using the QuantiTect SYBR Green RT-PCR Kit (QIAGEN) with 10 ng of starting mRNA isolated with RNeasy and QIAshredder kits (QIAGEN) from cells transfected with pmax-BAM factors. Messenger RNA concentrations were quantified with a NanoDrop ND-1000 Spectrophotometer (Thermo Scientific). PCR proceeded for 40 cycles in an ABI 7300

Real-Time PCR System (Carlsbad, CA). Target mRNA levels were normalized to endogenous GAPDH references, and presented as a fold-change increase relative to expression levels from untransfected PMEF mRNA collected 48 hours after seeding. Correct RT-PCR target amplicon lengths for exogenous pmax-BAM factors were verified with gel electrophoresis in a separate experiment. The primers (IDT, Coralville, Iowa) used were: Ascl1 forward (GCTGCAAACGCCGGCTCAAC); Ascl1 reverse (GCGGATGTACTCGACCGCCG); Ascl1 Endo forward (TGGCGGGTTCTCCGGTCTCGT); Ascl1 Endo reverse (TCCCCATTTGACGTCGTTGGCGA); Brn2 forward (CCATCGTACATGCCGAGCCGC); Brn2 reverse (GCGCGGTGATCCACTGGTGAG); Myt1l forward (CGGGTGTGATGGAACCGGCC); Myt1l reverse (GCCCTGTGCAGCCTGGAGTG); GAPDH forward (ACGGCCGCATCTTCTTGTGCA); GAPDH reverse (TTCTCGGCCTTGACTGTGCCG).

5.2.10 Immunofluorochemistry and Image Analysis

Transfected cells were washed briefly with PBS containing Ca^{2+} and Mg^{2+} (Mediatech), and fixed with 4% PFA (EMS) at RT for 20 minutes. Cells were then incubated for two hours at room temperature (RT) in blocking buffer containing 0.2% Triton X-100, 3% w/v BSA, 10% goat serum (Sigma-Aldrich), and combinations of the following primary antibodies with rabbit anti-Tuj1 (Covance, 1:500): mouse anti-MAP2 (Sigma-Aldrich, 1:500), mouse anti-synaptophysin (BD, 1:100), or mouse anti-Tau (BD, 1:50). The cells were then washed three times with PBS, and incubated for one hour at

RT in blocking buffer containing Alexa Fluor 488 goat anti-mouse IgG and Alexa Fluor 594 goat anti-rabbit IgG (Invitrogen), washed three times with PBS, and imaged with a Nikon Eclipse TE2000-U inverted fluorescence microscope (Tokyo, Japan) with a ProScanII motorized stage (Prior Scientific, Rockland, MA).

To quantify the relationship between Tuj1$^+$ cell generation and the number of serial BAM factor transfections, PMEFs were transfected in TCPS wells, stained for Tuj1, and scanned to produce large mosaic images of each complete culture area. These mosaics were processed with a FIJI (Fiji Is Just ImageJ, http://fiji.sc) macro to: automatically and uniformly threshold each image according to local contrast, exclude small debris, and to count the number of Tuj1$^+$ cells in each well. These counts were then divided by the number of PMEFs seeded in each well to calculate the efficiency of Tuj1$^+$ cell generation.

5.2.11 Electrophysiology

Non-virally-induced neuronal cells cultured on poly-D-lysine/laminin-coated glass coverslips (BD) were identified for patch clamp analysis by synapsin promoter-driven RFP expression [246] after 12-17 days of culture in N3 medium. One dose of p(CBA-ABOL)/BAM factors produced synapsin-RFP$^+$ cells that were too sparse to find readily with the patch clamping apparatus, and five doses kept unconverted PMEFs in serum-containing medium for an additional 4 days compared to three doses, allowing a layer of cells to develop on the back of the coverslips, which made it more difficult to

affix samples securely to our patching setup. So, we elected to patch cells that received three doses. Micropipettes had resistances between 3-7 MΩ, and were filled with internal solution containing: 130 mM $KMeSO_3$, 10 mM HEPES, 10 mM sodium phosphocreatine, 4 mM $MgCl_2$, 4 mM Na_2ATP, 0.4 mM Na_2GTP, 3 mM sodium L-ascorbic acid, with pH 7.24 and an osmolarity of 290 mM. The cells were perfused with artificial cerebral spinal fluid (ACSF) saturated with 5% O_2 and 95% CO_2 and containing: 130 mM NaCl, 2.5 mM KCl, 2 mM $NaHCO_3$, 1.25 mM NaH_2PO_4, 25 mM glucose, 2 mM $CaCl_2$, and 2 mM $MgCl_2$. Giga-ohm membrane seals were formed under voltage-clamp conditions. Action potentials were then recorded using an Axon Multiclamp 700B Microelectrode Amplifier (Molecular Devices, Sunnyvale, CA) by stepwise whole-cell current clamp injections, and analyzed with custom in-house MATLAB programs.

5.3 Results

5.3.1 Transfection and Toxicity of p(CBA-ABOL) Polyplexes

Of the four primary mouse embryonic fibroblast (PMEF) cell sources screened (PMEF-HL, PMEF-NL, and PMEF-CFL (Millipore), and PMEF (ATCC)), we found PMEF-HLs and ATCC PMEFs to be the most-efficiently transfected with p(CBA-ABOL) polyplexes and used them in all subsequent experiments. Fluorescence microscopy revealed that a 1.0 μg dose of pmax-GFP in p(CBA-ABOL) polyplexes produced high transfection efficiencies without noticeable toxicity (Figure 34). 2.0 μg doses also gave high transfection efficiencies, with some visibly rounded and dead cells, and 4.0 μg was

grossly toxic. A dose of 1.0 μg pmax-GFP delivered with p(CBA-ABOL) transfected cells more efficiently than the same dose delivered with Lipofectamine 2000. One and two doses of 1.0 μg pmax-GFP in p(CBA-ABOL) polyplexes were almost entirely nontoxic compared to untransfected controls, and a second transfection 48 hours later did not compound toxicity up to 2.0 μg (Figure 34). Lipofectamine 2000 was significantly more toxic than p(CBA-ABOL) when used to deliver the same DNA dose, and its toxicity compounded with a second serial dose.

Flow cytometric quantification of GFP expression confirmed high transfection efficiencies for 1.0 and 2.0 μg pmax-GFP doses in p(CBA-ABOL) polyplexes, significantly higher than with Lipofectamine 2000 lipoplexes (Figure 34). Further, a second dose maintained a high percentage of cells expressing GFP for an additional two days; without re-transfection, the percentage of GFP^+ cells fell relatively by 15 and 28% for 1.0 and 2.0 μg pmax-GFP in p(CBA-ABOL) polyplexes, respectively. Though 1.0 and 2.0 μg doses of pmax-GFP in p(CBA-ABOL) polyplexes elicited similar percentages of GFP^+ cells, the median fluorescence intensity (MFI) change of GFP^+ cells over non-fluorescent negative controls revealed that cells transfected with a 2.0 μg DNA dose had significantly higher GFP expression levels (Figure 34).

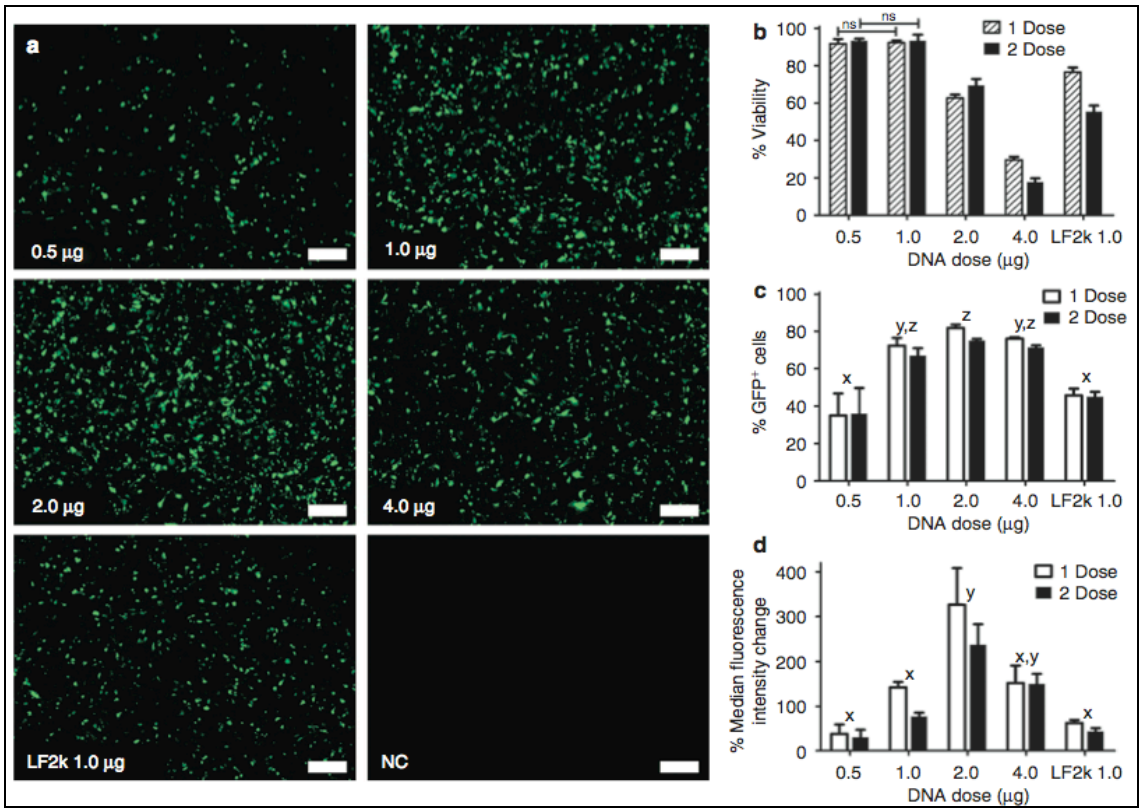

Figure 34. Optimization of p(CBA-ABOL) Transfection in PMEF Cells
(a) Fluorescence micrographs of PMEF-HLs transfected with increasing doses of DNA in p(CBA-ABOL)/pmax-GFP polyplexes (500 µm scale bars), with 1.0 µg of pmax-GFP delivered with Lipofectamine 2000 (LF2k) included for comparison. Images were taken 24 hours after transfection. (b) AlamarBlue toxicity assay multiplexed with (c) flow cytometric measurement of GFP transfection efficiency and (d) % median fluorescence intensity increase of GFP^+ cells compared to non-fluorescent control transfections for one and two doses of p(CBA-ABOL)/pmax-GFP polyplexes, assayed 24h after transfection. 1.0 µg of pmax-GFP delivered with Lipofectamine 2000 (LF2k) is again included for comparison. Error bars represent mean + SEM of three separate experiments performed in triplicate. Two-way ANOVA were performed with $P < 0.05$ considered significant. The main effect of DNA mass was significant in (b-d), and the main effect of DNA dose # was significant in (b). Letters (x,y,z) not shared between columns denote significant comparisons between DNA masses by Tukey post-hoc tests ($P < 0.05$) of one-way ANOVA across DNA masses, with data from one and two doses pooled in (c) and (d), due to absence of a main effect of dose # by two-way ANOVA. All comparisons of viability (b) across DNA mass within a given dose # were significant, other than those between 0.5 and 1.0 µg pmax-GFP in p(CBA-ABOL) polyplexes (marked ns – not significant).

5.3.2 Delivery and Expression of Reprogramming Factor Genes

An equimolar ratio of 1.0 μg pmax-BAM neuronal reprogramming factors in p(CBA-ABOL) polyplexes was delivered to PMEF-HLs according to the scheme in (Figure 35). Twenty-four hours after the initial transfection, each of the exogenous BAM factor transcripts was expressed at levels that were orders of magnitude higher than non-transfected PMEFs (Figure 35). Ectopic expression of pmax-BAM factors diminished by approximately two orders of magnitude by day 10 of culture in N3 medium as the plasmids were silenced, diluted, or degraded, for both one and three doses. Endogenous Ascl1 was activated in some cells by day 10 in N3 medium, as measured with primers targeted against an untranslated region (UTR) of the endogenous transcript not present in the exogenous transcript. Tuj1 and MAP2 transcripts were quantified but not detectably increased by transfection.

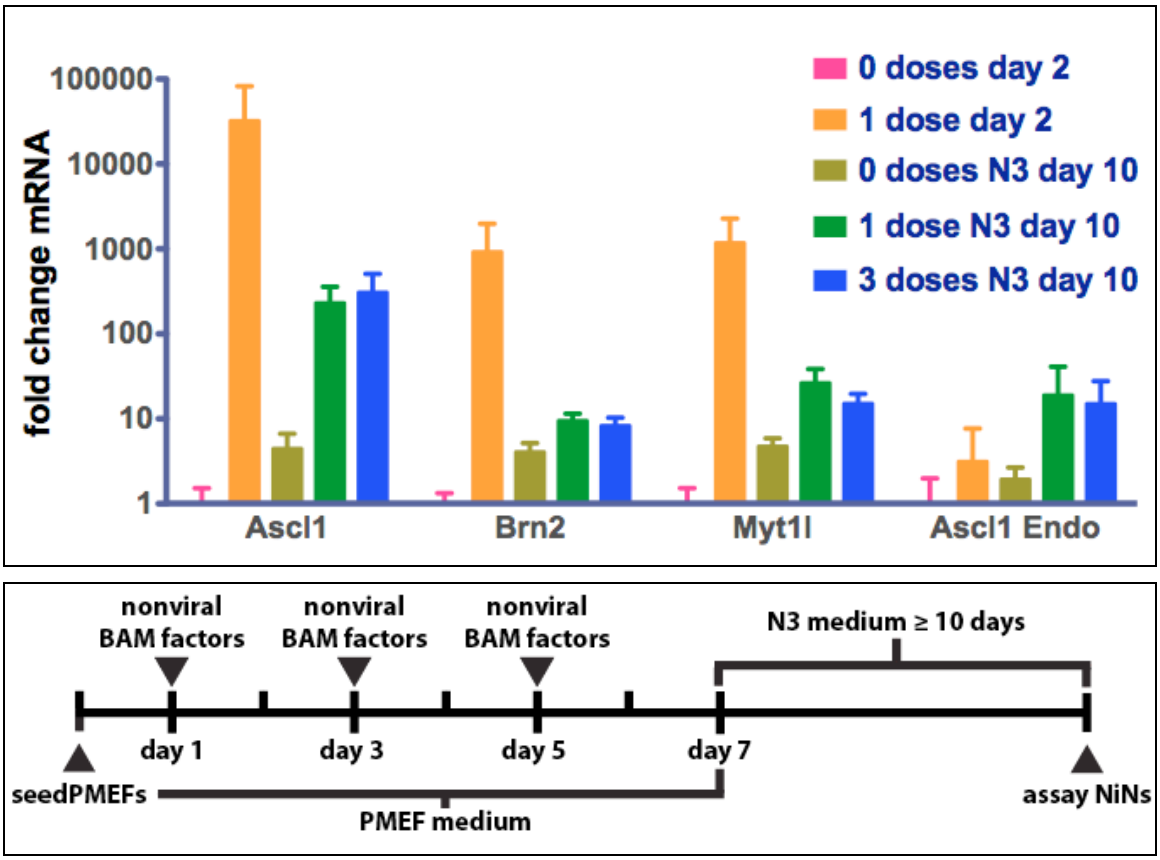

Figure 35. Reprogramming Factor Expression and Dosing Strategy
Real-time comparative C_T RT-PCR of ectopic neuronal reprogramming factors (Ascl1, Brn2, Myt1l) and endogenous Ascl1 (Ascl1 Endo) mRNA expression. PMEFs were transfected with one or three doses of 1.0 μg pmax-BAM factors complexed with p(CBA-ABOL), and total mRNA was collected 24h after transfection (day 2) or after 10 days of culture in N3. Error bars represent the range of transcript produced by the standard deviation about a mean C_T value (n = 3). NiN generation scheme: On day zero, PMEFs were seeded on TCPS wells or poly-D-lysine/laminin-coated glass coverslips in complete medium containing serum. 24 hours later, the first transfection was performed. One to four additional doses were then administered every 48 hours. Beginning 48 hours after administration of the final dose, the cells were cultured for a minimum of 10 additional days before assay in serum-free N3 neural induction medium containing FGF2, which was replaced every 48 hours, or every 24 hours beyond day 10 in N3 for longer-term experiments.

5.3.3 Serial Doses of Reprogramming Factors Generate Tuj1$^+$ Cells

One dose of 1.0 μg pmax-BAM neuronal reprogramming factors in p(CBA-ABOL) polyplexes produced rare and isolated Tuj1$^+$ cells, while three and particularly five doses generated networks of Tuj1$^+$ cells showing varying degrees of neuronal and fibroblastic morphologies (Figure 36). Neuron-like Tuj1$^+$ processes increased in length and complexity with increased culture time in N3 medium. Untransfected PMEFs were not reactive to antibodies against Tuj1. Automated microscopy and image analysis of large culture regions were used to quantify the efficiency of Tuj1$^+$ conversion relative to the number of PMEFs seeded (Figure 36). Five doses produced significantly more Tuj1$^+$ cells than one or three doses. The increase in efficiency with dose is visually evident in the mosaic images of 24-well plates. When three or five doses of pmax-BAM factors were delivered to normal human dermal fibroblasts, a small number of MAP2$^+$ cells were detectable. While efficient reprogramming of adult human cells likely requires the addition of NeuroD1 or other additional factors, this result suggests that the nonviral transdifferentiation strategy could eventually be extended to adult human cells.

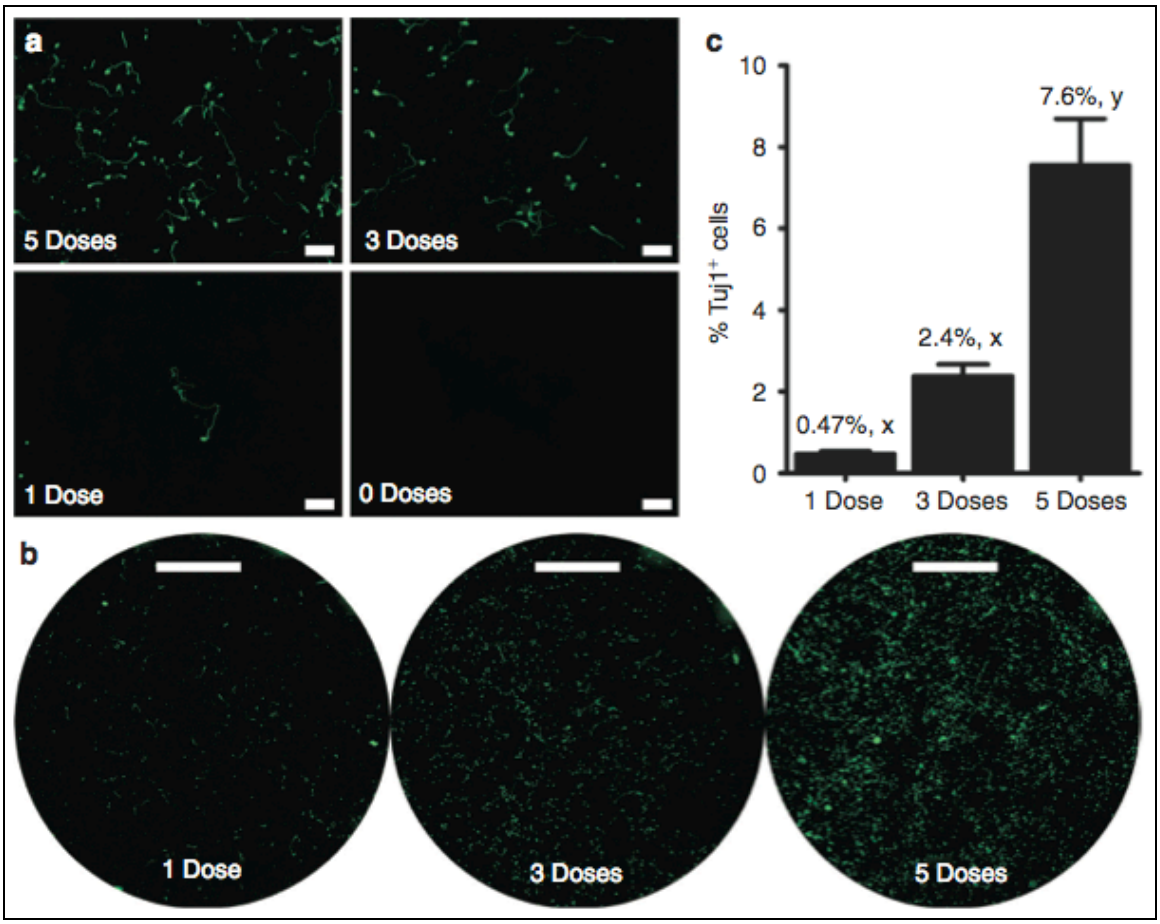

Figure 36. Reprogramming Efficiency following Multiple Serial Doses
(a) Tuj1 stain of cells transfected with one to five doses of 1.0 μg pmax-BAM factors in p(CBA-ABOL) polyplexes after a minimum of 14 days in N3 medium following transfection. (200 μm scale bars) (b) Large mosaic images of the entire culture area (2.5 mm scale bar) acquired for image analysis-based quantification of the number of $Tuj1^+$ cells normalized to the number of PMEFs seeded (c), after a minimum of 10 days in N3 following transfection. Letters (x,y) not shared between columns denote significant comparisons by Tukey post-hoc tests of a one-way ANOVA ($P < 0.05$). Error bars represent the mean + SEM of three separate experiments performed in triplicate.

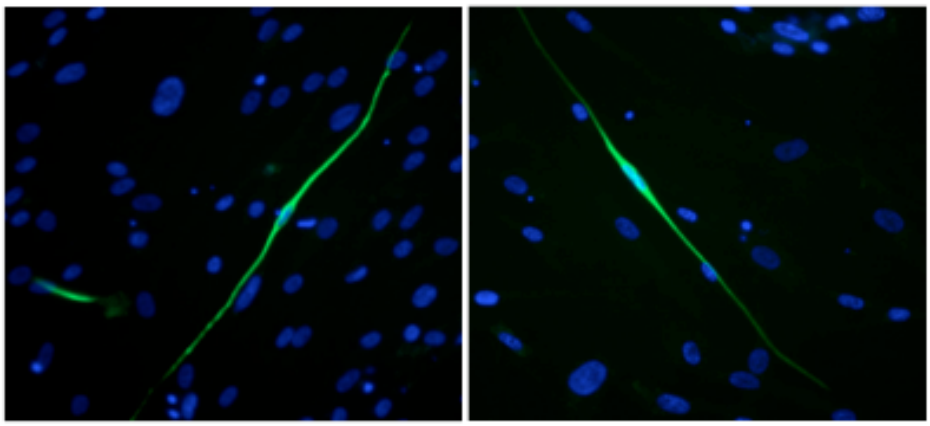

Figure 37. Generation of MAP2^{+} Human Cells
While less efficient, the reprogramming of human dermal fibroblasts to MAP2^{+} neuronal cells has been accomplished with nonviral delivery of BAM factors to normal human dermal fibroblasts

5.3.4 Induced Neuronal Cells Express Pan-Neuronal Proteins

After confirming the feasibility of nonviral neuronal transdifferentiation using the BAM factors, we added an additional set of plasmids to give the best chance of producing NiNs with active membrane properties. The CMV promoter is generally inactive in cortical neurons [247], and it is not known if or at what point this silencing could occur during neuronal transdifferentiation. We therefore added a parallel plasmid cocktail with serial transfections of 2.0 μg pUNO-AM/pmax-B factors, which utilize the EF1α/HTLV promoter for Ascl1 and Myt1l expression instead of the CMV promoter in pmax-BAM plasmids, and would potentially take advantage of increased expression levels with 2.0 μg of plasmid compared to the 1.0 μg dose.

Distal enrichment of tau (Figure 38), characteristic of neurons, was visible for a subset of Tuj1$^+$ cells (center and right panels). Tuj1$^+$ cells with fibroblastic morphologies were not tau$^+$ (red cells, left panel). Tuj1$^+$ cells with neuronal morphology were also reactive to MAP2 antibodies (second row). Synaptophysin punctae were visible in a subset of Tuj1$^+$ cells, a protein characteristic of synaptic vesicles (third row). Synapsin-RFP was also visible in long, branching processes. Synapsin-RFP$^+$ cells were less common than any of those detected by immunofluorescence. Though less prevalent, synapsin-RFP$^+$ processes were present at sufficient densities and lengths to intersect with neighboring cells (fourth row), particularly for those transfected with the pUNO-AM/pmax-B cocktail (right panel). A worst case estimate of synapsin-RFP$^+$ cells counted compared to Tuj1$^+$ cells quantified in Figure 38 provides that approximately 0.1% - 1% of Tuj1$^+$ cells are also synapsin-RFP$^+$ for three doses of 1.0 μg pmax-BAM factors.

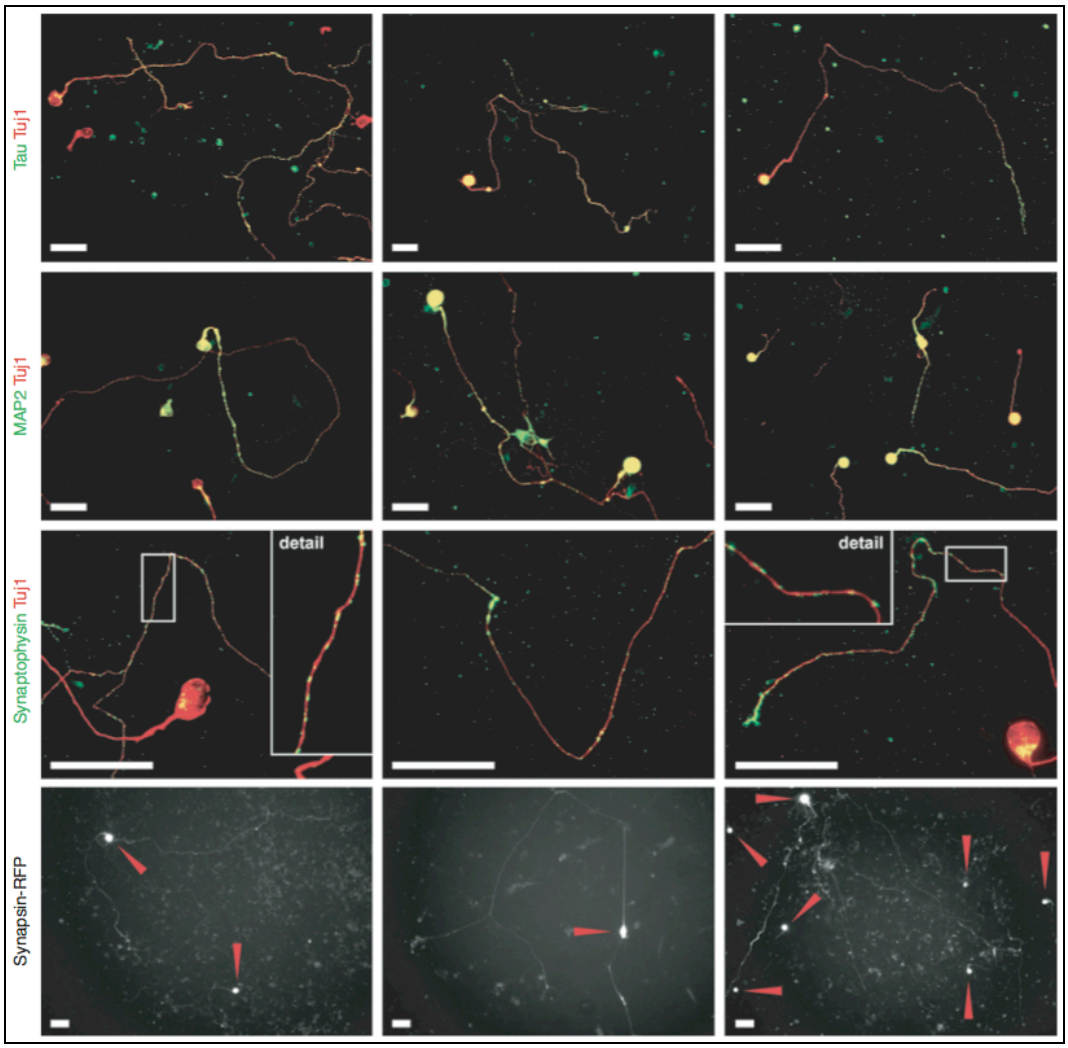

Figure 38. Immunofluorochemistry and Synapsin Reporter Activity in NiNs Generated with p(CBA-ABOL)/DNA Polyplexes

All scale bars are 50 μm. Tau stain (first row): three doses of 1.0 μg pmax-BAM factors, ≥ 10 days in N3 medium, on TCPS. MAP2 stain (second row): three doses of 1.0 μg pmax-BAM factors (left panel), or 2.0 μg pUNO-AM/pmax-B factors (center and right panels), 16 days in N3, on poly-D-lysine/laminin-coated coverslips. Synaptophysin stain (third row): five (left and center panels) or three (right panel) doses of 1.0 μg pmax-BAM factors, 17 days in N3, on PDL/laminin-coated coverslips. Expression of RFP under control of the synapsin promoter (fourth row): three doses of 1.0 μg pmax-BAM factors (left and center panels), or 2.0 μg pUNO-AM/pmax-B factors (right panel), ≥ 10 days in N3, on PDL/laminin-coated coverslips. Synapsin-RFP images have not been pseudo-colored red, in order to maximize visual contrast for thin cellular processes. Arrows indicate synapsin-RFP^{+} cell bodies.

5.3.5 Microfluidic Nanomanufacturing Improves the Efficiency of Nonviral Neuronal Cellular Reprogramming

To test the potential of microfluidic nanomanufactured polyplexes to enhance the efficiency of nonviral neuronal reprogramming, 0.5 μg doses of pUNO-BAM factor genes were delivered to passage two ATCC PMEF cells. Since we had seen that reprogramming factors driven by the EF1α/HTLV promoter tend to generate more mature NiNs in greater quantities, we used strictly pUNO constructs throughout the testing of MAC p(CBA-ABOL) polyplexes (Figure 39). This required the cloning of pUNO-Brn2 by excising the Brn2 coding region from pmax-Brn2 and substituting it in place of Ascl1 in pUNO-Ascl1. Prior to use, pUNO-Brn2 sequence and activity was validated by sequencing, immunocytochemistry, and Western blot (Figure 39).

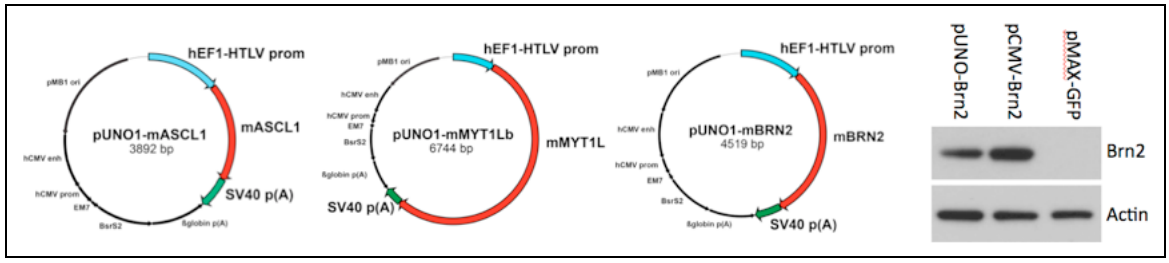

Figure 39. Schematic of pUNO-BAM Factors and Validtion of pUNO-Brn2 Activity

There was reason to believe that MAC polyplex assembly would improve nonviral neuronal transdifferentiation. In all of our experiments, we delivered the BAM factors each on a separate plasmid. Previous reports have clearly demonstrated the importance of co-expression of all three BAM factors to produce iNs with mature

electrophysiological phenotypes [6], which we expected to occur for a subset of cells transfected with our system. Figure 40 below illustrates the variability in co-expression of GFP, RFP, and luciferase reporter constructs co-delivered within p(CBA-ABOL) polyplexes to PMEF cells. While many cells express both fluorescent reporters, the levels of expression vary significantly and some cells appear positive for only one transgene. When extrapolated to the case of BAM factor expression, it is no surprise that there exists significant variability in the resultant downstream responses, namely neuronal protein expression and electrophysiological capacity, given the variability in BAM factor co-expression the cells would have encountered during conversion. It follows that even a modest increase in transfection levels achieved through the use of microfluidic nanomanufacturing could yield a nonlinear improvement in neuronal conversion. In addition to improving transfection efficiency, MAC assembly might offer benefits in terms of co-transfection of multiple constructs. MAC particles tend to have more uniform physical properties, so it stands to reason that their compositional uniformity may also be enhanced.

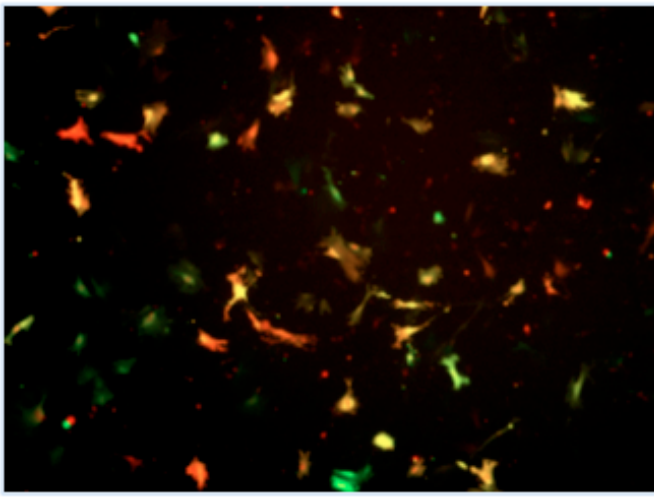

Figure 40. Co-transfection of GFP, RFP, and Luciferase Reporter Constructs Delivered by p(CBA-ABOL) Polyplexes to PMEF Cells
Delivery of fluorescent reporter constructs illustrates the expected variability in cellular co-expression of BAM factors during nonviral neuronal reprogramming.

Quantifying the efficiency of MAC particle mediated nonviral reprogramming was performed as previously described. The gross conversion efficiency measured by the percent Tuj1^{+} cells was determined as before by automated microscopy and image cytometry of entire culture wells. Single and repeated transfections of PMEFs were performed, along with bulk controls, and assayed 10 days after the final transfection. In the case of single transfections, we found that 1.2 ± 0.6 percent of cells were converted with bulk nanoparticles, while 8.1 ± 0.8 percent were converted with MAC polyplexes (Figure 41). Due to the increased susceptibility of ATCC PMEFs to cytotoxicity, the efficiency of conversion mediated by serial transfections exhibited significant variability. Conversion efficiencies as high as 21 percent were recorded, which represents in improvement upon the maximum achieved in prior nonviral reports, but the variability

precluded the establishment of statistical significance. However, the improvement in neuronal conversion efficiency derived from the use of microfluidic nanomanufactured p(CBA-ABOL) BAM factor polyplexes in place of bulk prepared particles is evident in the single dose experiments.

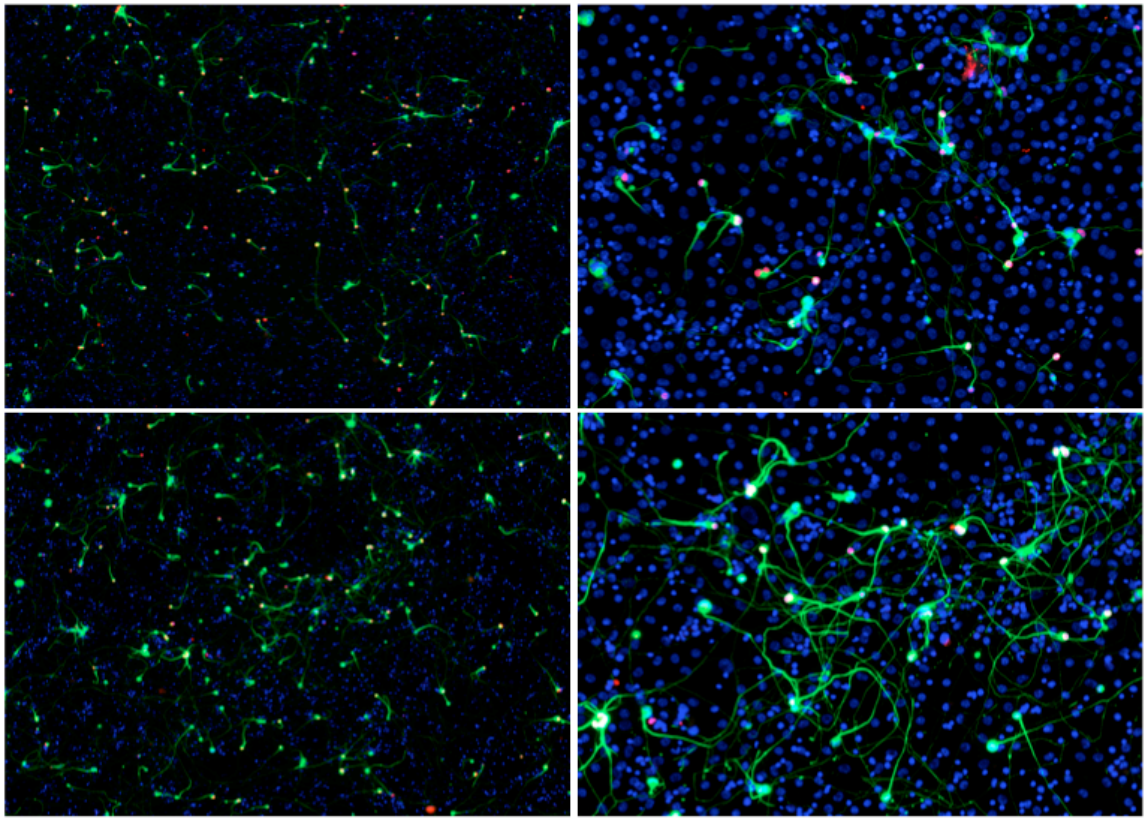

Figure 41. Enhancement of Cellular Reprogramming with Nanomanufactured Polyplexes
Using microfluidic nanomanufactured complexes to deliver the BAM factors, we are able to improve the efficiency of nonviral neuronal reprogramming, achieving a 6-fold increase with a single dose.

5.3.6 Substrate Topography Improves the Efficiency of Nonviral Neuronal Cellular Reprogramming

To assess the potential of cell-substrate interactions to influence the process of nonviral neuronal transdifferentiation, we applied the reprogramming protocol on multi-architecture (MARC) chips fabricated from PDMS containing 17 distinct topographies consisting of micro-, nano-, and hierarchical combination pattern features (Table 3).

Table 3: Multi-Architecture (MARC) Chip Topographies

ID #	Pattern Description
1	250 nm lines, 250 nm space, 250 nm depth
2	250 nm lines, 250 nm space, 150 nm depth
3	460 nm lines, 70 nm space
4	2 μm lines, 2 μm space
5	1 μm lines, 2 μm space
6	2 μm lines, 1 μm space
7	2 μm lines ⊥ 250 nm line
8	2 μm lines // 250 nm line
9	2 μm lines 250 nm pillar
10	1 μm pitch microlens concave
11	1 μm pitch microlens convex
12	1.8 μm diameter, 2 μm pitch microlens concave
13	1.8 μm diameter, 2 μm pitch microlens convex
14	2 μm pillars, 12 μm pitch
15	1 μm holes, 9 μm pitch
16	250 nm pillars
17	Control – no pattern – plain PDMS

First, we tested whether any of the patterns would result in increased transfection efficiency using p(CBA-ABOL) polyplexes. We delivered 0.25 cm^{-2} doses of pmax-GFP to PMEF cells seeded on MARC chips and quantified transfection efficiency by image cytometry after 24 hours. We found no significant difference in the fraction of cells that were GFP^+ amongst the different patterned regions. Image cytometry was used for quantification, instead of flow cytometry, because it is not straightforward to isolate cells from separate patterned regions on the MARC chip. We next delivered single 0.25 cm^{-2} doses of pUNO-BAM factors in p(CBA-ABOL) polyplexes to PMEFs on MARC chips to screen for influence on the reprogramming process. After transfection and maturation, cells were stained for Tuj1 and quantified by image cytometry. PMEFs cultured on flat PDMS were converted to $Tuj1^+$ cells at a rate of 0.8 ± 0.4 percent. The majority of patterns tested did not yield a significant effect on the reprogramming efficiency in either direction. However, we identified five patterns that did result in a significantly higher rate of conversion to $Tuj1^+$ cells (Figures 42 and 43). These patterns included 2 μm pillars with 12 μm pitch, 1 μm holes with 9 μm pitch, 2 μm lines with hierarchical perpendicular 250 nm lines, 2 μm lines with hierarchical parallel 250 nm lines, and 2 μm lines with hierarchical 250 nm pillars. Interestingly, isolation of the components of the hierarchical patterns did not yield the same effects. Microgratings (patterns 4 and 5) or nanogratings (patterns 1 and 2) alone are insufficient to improve the

conversion efficiency. However, their hierarchical combination results in a significant increase in the production of Tuj1$^+$ NiNs.

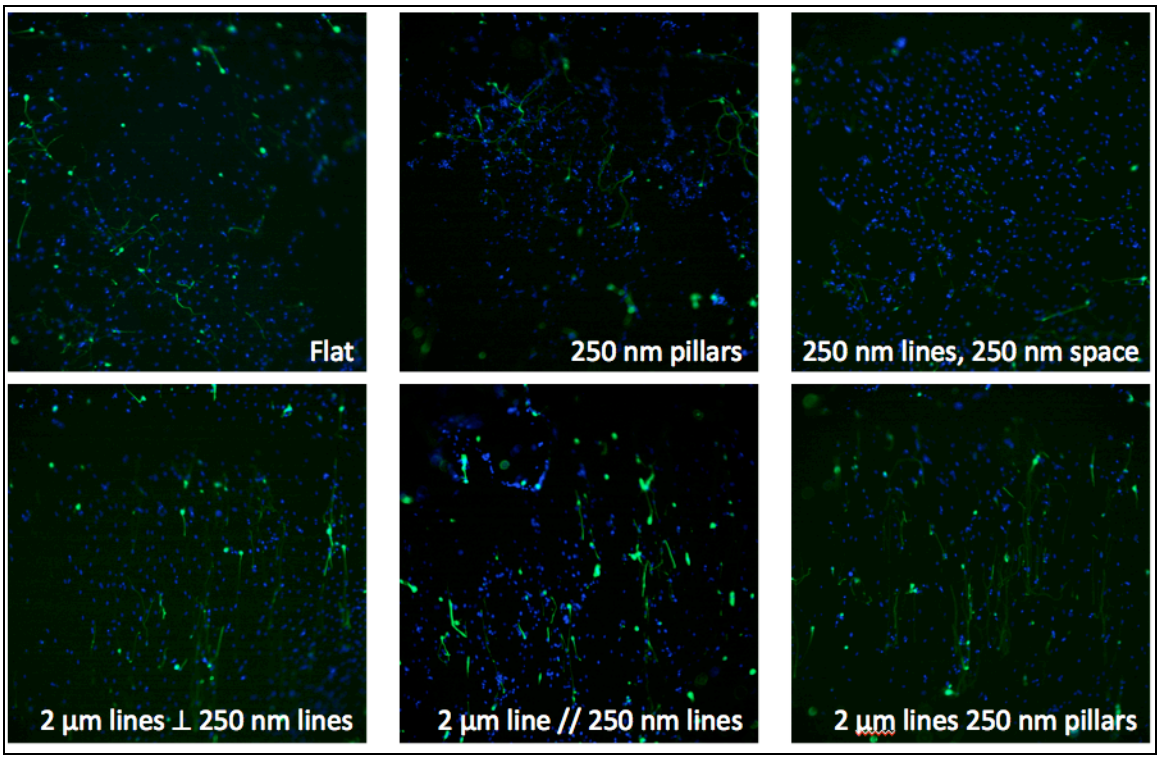

Figure 42. Tuj1 Immunostaining of PMEFs Reprogrammed on MARC Chips with pUNO-BAM Factors Delivered by p(CBA-ABOL) Polyplexes
PMEFs cultured on flat PDMS were converted to Tuj1$^+$ cells at a rate of 0.8 ± 0.4 percent. Five patterns resulted in a significantly higher rate of conversion to Tuj1$^+$ cells. These patterns included 2 µm pillars with 12 µm pitch, 1 µm holes with 9 µm pitch, 2 µm lines with hierarchical perpendicular 250 nm lines, 2 µm lines with hierarchical parallel 250 nm lines, and 2 µm lines with hierarchical 250 nm pillars. Interestingly, isolation of the components of the hierarchical patterns did not yield the same effects. Microgratings or nanogratings alone are insufficient to improve the conversion efficiency. However, their hierarchical combination results in a significant increase in the production of Tuj1$^+$ NiNs.

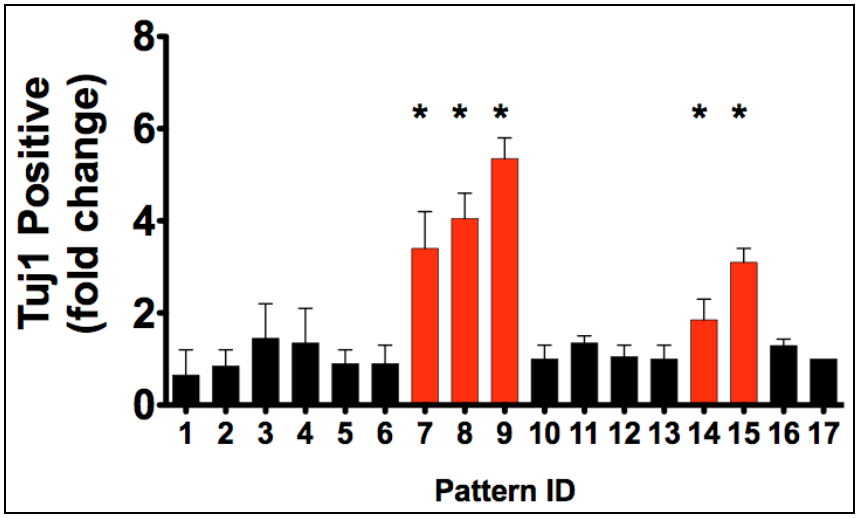

Figure 43. Enhancement of Cellular Reprogramming with Substrate Topography
Quantification of the generation of Tuj1^{+} cells on distinct MARC chip patterns following normalization to the transfection efficiency measured for each pattern.

5.3.7 Nonvirally-Induced Neuronal Cells Exhibit Electrophysiological Function

Given the increased heterogeneity in maturity and completeness of NiNs compared to conventional iNs, we expected that upstream markers of neurogenesis, such as tau [6] or MAP2 promoter activity [230], would likely be less useful in NiNs for predicting active membrane properties. Accordingly, we transduced NiNs with a lentiviral reporter driving expression of RFP under the control of the highly neuron-specific synapsin I promoter [248, 249], in order to help us identify the most-mature NiNs for electrophysiological characterization. This lentivirus may have a natural tropism for excitatory cortical neurons [246], which are similar to the predominant subtype generated by ectopic BAM expression in PMEFs [6].

The presence of synapsin-RFP in long processes of NiNs was used to identify cells for electrophysiological recording. Twelve out of thirteen synapsin-RFP$^+$ cells produced with three doses of 1.0 μg pmax-BAM factors fired single action potentials in response to depolarizing current injection as shown in (Figure 44). These cells had an average resting membrane potential of -46.3 ± 2.2 mV (mean ± SEM, n = 12), and an average input resistance of 1.7 ± 0.3 GΩ (mean ± SEM, n = 11). Twelve out of thirteen synapsin-RFP$^+$ cells produced with three doses of 2.0 μg pUNO-AM/pmax-B factors fired at least one action potential in response to depolarizing current injection. Further, 5/13 of these cells fired multiple action potentials as shown in Figure 44, and 7/13 fired single action potentials. One cell was observed firing spontaneous trains of action potentials (Figure 44, 0 pA), and rebound action potentials were also recorded. These cells had an average resting membrane potential of -41.7 ± 2.4 mV (mean ± SEM, n = 12), and an average input resistance of 1.5 ± 0.2 GΩ (mean ± SEM, n = 12). Results are for recordings with freely-fluctuating resting membrane potentials, though maintaining the cells at ~ -65 mV with holding current between recordings did occasionally result in more-clearly defined trains of action potentials. Qualitatively, we observed that cells firing trains of action potentials tended to be larger and expressed synapsin-RFP more-strongly than those firing only once.

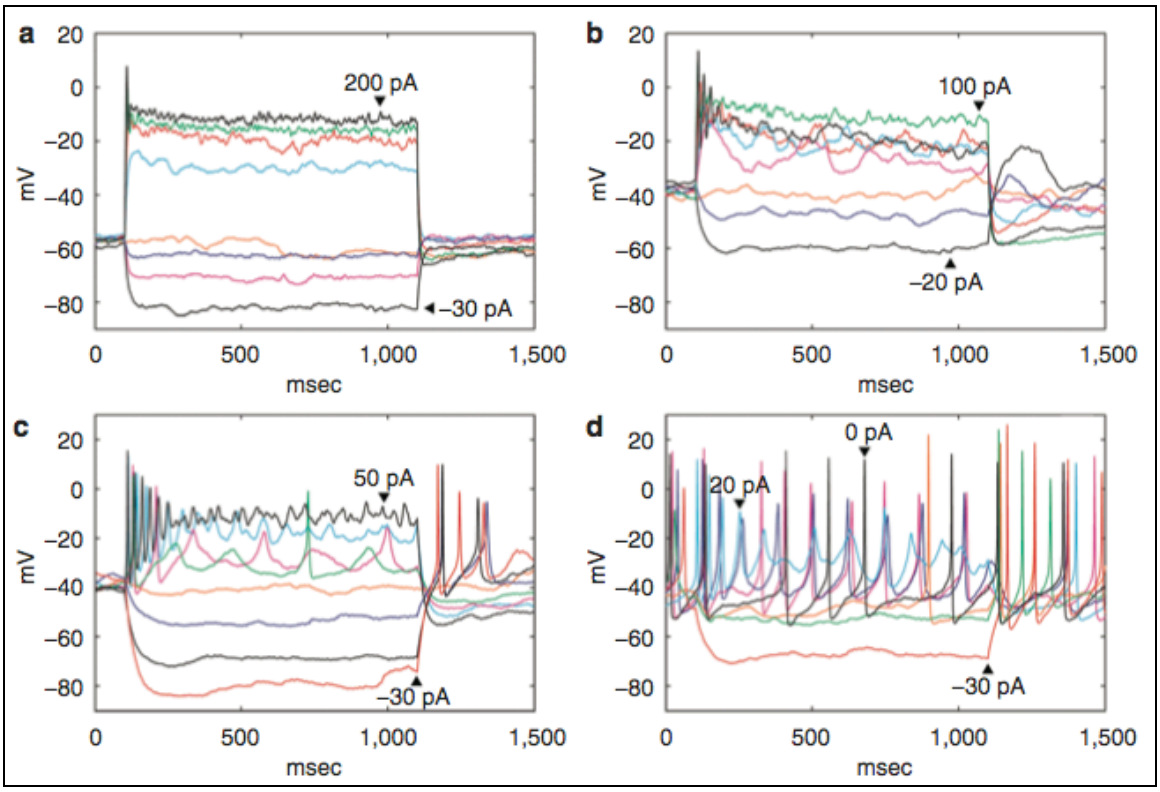

Figure 44. Electrophysiological Activity of NiNs
Current clamp in the whole-cell configuration of synapsin-RFP^{+} NiNs generated with p(CBA-ABOL)/DNA polyplexes. (a) and (b) are traces of cells that received three doses of 1.0 μg pmax-BAM factors, after 16-17 days of culture in N3 medium, on poly-D-lysine/laminin-coated coverslips. (c) and (d) are traces of cells that received three doses of 2.0 μg pUNO-AM/pmax-B factors, on day 12 of culture in N3, on PDL/laminin-coated coverslips.

5.4 Discussion

Our aim in this study was to demonstrate nonviral direct neuronal transdifferentiation in an effort to bring cellular reprogramming one step closer to viable clinical translation. We hypothesized that multiple doses of reprogramming factors would be required to generate non-virally-induced neuronal cells (NiNs) efficiently. We

used the three neuronal reprogramming factors Brn2, Ascl1, and Myt1l (BAM) in separate nonviral plasmids. Accordingly, we expect the proportion of cells that receive and express all three transgenes to be lower than that of those expressing only one or two [250]. The fraction of cells co-expressing all three can be roughly estimated by considering the fraction of cells positive for a single reporter, and raising it to the power n = number of transgenes that must be co-expressed. This worst-case is mitigated somewhat by our inclusion of all three factors in the same polyplexes, such that they are co-delivered, but it is helpful to realize the large benefit high transfection efficiencies have on co-expression of multiple plasmids. Previous reports have clearly demonstrated the importance of co-expression of all three BAM factors to produce iNs with mature electrophysiological phenotypes [6], which we expected to occur for a subset of cells transfected with our system. Poly(CBA-ABOL) is a highly-efficient and non-toxic gene carrier that is rapidly degraded upon delivery to the reducing intracellular environment, for favorable unpacking [22]. In our hands, p(CBA-ABOL) outperforms most commercially-available transfection reagents in vitro. The high efficiency and low cytotoxicity of this gene carrier is key to the success of the current study, as serial multiple-plasmid transfections are helpful for efficient NiN generation.

Optimization of PMEF transfection demonstrated that p(CBA-ABOL) polyplexes are nontoxic for doses that elicit robust transgene expression. A 2.0 μg dose was identified as the highest dose suitable for serial delivery without toxicity concern.

Poly(CBA-ABOL) is more efficient and less toxic than Lipofectamine 2000, which we deemed to be inappropriate for multiple dose delivery due to its compounding toxicity. Maintenance of high transfection efficiencies upon administration of a second dose is likely due to re-transfection of fibroblasts silencing the transgenes, as well as from transfection of newly-divided PMEFs replacing those lost to toxicity. The increase in expression levels for 2.0 μg compared to 1.0 μg is important, particularly if there is a threshold level of reprogramming factor that must be expressed in a given cell to induce transdifferentiation [251, 252].

Using 1.0 μg of pmax-BAM factors, we observed dramatic ectopic expression of BAM factor mRNA and endogenous activation of Ascl1, but no upregulation of MAP2 or Tuj1 mRNA. However, the presence of Tuj1 and MAP2 at the protein level highlights the necessity of FACS enrichment or single-cell PCR [253] when attempting to analyze NiN mRNA amidst a background population of unconverted cells. The exogenous BAM factors were silenced to a large extent by day 10 in N3 medium, supporting the use of this technique as a transient expression system. Integration of nonviral DNA vectors occurs rarely [237, 239, 254], but direct neuronal transdifferentiation is superior to iPSC systems in this regard in that sporadic BAM factor reactivation would lead to growth arrest, rather than cell proliferation.

The morphological heterogeneity of Tuj1$^+$ cells generated by our technique is further confirmation of Tuj1$^+$ as an early or promiscuous marker of induced

neurogenesis [252]. However, a subset of these cells have more complete neuronal morphologies and phenotypes, and increasing the number of Tuj1$^+$ cells is therefore likely predictive of an increased number of more-mature NiNs at downstream analysis points. The nonlinear improvement in the efficiency of Tuj1 induction with an increasing number of serial transfections may be a consequence of the re-transfection of individual cells that did not initially express sufficient transcription factor to surpass the threshold required for transdifferentiation, and also of the potential continued proliferation and subsequent transfection of unconverted PMEFs.

In accordance with the mixture of fibroblastic and neuron-like Tuj1$^+$ cell morphologies, immunofluorochemistry revealed a similar heterogeneity in the expression of pan-neuronal markers. Delivering separate transcription factors with both pmax-BAM and pUNO-BAM plasmids resulted in some more-mature NiNs that expressed MAP2, distal tau enrichment, Tuj1, synaptophysin punctae, and had synapsin promoter activity, as well as some less-mature cells that expressed only subsets of these markers. These less-complete neuron-like cells may have received an inappropriate timing, amount, or mixture of transcription factors, or may have been in the process of becoming fully-reprogrammed NiNs. Though heterogeneous on the population level, the presence of non-virally-induced markers of maturing neuronal cells (synapsin promoter activity, synaptophysin punctae) foreshadowed the neuron-like electrophysiological properties exhibited by these cells.

The synapsin-RFP reporter was excellent at predicting which cells would fire action potentials, with 24/26 patched cells firing. These cells had heterogeneous resting membrane potentials, action potential thresholds, action potential amplitudes, and number of action potentials. We observed action potentials after hyperpolarization, and spontaneous action potentials for NiNs generated with 2.0 μg pUNO-AM/pmax-B factors. These heterogeneous active membrane properties are again likely indicative of the disparate combinations of BAM factors the cells receive during nonviral transdifferentiation, producing NiNs in different stages of maturity and completion.

NiNs generated with pmax-BAM factors were electrophysiologically similar to iNs produced with lentiviral transduction of Ascl1 only [6]. Ascl1 is the only member of the BAM factors that is able to generate cells with active membrane responses on its own. As such, if a population of cells tends to receive a supra-threshold dose of only one of the transcription factors, Ascl1 cells may be the only ones detected as synapsin-RFP^{+}. pmax-BAM vectors may be silenced before an expression time has been reached that is sufficient for Brn2 or Myt1l to act, or the more-prevalent pmax-Ascl1 transcript may have out-competed pmax-Brn2 and -Myt1l for translational machinery [255]. The 2.0 μg dose of pUNO-AM/pmax-B factors may have elicited higher (or more balanced) overall expression levels compared to 1.0 μg of pmax-BAM factors. The use of separate plasmids would allow simple alteration of BAM plasmid ratios to correct such an imbalance, if necessary.

It is now established that functional NiNs can be produced by nonviral gene delivery methods, and that the transfection process plays a large role in the efficiency of reprogramming. Furthermore, it has already been demonstrated that microfluidic nanomanufactured particles are capable of transfecting a greater number of PMEF cells than bulk-prepared particles, while also producing much higher overall transgene expression levels. It was natural to combine these two capabilities to improve the transdifferentiation of fibroblasts to functional neuronal cells. Some groups have generated polycistronic BAM expression constructs, which certainly increase the likelihood of co-expression within cells and likely increase the reprogramming efficiency. However, such approaches prevent the straightforward substitution of factors and adjustment of their ratios. As the field expands and new factors continue to emerge to direct transdifferentiation toward specific neuronal subtypes, the facile substitution and adjustment of factors will remain necessary, at least in the preliminary stages of optimization. Even with these limitations, we were able to increase the conversion efficiency of a single dose by more than four times, and achieve greater than twenty percent conversion with serial dosing.

In addition to their genetic programs, cells respond to topographical cues from their extracellular microenvironment during development and maintenance. Contact guidance is a mechanism by which physical stimuli induce cellular responses. Neurons migrate along tracks of radial glia during development, while axon regeneration

following peripheral nerve injury takes places along tracks created by Schwann cells [256]. The effects of substrate topography, including isotropic pits and pillars, anisotropic gratings, and random and aligned electrospun fibers, on the rate and fate of neuron progenitor and stem cell differentiation have also been studied [257]. It has recently been shown that the incorporation of substrate topography into the tissue culture polystyrene used for lentiviral neuronal transdifferentiation can improve the yield and purity of the iNs produced [258]. They found that 5 μm gratings improved both of these parameters. However, in vivo cells experience a wide variety of features that range from the microscale to nanoscale, and studying a limited range of microscale patterns is unlikely to capture the full range of influence. Topography feature size affects progenitor and stem cell differentiation, cell morphology, and neurite length, alignment, and branching [257]. We found, by testing 17 distinct patterns simultaneously in the same culture, that the inclusion of both microscale and nanoscale features into the same substrate was necessary to achieve the greatest improvement in reprogramming efficiency. Further, both isotropic and anisotropic patterns demonstrated ability to improve nonviral neuronal transdifferentiation.

These results are the first example of nonviral direct neuronal transdifferentiation. We believe this method will prove useful in the nonviral production of subtype-specific neuronal cells, as well as provide an accessible means of generating iNs without lentivirus. Lentiviral protocols have demonstrated that adult human cells

may be intrinsically more resistant to neuronal transdifferentiation than are embryonic mouse cells, and as such our nonviral approach can benefit from further increases in efficiency as it is deployed in human cells. The effectiveness of the nonviral technique will undoubtedly improve as polycistronic vectors for iN generation become more readily available [230, 232], which, by removing redundant plasmid backbone sequences will increase the effective dose of each factor, and ensure co-expression of all factors in transfected cells. Work is underway to modify these polycistronic vectors for nonviral use in adult human cells to generate human NiNs at a sufficient density to allow study of their synaptic properties, their designation as "fully-mature" iNs [252], and to achieve a therapeutic efficiency. The recent discovery that small molecules can greatly boost the efficiency of neuronal transdifferentiation is also expected to help reach this goal [259]. Subtype-specific human NiN generation will likely require a longer pulse of ectopic expression [171], which will further rely on the unique non-toxicity of p(CBA-ABOL). Though the non-integrative requirement for ex vivo generation of non-proliferative therapeutic NiNs is relaxed compared to iPSCs, mRNA vectors will be of interest, but may need to be delivered even more frequently to maintain sufficient expression levels given their significantly shorter intracellular half-lives.

When the scalability of p(CBA-ABOL) synthesis is taken together with successful demonstration of iMN [231] and iDA [171] engraftment and iDA functional improvement in animal models of Parkinson's [172, 229], the goal of cell replacement

therapies using iNs for a number of neurodegenerative diseases seems attainable. For example, if this nonviral method is modified with a different TF cocktail to produce functional dopaminergic neurons with five 1 μg doses at a 7.5% efficiency, only ~ 0.5% of a typical p(CBA-ABOL) synthesis and ~ 1% of a Plasmid Giga Kit product would be required to generate enough neurons to produce phenotype correction in a Parkinsonian rat [172]. The benefit-to-risk ratio of neuroprotective AAV gene therapy to combat PD is already deemed high enough to warrant clinical trials [260], so the introduction of an ethically and technically viable autologous nonviral source of neuronal cells should be of great therapeutic value. The reduced risk of insertion mutagenesis with this nonviral approach should lower the entry barrier for a variety of neurological diseases even further. Further, our demonstration of NiN generation is suggestive of the feasibility of other forms of nonviral inter-lineage direct transdifferentiation [261-265].

6. Conclusions and Future Perspectives

6.1 Conclusions

This dissertation describes efforts to extend, evaluate, improve, and apply a reliable and scalable microfluidic nanomanufacturing platform to generate polymer-nucleic acid nanocomplexes with better-controlled characteristics and improved functional performance. Through these results, we have contributed to the improvement of nonviral gene transfer and cellular reprogramming by: 1) selecting and synthesizing a promising polymeric gene carrier while optimizing its delivery strategy to facilitate serial dosing without compounding cytotoxicity, 2) implementing emulsion-based microfluidic nanomanufacturing techniques to improve the physicochemical characteristics and functional performance of the chosen nanoparticles, and 3) applying these more potent nanoparticles to increase the efficiency of nonviral cellular reprogramming of fibroblasts to functional induced neurons.

We first attempted to improve upon the modestly successful high molecular weight chitosan carrier system that has been used previously. However, efforts to solve the known issue of overly stable binding through payload substitution, adjustment of molecular weight and charge density, and the addition of the ternary anionic component PGA all proved inadequate to significantly improve transfection levels. We subsequently pivoted our efforts to an alternative carrier system - a bioreducible linear poly(amido amine) able to give sustained, robust transgene expression through serial

dosing. Poly(CBA-ABOL) possesses an inherent degradative response mechanism to changes encountered in the redox environment while transitioning from the extracellular space to the cytoplasmic domain. It is designed to unpack efficiently within cells, and to break down quickly to minimize associated sequelae. Following selection and synthesis of this promising carrier, we showed that it forms polyplexes of appropriate size and charge, dissociates readily upon challenge with intracellular concentrations of reducing agents, and transfects cells efficiently. We also demonstrated its ability to achieve modest levels of transfection in vivo, and show that its favorable cytotoxicity profiles allows for repeated dosing in order to sustain high transgene expression levels.

Next, we reported the benefits of applying a microfluidic nanomanufacturing approach to better control the preparation of polyplexes and to produce more uniform and more potent delivery systems. While polymer-DNA nanocomplexes have been synthesized by microfluidics, to our knowledge this is the first example of the production of polymer-RNA nanocomplexes with a droplet-based microfluidic nanomanufacturing approach, as well as the first time that QD-FRET has been used in combination with flow cytometry to quantify the intracellular unpacking of polymer-DNA nanocomplexes. We have demonstrated that nanomanufactured polyplexes exhibit significant and consistent decreases in size, zeta potential, and polydispersity relative to complexes synthesized by traditional bulk methods. Both DNA- and RNA-

loaded nanocomplexes exhibit increased colloidal and binding stability, as quantified by fluorescence-based competitive binding assays. Transfection was significantly improved in a broad range of cell types, in terms of both the number of cells transfected and gross transgene expression. We ascribed this improvement in part to a more gradual release of nucleic acids offered by the more stable microfluidic nanomanufactured nanocomplexes, evidenced by the retarded decline of intracellular QD-FRET emission.

The increased transfection efficiency and diminished toxicity of p(CBA-ABOL) nanomanufactured particles are especially advantageous in applications requiring high levels of transgene expression and repeated administration. One such application is the nonviral direct cellular reprogramming of fibroblasts to neurons. In an effort to address the lack of a safe and ethical source of therapeutic cells to treat neurodegenerative diseases, we developed a nonviral transfection strategy to deliver genes encoding the transcription factors necessary to convert fibroblasts directly to functional neuronal cells. Nonviral cellular reprogramming strategies eliminate the integration of viral DNA sequences and represent a potentially safer alternative to viral transdifferentiation methods. Our method produced neuronal cells with appropriate morphological changes, activation and expression of endogenous neuronal markers, and electrophysiological function. Delivery of the reprogramming factors with microfluidic nanomanufactured particles significantly improved the efficiency of this nonviral neuronal transdifferentiation, which is a critical parameter in the effort to generate a

sufficient supply cells for potential transplantation given the postmitotic, non-proliferative nature of neurons. To achieve the primary goal of sustained and robust transgene expression, this work endeavored, through optimization of polymer-nucleic acid nanocomplex formulation and application, to alleviate the paucity of uniform, potent, biocompatible, and reproducibly generated gene carriers that are able to satisfy the contrary requirements of adequate nucleic acid protection and efficient release.

6.2 Future Perspectives

By validating the merits of microfluidic nanomanufacturing with a range of carriers, nucleic acid payloads, and cell types, we have provided justification for the further translation of the platform. Due to the role of physical particle properties in uptake, endocytosis, circulatory retention, and toxicity, the development of precise structure-function correlations requires a reliable technique to produce uniform particles. The increased consistency of nanomanufactured particles, and subsequent reduced variances in cellular and systemic processing, has the potential provide more accurate mechanistic and pharmacodynamic data for the rational design of better gene carriers. Furthermore, nonviral gene delivery will continue to demand more sophisticated delivery systems, such as multi-functional particles endowed with targeting, imaging and environmental-sensitive functionalities. Better control of the self-assembly of these types of particles will be even more critical. We have not explicitly

addressed the scale-up issue, however the microfluidics approach is certainly scalable using arrayed channel designs and parallel chips.

Our protocol for nonviral neuronal cellular reprogramming is expected to be readily adaptable to other direct transdifferentiation strategies as new reprogramming factors are identified. The capacity of our carrier system to deliver a variety of nucleic acid payloads provides the opportunity to deliver alternative payloads including mRNA, siRNA, and protein factors should they eventually prove superior to plasmid DNA in some applications. Safe and efficient cellular reprogramming may represent the most realistic treatment on the horizon for neurodegenerative disease in the near-term. Further development of the physical culture conditions and nonviral carrier systems used to transfer reprogramming factors promises to not only continue to add to our collective understanding of transdifferentiation processes, but also move the technology closer to successful translation. If in situ transdifferentiation proves necessary, the many years of engineering spent developing nonviral carriers for in vivo delivery will provide an excellent starting point. Whether the future calls for in vivo or ex vivo nonviral cellular reprogramming, there will be a demand for a reproducible and scalable platform to produce uniform and potent delivery systems. Microfluidic nanomanufacturing of polymer-nucleic acid nanocomplexes represents an important step forward in addressing this critical need.

References

1. Ferrari, S., D.M. Geddes, and E.W. Alton, *Barriers to and new approaches for gene therapy and gene delivery in cystic fibrosis.* Adv Drug Deliv Rev, 2002. **54**(11): p. 1373-93.

2. Walsh, C.E., *Gene therapy progress and prospects: gene therapy for the hemophilias.* Gene Ther, 2003. **10**(12): p. 999-1003.

3. Vile, R.G., S.J. Russell, and N.R. Lemoine, *Cancer gene therapy: hard lessons and new courses.* Gene Ther, 2000. **7**(1): p. 2-8.

4. Mulligan, R.C., *The basic science of gene therapy.* Science, 1993. **260**(5110): p. 926-32.

5. Fant, K., B. Norden, and P. Lincoln, *Using ethidium to probe nonequilibrium states of DNA condensed for gene delivery.* Biochemistry, 2011. **50**(7): p. 1125-7.

6. Vierbuchen, T., et al., *Direct conversion of fibroblasts to functional neurons by defined factors.* Nature, 2010. **463**(7284): p. 1035-41.

7. Varga, C.M., K. Hong, and D.A. Lauffenburger, *Quantitative analysis of synthetic gene delivery vector design properties.* Mol Ther, 2001. **4**(5): p. 438-46.

8. Dinh, A.T., et al., *Understanding intracellular transport processes pertinent to synthetic gene delivery via stochastic simulations and sensitivity analyses.* Biophys J, 2007. **92**(3): p. 831-46.

9. Schaffer, D.V., et al., *Vector unpacking as a potential barrier for receptor-mediated polyplex gene delivery.* Biotechnol Bioeng, 2000. **67**(5): p. 598-606.

10. Pollard, H., et al., *Polyethylenimine but not cationic lipids promotes transgene delivery to the nucleus in mammalian cells.* J Biol Chem, 1998. **273**(13): p. 7507-11.

11. Thomas, M. and A.M. Klibanov, *Non-viral gene therapy: polycation-mediated DNA delivery.* Appl Microbiol Biotechnol, 2003. **62**(1): p. 27-34.

12. Huth, S., et al., *Interaction of polyamine gene vectors with RNA leads to the dissociation of plasmid DNA-carrier complexes.* J Gene Med, 2006. **8**(12): p. 1416-24.

13. Koping-Hoggard, M., et al., *Improved chitosan-mediated gene delivery based on easily dissociated chitosan polyplexes of highly defined chitosan oligomers.* Gene Ther, 2004. **11**(19): p. 1441-52.

14. Kiang, T., et al., *The effect of the degree of chitosan deacetylation on the efficiency of gene transfection.* Biomaterials, 2004. **25**(22): p. 5293-301.

15. Jones, N.A., et al., *Polymer chemical structure is a key determinant of physicochemical and colloidal properties of polymer-DNA complexes for gene delivery.* Biochimica Et Biophysica Acta-Gene Structure and Expression, 2000. **1517**(1): p. 1-18.

16. Forrest, M.L., et al., *Partial acetylation of polyethylenimine enhances in vitro gene delivery.* Pharm Res, 2004. **21**(2): p. 365-71.

17. Gabrielson, N.P. and D.W. Pack, *Acetylation of polyethylenimine enhances gene delivery via weakened polymer/DNA interactions.* Biomacromolecules, 2006. **7**(8): p. 2427-35.

18. Liu, X., J.W. Yang, and D.M. Lynn, *Addition of "charge-shifting" side chains to linear poly(ethyleneimine) enhances cell transfection efficiency.* Biomacromolecules, 2008. **9**(7): p. 2063-71.

19. Mao, H.Q. and K.W. Leong, *Design of Polyphosphoester-DNA Nanoparticles for Non-Viral Gene Delivery.* Adv Genet, 2005. **53PA**: p. 275-306.

20. Oupicky, D., A.L. Parker, and L.W. Seymour, *Laterally stabilized complexes of DNA with linear reducible polycations: Strategy for triggered intracellular activation of DNA delivery vectors.* Journal of the American Chemical Society, 2002. **124**(1): p. 8-9.

21. Gosselin, M.A., W.J. Guo, and R.J. Lee, *Efficient gene transfer using reversibly cross-linked low molecular weight polyethylenimine.* Bioconjugate Chemistry, 2001. **12**(6): p. 989-994.

22. Lin, C., et al., *Novel bioreducible poly(amido amine)s for highly efficient gene delivery.* Bioconjug Chem, 2007. **18**(1): p. 138-45.

23. Lin, C. and J.F. Engbersen, *The role of the disulfide group in disulfide-based polymeric gene carriers.* Expert Opin Drug Deliv, 2009. **6**(4): p. 421-39.

24. Lin, C., et al., *Random and block copolymers of bioreducible poly(amido amine)s with high- and low-basicity amino groups: study of DNA condensation and buffer capacity on gene transfection.* J Control Release, 2007. **123**(1): p. 67-75.

25. Miyata, K., et al., *Block catiomer polyplexes with regulated densities of charge and disulfide cross-linking directed to enhance gene expression.* Journal of the American Chemical Society, 2004. **126**(8): p. 2355-2361.

26. Oishi, M., K. Kataoka, and Y. Nagasaki, *pH-responsive three-layered PEGylated polyplex micelle based on a lactosylated ABC triblock copolymer as a targetable and endosome-disruptive nonviral gene vector.* Bioconjugate Chemistry, 2006. **17**(3): p. 677-688.

27. Sethuraman, V.A., K. Na, and Y.H. Bae, *pH-responsive sulfonamide/PEI system for tumor specific gene delivery: an in vitro study.* Biomacromolecules, 2006. **7**(1): p. 64-70.

28. Kim, Y.H., et al., *Polyethylenimine with acid-labile linkages as a biodegradable gene carrier.* J Control Release, 2005. **103**(1): p. 209-19.

29. Hinrichs, W.L.J., et al., *Thermosensitive polymers as carriers for DNA delivery.* Journal of Controlled Release, 1999. **60**(2-3): p. 249-259.

30. Kurisawa, M., M. Yokoyama, and T. Okano, *Gene expression control by temperature with thermo-responsive polymeric gene carriers.* Journal of Controlled Release, 2000. **69**(1): p. 127-137.

31. Bisht, H.S., et al., *Temperature-controlled properties of DNA complexes with poly(ethylenimine)-graft-poly(N-isopropylacrylamide).* Biomacromolecules, 2006. **7**(4): p. 1169-1178.

32. Oupicky, D., et al., *Temperature-controlled behavior of self-assembly gene delivery vectors based on complexes of DNA with poly(L-lysine)-graft-poly(N-isopropylacrylamide).* Macromolecules, 2003. **36**(18): p. 6863-6872.

33. Lavigne, M.D., et al., *Enhanced gene expression through temperature profile-induced variations in molecular architecture of thermoresponsive polymer vectors.* Journal of Gene Medicine, 2007. **9**(1): p. 44-54.

34. Sun, S.J., et al., *A thermoresponsive chitosan-NIPAAm/vinyl laurate copolymer vector for gene transfection.* Bioconjugate Chemistry, 2005. **16**(4): p. 972-980.

35. Zintchenko, A., M. Ogris, and E. Wagner, *Temperature dependent gene expression induced by PNIPAM-based copolymers: Potential of hyperthermia in gene transfer.* Bioconjugate Chemistry, 2006. **17**(3): p. 766-772.

36. Chilkoti, A., M.R. Dreher, and D.E. Meyer, *Design of thermally responsive, recombinant polypeptide carriers for targeted drug delivery.* Advanced Drug Delivery Reviews, 2002. **54**(8): p. 1093-1111.

37. Chen, T.H.H., Y. Bae, and D.Y. Furgeson, *Intelligent biosynthetic nanobiomaterials (IBNs) for hyperthermic gene delivery.* Pharmaceutical Research, 2008. **25**(3): p. 683-691.

38. Kim, M.S., et al., *Preparation and characterization of MPEG-PCL diblock copolymers with thermo-responsive sol-gel-sol phase transition.* Journal of Polymer Science Part a-Polymer Chemistry, 2006. **44**(18): p. 5413-5423.

39. Handwerger, R.G., M.-S. Kim, and S.L. Diamond, *Crosslinked PEI Polyplexes for Light-Triggered DNA Release.* Mol Ther, 2006. **13**(S1): p. S415-S416.

40. Lepage, M., et al., *MRI observation of the light-induced release of a contrast agent from photo-controllable polymer micelles.* Physics in Medicine and Biology, 2007. **52**(10): p. N249-N255.

41. Jiang, J.Q., X. Tong, and Y. Zhao, *A new design for light-breakable polymer micelles.* Journal of the American Chemical Society, 2005. **127**(23): p. 8290-8291.

42. Lee, H.I., et al., *Light-induced reversible formation of polymeric micelles.* Angewandte Chemie-International Edition, 2007. **46**(14): p. 2453-2457.

43. Truong-Le, V.L., et al., *Gene transfer by DNA-gelatin nanospheres.* Arch Biochem Biophys, 1999. **361**(1): p. 47-56.

44. Liang, D.C., et al., *Pre-deliver chitosanase to cells: a novel strategy to improve gene expression by endocellular degradation-induced vector unpacking.* Int J Pharm, 2006. **314**(1): p. 63-71.

45. Zuo, A., et al., *Improved transfection efficiency of CS/DNA complex by co-transfected chitosanase gene.* Int J Pharm, 2008. **352**(1-2): p. 302-8.

46. Kuhn, S.J., et al., *Proteolytic surface functionalization enhances in vitro magnetic nanoparticle mobility through extracellular matrix.* Nano Lett, 2006. **6**(2): p. 306-12.

47. Godbey, W.T., K.K. Wu, and A.G. Mikos, *Tracking the intracellular path of poly(ethylenimine)/DNA complexes for gene delivery.* Proceedings of the National Academy of Sciences of the United States of America, 1999. **96**(9): p. 5177-5181.

48. Zaric, V., et al., *Effective polyethylenimine-mediated gene transfer into human endothelial cells.* J Gene Med, 2004. **6**(2): p. 176-84.

49. Foerster, T., *Intermolecular energy transference and fluorescence.* Ann. Phys., 1948. **2**: p. 55.

50. Jares-Erijman, E.A. and T.M. Jovin, *FRET imaging.* Nat Biotechnol, 2003. **21**(11): p. 1387-95.

51. Stryer, L., *Fluorescence Energy-Transfer as a Spectroscopic Ruler.* Annual Review of Biochemistry, 1978. **47**: p. 819-846.

52. Itaka, K., et al., *Evaluation by fluorescence resonance energy transfer of the stability of nonviral gene delivery vectors under physiological conditions.* Biomacromolecules, 2002. **3**(4): p. 841-845.

53. Itaka, K., et al., *In situ single cell observation by fluorescence resonance energy transfer reveals fast intra-cytoplasmic delivery and easy release of plasmid DNA complexed with linear polyethylenimine.* Journal of Gene Medicine, 2004. **6**(1): p. 76-84.

54. Kong, H.J., et al., *Non-viral gene delivery regulated by stiffness of cell adhesion substrates.* Nature Materials, 2005. **4**(6): p. 460-464.

55. McGrath, N. and M. Barroso, *Quantum dots as fluorescence resonance energy transfer donors in cells.* Journal of Biomedical Optics, 2008. **13**(3): p. -.

56. Lee, J.I., K.S. Ha, and H.S. Yoo, *Quantum-dot-assisted fluorescence resonance energy transfer approach for intracellular trafficking of chitosan/DNA complex.* Acta Biomaterialia, 2008. **4**(4): p. 791-798.

57. Chen, H.H., et al., *Quantitative comparison of intracellular unpacking kinetics of polyplexes by a model constructed from quantum dot-FRET.* Mol Ther, 2008. **16**(2): p. 324-32.

58. Ho, Y.P., et al., *Evaluating the intracellular stability and unpacking of DNA nanocomplexes by quantum dots-FRET.* J Control Release, 2006. **116**(1): p. 83-9.

59. Chen, H.H., et al., *Simultaneous non-invasive analysis of DNA condensation and stability by two-step QD-FRET.* Nano Today, 2009. **4**(2): p. 125-134.

60. Bacia, K. and P. Schwille, *A dynamic view of cellular processes by in vivo fluorescence auto- and cross-correlation spectroscopy.* Methods, 2003. **29**(1): p. 74-85.

61. Remaut, K., et al., *Can we better understand the intracellular behavior of DNA nanoparticles by fluorescence correlation spectroscopy?* J Control Release, 2007. **121**(1-2): p. 49-63.

62. Lucas, B., et al., *Studying the intracellular dissociation of polymer-oligonucleotide complexes by dual color fluorescence fluctuation spectroscopy and confocal imaging.* Biochemistry, 2005. **44**(29): p. 9905-12.

63. Kulkarni, R.P., et al., *Quantitating intracellular transport of polyplexes by spatio-temporal image correlation spectroscopy.* Proc Natl Acad Sci U S A, 2005. **102**(21): p. 7523-8.

64. Remaut, K., et al., *FRET-FCS as a tool to evaluate the stability of oligonucleotide drugs after intracellular delivery.* J Control Release, 2005. **103**(1): p. 259-71.

65. Burke, R.S. and S.H. Pun, *Extracellular barriers to in Vivo PEI and PEGylated PEI polyplex-mediated gene delivery to the liver.* Bioconjug Chem, 2008. **19**(3): p. 693-704.

66. Ruponen, M., et al., *Extracellular glycosaminoglycans modify cellular trafficking of lipoplexes and polyplexes.* J Biol Chem, 2001. **276**(36): p. 33875-80.

67. Ruponen, M., et al., *Extracellular and intracellular barriers in non-viral gene delivery.* J Control Release, 2003. **93**(2): p. 213-7.

68. Mullen, P.M., et al., *Strength of conjugate binding to plasmid DNA affects degradation rate and expression level in vivo.* Biochim Biophys Acta, 2000. **1523**(1): p. 103-10.

69. Fischer, D., et al., *Effect of poly(ethylene imine) molecular weight and pegylation on organ distribution and pharmacokinetics of polyplexes with oligodeoxynucleotides in mice.* Drug Metab Dispos, 2004. **32**(9): p. 983-92.

70. Merdan, T., et al., *PEGylation of poly(ethylene imine) affects stability of complexes with plasmid DNA under in vivo conditions in a dose-dependent manner after intravenous injection into mice.* Bioconjug Chem, 2005. **16**(4): p. 785-92.

71. Oupicky, D., et al., *Effect of albumin and polyanion on the structure of DNA complexes with polycation containing hydrophilic nonionic block.* Bioconjug Chem, 1999. **10**(5): p. 764-72.

72. Mishra, S., P. Webster, and M.E. Davis, *PEGylation significantly affects cellular uptake and intracellular trafficking of non-viral gene delivery particles.* European Journal of Cell Biology, 2004. **83**(3): p. 97-111.

73. Wolff, J.A. and V. Budker, *The mechanism of naked DNA uptake and expression.* Adv Genet, 2005. **54**: p. 3-20.

74. Wolff, J.A., et al., *Direct gene transfer into mouse muscle in vivo.* Science, 1990. **247**(4949 Pt 1): p. 1465-8.

75. Roy, K., et al., *Oral gene delivery with chitosan--DNA nanoparticles generates immunologic protection in a murine model of peanut allergy.* Nat Med, 1999. **5**(4): p. 387-91.

76. Mao, Y. and J.E. Schwarzbauer, *Stimulatory effects of a three-dimensional microenvironment on cell-mediated fibronectin fibrillogenesis.* J Cell Sci, 2005. **118**(Pt 19): p. 4427-36.

77. Gruber, H.E. and E.N. Hanley, Jr., *Human disc cells in monolayer vs 3D culture: cell shape, division and matrix formation.* BMC Musculoskelet Disord, 2000. **1**: p. 1.

78. Ruponen, M., S. Yla-Herttuala, and A. Urtti, *Interactions of polymeric and liposomal gene delivery systems with extracellular glycosaminoglycans: physicochemical and transfection studies.* Biochim Biophys Acta, 1999. **1415**(2): p. 331-41.

79. Goodman, T.T., C.P. Ng, and S.H. Pun, *3-D tissue culture systems for the evaluation and optimization of nanoparticle-based drug carriers.* Bioconjug Chem, 2008. **19**(10): p. 1951-9.

80. Kim, Y., et al., *Polymeric worm micelles as nano-carriers for drug delivery.* Nanotechnology, 2005. **16**(7): p. S484-S491.

81. Kuhn, S.J., D.E. Hallahan, and T.D. Giorgio, *Characterization of superparamagnetic nanoparticle interactions with extracellular matrix in an in vitro system.* Ann Biomed Eng, 2006. **34**(1): p. 51-8.

82. DeRouchey, J., et al., *Monomolecular assembly of siRNA and poly(ethylene glycol)-peptide copolymers.* Biomacromolecules, 2008. **9**(2): p. 724-32.

83. Ng, C.P. and S.H. Pun, *A perfusable 3D cell-matrix tissue culture chamber for in situ evaluation of nanoparticle vehicle penetration and transport.* Biotechnol Bioeng, 2008. **99**(6): p. 1490-501.

84. Nederman, T. and P. Twentyman, *Spheroids for studies of drug effects.* Recent Results Cancer Res, 1984. **95**: p. 84-102.

85. Han, M., et al., *Enhanced Percolation and Gene Expression in Tumor Hypoxia by PEGylated Polyplex Micelles.* Mol Ther, 2009.

86. Mellor, H.R., et al., *Optimising non-viral gene delivery in a tumour spheroid model.* J Gene Med, 2006. **8**(9): p. 1160-70.

87. Han, M., et al., *Transfection study using multicellular tumor spheroids for screening non-viral polymeric gene vectors with low cytotoxicity and high transfection efficiencies.* J Control Release, 2007. **121**(1-2): p. 38-48.

88. Goodman, T.T., P.L. Olive, and S.H. Pun, *Increased nanoparticle penetration in collagenase-treated multicellular spheroids.* Int J Nanomedicine, 2007. **2**(2): p. 265-74.

89. Nederman, T., et al., *Demonstration of an extracellular matrix in multicellular tumor spheroids.* Cancer Res, 1984. **44**(7): p. 3090-7.

90. Artursson, P. and J. Karlsson, *Correlation between oral drug absorption in humans and apparent drug permeability coefficients in human intestinal epithelial (Caco-2) cells.* Biochem Biophys Res Commun, 1991. **175**(3): p. 880-5.

91. Artursson, P., *Epithelial transport of drugs in cell culture. I: A model for studying the passive diffusion of drugs over intestinal absorptive (Caco-2) cells.* J Pharm Sci, 1990. **79**(6): p. 476-82.

92. Meng, Q.H., et al., *Efficient transfection of non-proliferating human airway epithelial cells with a synthetic vector system.* J Gene Med, 2004. **6**(2): p. 210-21.

93. Molestina, R.E., et al., *Infection of human endothelial cells with Chlamydia pneumoniae stimulates transendothelial migration of neutrophils and monocytes.* Infect Immun, 1999. **67**(3): p. 1323-30.

94. Kerneis, S., et al., *Conversion by Peyer's patch lymphocytes of human enterocytes into M cells that transport bacteria.* Science, 1997. **277**(5328): p. 949-52.

95. Kerneis, S., et al., *Molecular studies of the intestinal mucosal barrier physiopathology using cocultures of epithelial and immune cells: a technical update.* Microbes Infect, 2000. **2**(9): p. 1119-24.

96. Hilgendorf, C., et al., *Caco-2 versus Caco-2/HT29-MTX co-cultured cell lines: permeabilities via diffusion, inside- and outside-directed carrier-mediated transport.* J Pharm Sci, 2000. **89**(1): p. 63-75.

97. Gersting, S.W., et al., *Gene delivery to respiratory epithelial cells by magnetofection.* J Gene Med, 2004. **6**(8): p. 913-22.

98. Lang, D.S., et al., *A novel human ex vivo model for the analysis of molecular events during lung cancer chemotherapy.* Respir Res, 2007. **8**: p. 43.

99. Torche, A.M., et al., *Ex vivo and in situ PLGA microspheres uptake by pig ileal Peyer's patch segment.* Int J Pharm, 2000. **201**(1): p. 15-27.

100. Conner, S.D. and S.L. Schmid, *Regulated portals of entry into the cell.* Nature, 2003. **422**(6927): p. 37-44.

101. Rejman, J., et al., *Size-dependent internalization of particles via the pathways of clathrin- and caveolae-mediated endocytosis.* Biochem J, 2004. **377**(Pt 1): p. 159-69.

102. Ganta, S., et al., *A review of stimuli-responsive nanocarriers for drug and gene delivery.* J Control Release, 2008. **126**(3): p. 187-204.

103. Murthy, N., et al., *Design and synthesis of pH-responsive polymeric carriers that target uptake and enhance the intracellular delivery of oligonucleotides.* J Control Release, 2003. **89**(3): p. 365-74.

104. Verbaan, F.J., et al., *Steric stabilization of poly(2-(dimethylamino)ethyl methacrylate)-based polyplexes mediates prolonged circulation and tumor targeting in mice.* J Gene Med, 2004. **6**(1): p. 64-75.

105. Schaffer, D.V. and D.A. Lauffenburger, *Optimization of cell surface binding enhances efficiency and specificity of molecular conjugate gene delivery.* J Biol Chem, 1998. **273**(43): p. 28004-9.

106. Akita, H., et al., *Quantitative three-dimensional analysis of the intracellular trafficking of plasmid DNA transfected by a nonviral gene delivery system using confocal laser scanning microscopy.* Mol Ther, 2004. **9**(3): p. 443-51.

107. Hama, S., et al., *Quantitative comparison of intracellular trafficking and nuclear transcription between adenoviral and lipoplex systems.* Mol Ther, 2006. **13**(4): p. 786-94.

108. Grigsby, C.L. and K.W. Leong, *Balancing protection and release of DNA: tools to address a bottleneck of non-viral gene delivery.* J R Soc Interface, 2010. **7 Suppl 1**: p. S67-82.

109. Kiang, T., et al., *Formulation of chitosan-DNA nanoparticles with poly(propyl acrylic acid) enhances gene expression.* Journal of Biomaterials Science Polymer Edition, 2004. **15**(11): p. 1405-21.

110. Suh, J., D. Wirtz, and J. Hanes, *Efficient active transport of gene nanocarriers to the cell nucleus.* Proceedings of the National Academy of Sciences of the United States of America, 2003. **100**(7): p. 3878-82.

111. Panyam, J. and V. Labhasetwar, *Dynamics of endocytosis and exocytosis of poly(D,L-lactide-co-glycolide) nanoparticles in vascular smooth muscle cells.* Pharmaceutical Research, 2003. **20**(2): p. 212-20.

112. Lucas, B., et al., *Towards a better understanding of the dissociation behavior of liposome-oligonucleotide complexes in the cytosol of cells.* Journal of Controlled Release, 2005. **103**(2): p. 435-50.

113. Godbey, W.T., K.K. Wu, and A.G. Mikos, *Tracking the intracellular path of poly(ethylenimine)/DNA complexes for gene delivery.* Proc Natl Acad Sci U S A, 1999. **96**(9): p. 5177-81.

114. Lakowicz, J.R., *Principles of Fluorescence Spectroscopy*. 4th ed. 2006: Kluwer Academic/Plenum.

115. Clapp, A.R., I.L. Medintz, and H. Mattoussi, *Forster resonance energy transfer investigations using quantum-dot fluorophores.* Chemphyschem, 2006. **7**(1): p. 47-57.

116. Ho, Y.P., et al., *Multiplexed hybridization detection with multicolor colocalization of quantum dot nanoprobes.* Nano Lett, 2005. **5**(9): p. 1693-7.

117. Bruchez, M., et al., *Semiconductor nanocrystals as fluorescent biological labels.* Science, 1998. **281**(5385): p. 2013-2016.

118. Chan, W.C.W. and S.M. Nie, *Quantum dot bioconjugates for ultrasensitive nonisotopic detection.* Science, 1998. **281**(5385): p. 2016-2018.

119. Medintz, I.L. and H. Mattoussi, *Quantum dot-based resonance energy transfer and its growing application in biology.* Physical Chemistry Chemical Physics, 2009. **11**(1): p. 17-45.

120. Clapp, A.R., et al., *Can luminescent quantum dots be efficient energy acceptors with organic dye donors?* J Am Chem Soc, 2005. **127**(4): p. 1242-50.

121. Kong, H.J., et al., *Non-viral gene delivery regulated by stiffness of cell adhesion substrates.* Nature materials, 2005. **4**(6): p. 460-4.

122. Chen, H.H., et al., *Quantitative comparison of intracellular unpacking kinetics of polyplexes by a model constructed from quantum dot-FRET.* Mol Ther, 2008. **16**(2): p. 324-32.

123. Lauffenburger, D.A., C.M. Varga, and K. Hong, *Quantitative analysis of synthetic gene delivery vector design properties.* Molecular Therapy, 2001. **4**(5): p. 438-446.

124. Lauffenburger, D.A., et al., *Quantitative comparison of polyethylenimine formulations and adenoviral vectors in terms of intracellular gene delivery processes.* Gene Therapy, 2005. **12**(13): p. 1023-1032.

125. Mitragotri, S., et al., *Understanding intracellular transport processes pertinent to synthetic gene delivery via stochastic simulations and sensitivity analyses.* Biophysical Journal, 2007. **92**(3): p. 831-846.

126. Ulasov, A.V., et al., *Properties of PEI-based polyplex nanoparticles that correlate with their transfection efficacy.* Mol Ther, 2011. **19**(1): p. 103-12.

127. Lee, J.I., K.-S. Ha, and H.S. Yoo, *Quantum-dot-assisted fluorescence resonance energy transfer approach for intracellular trafficking of chitosan/DNA complex.* Acta Biomater, 2008. **4**(4): p. 791-8.

128. Lim, T.C., et al., *Intercalating dye as an acceptor in quantum-dot-mediated FRET.* Nanotechnology, 2008. **19**(7): p. 075701.

129. Shaheen, S.M., et al., *Quantitative analysis of condensation/decondensation status of pDNA in the nuclear sub-domains by QD-FRET.* Nucleic Acids Res, 2011. **39**(7): p. e48.

130. Jiang, X., et al., *Dual-sensitive micellar nanoparticles regulate DNA unpacking and enhance gene-delivery efficiency.* Adv Mater Weinheim, 2010. **22**(23): p. 2556-60.

131. Chen, H.H., et al., *Simultaneous Non-invasive Analysis of DNA Condensation and Stability by Two-step QD-FRET.* Nano Today, 2009. **4**(2): p. 125-134.

132. Lee, H., I.-K. Kim, and T.G. Park, *Intracellular trafficking and unpacking of siRNA/quantum dot-PEI complexes modified with and without cell penetrating peptide: confocal and flow cytometric FRET analysis.* Bioconjug Chem, 2010. **21**(2): p. 289-95.

133. Qi, L. and X. Gao, *Quantum dot-amphipol nanocomplex for intracellular delivery and real-time imaging of siRNA.* ACS Nano, 2008. **2**(7): p. 1403-10.

134. Wu, Y., et al., *Uptake and intracellular fate of multifunctional nanoparticles: a comparison between lipoplexes and polyplexes via quantum dot mediated Forster resonance energy transfer.* Mol Pharm, 2011. **8**(5): p. 1662-8.

135. Zhang, B., et al., *Sensing polymer/DNA polyplex dissociation using quantum dot fluorophores.* ACS nano, 2011. **5**(1): p. 129-38.

136. Ho, Y.P., et al., *The convergence of quantum-dot-mediated fluorescence resonance energy transfer and microfluidics for monitoring DNA polyplex self-assembly in real time.* Nanotechnology, 2009. **20**(9): p. 095103.

137. Bagalkot, V., et al., *Quantum dot-aptamer conjugates for synchronous cancer imaging, therapy, and sensing of drug delivery based on bi-fluorescence resonance energy transfer.* Nano Letters, 2007. **7**(10): p. 3065-70.

138. Lavertu, M., et al., *High efficiency gene transfer using chitosan/DNA nanoparticles with specific combinations of molecular weight and degree of deacetylation.* Biomaterials, 2006. **27**(27): p. 4815-24.

139. Srinivasan, C., et al., *Labeling and intracellular tracking of functionally active plasmid DNA with semiconductor quantum dots.* Mol Ther, 2006. **14**(2): p. 192-201.

140. Smith, A.M., et al., *Bioconjugated quantum dots for in vivo molecular and cellular imaging.* Adv Drug Deliv Rev, 2008. **60**(11): p. 1226-40.

141. Michalet, X., et al., *Quantum dots for live cells, in vivo imaging, and diagnostics.* Science, 2005. **307**(5709): p. 538-44.

142. Ho, Y.P. and K.W. Leong, *Quantum dot-based theranostics.* Nanoscale, 2010. **2**(1): p. 60-8.

143. Braun, C.S., et al., *A stopped-flow kinetic study of the assembly of nonviral gene delivery complexes.* Biophys J, 2005. **88**(6): p. 4146-58.

144. Ho, Y.P., et al., *Tuning physical properties of nanocomplexes through microfluidics-assisted confinement.* Nano Lett, 2011. **11**(5): p. 2178-82.

145. Gratton, S.E., et al., *The pursuit of a scalable nanofabrication platform for use in material and life science applications.* Acc Chem Res, 2008. **41**(12): p. 1685-95.

146. Rolland, J.P., et al., *Direct fabrication and harvesting of monodisperse, shape-specific nanobiomaterials.* J Am Chem Soc, 2005. **127**(28): p. 10096-100.

147. Tao, L., et al., *Lithographically defined uniform worm-shaped polymeric nanoparticles.* Nanotechnology, 2010. **21**(9): p. 095301.

148. Koh, C.G., et al., *Delivery of antisense oligodeoxyribonucleotide lipopolyplex nanoparticles assembled by microfluidic hydrodynamic focusing.* J Control Release, 2010. **141**(1): p. 62-9.

149. Koh, C.G., et al., *Delivery of polyethylenimine/DNA complexes assembled in a microfluidics device.* Mol Pharm, 2009. **6**(5): p. 1333-42.

150. Hsieh, A.T., et al., *Nonviral gene vector formation in monodispersed picolitre incubator for consistent gene delivery.* Lab Chip, 2009. **9**(18): p. 2638-43.

151. Gary, D.J., N. Puri, and Y.Y. Won, *Polymer-based siRNA delivery: perspectives on the fundamental and phenomenological distinctions from polymer-based DNA delivery.* J Control Release, 2007. **121**(1-2): p. 64-73.

152. Molsa, P.K., R.J. Marttila, and U.K. Rinne, *Survival and cause of death in Alzheimer's disease and multi-infarct dementia.* Acta Neurol Scand, 1986. **74**(2): p. 103-7.

153. Gao, A., et al., *Potential therapeutic applications of differentiated induced pluripotent stem cells (iPSCs) in the treatment of neurodegenerative diseases.* Neuroscience, 2013. **228**: p. 47-59.

154. Dorsey, E.R., et al., *Projected number of people with Parkinson disease in the most populous nations, 2005 through 2030.* Neurology, 2007. **68**(5): p. 384-6.

155. Korecka, J.A., J. Verhaagen, and E.M. Hol, *Cell-replacement and gene-therapy strategies for Parkinson's and Alzheimer's disease.* Regen Med, 2007. **2**(4): p. 425-46.

156. Astradsson, A., et al., *Recent advances in cell-based therapy for Parkinson disease.* Neurosurg Focus, 2008. **24**(3-4): p. E6.

157. Freed, C.R., et al., *Transplantation of embryonic dopamine neurons for severe Parkinson's disease.* N Engl J Med, 2001. **344**(10): p. 710-9.

158. Mendez, I., et al., *Simultaneous intrastriatal and intranigral fetal dopaminergic grafts in patients with Parkinson disease: a pilot study. Report of three cases.* J Neurosurg, 2002. **96**(3): p. 589-96.

159. Peschanski, M., et al., *Bilateral motor improvement and alteration of L-dopa effect in two patients with Parkinson's disease following intrastriatal transplantation of foetal ventral mesencephalon.* Brain, 1994. **117 (Pt 3)**: p. 487-99.

160. Lindvall, O., et al., *Grafts of fetal dopamine neurons survive and improve motor function in Parkinson's disease.* Science, 1990. **247**(4942): p. 574-7.

161. Olanow, C.W., et al., *A double-blind controlled trial of bilateral fetal nigral transplantation in Parkinson's disease.* Ann Neurol, 2003. **54**(3): p. 403-14.

162. Perrier, A.L., et al., *Derivation of midbrain dopamine neurons from human embryonic stem cells.* Proc Natl Acad Sci U S A, 2004. **101**(34): p. 12543-8.

163. Sonntag, K.C., et al., *Enhanced yield of neuroepithelial precursors and midbrain-like dopaminergic neurons from human embryonic stem cells using the bone morphogenic protein antagonist noggin.* Stem Cells, 2007. **25**(2): p. 411-8.

164. Bjorklund, L.M., et al., *Embryonic stem cells develop into functional dopaminergic neurons after transplantation in a Parkinson rat model.* Proc Natl Acad Sci U S A, 2002. **99**(4): p. 2344-9.

165. Sonntag, K.C., et al., *Context-dependent neuronal differentiation and germ layer induction of Smad4-/- and Cripto-/- embryonic stem cells.* Mol Cell Neurosci, 2005. **28**(3): p. 417-29.

166. Moghadam, F.H., et al., *Transplantation of primed or unprimed mouse embryonic stem cell-derived neural precursor cells improves cognitive function in Alzheimerian rats.* Differentiation, 2009. **78**(2-3): p. 59-68.

167. Gage, F.H., et al., *Intrahippocampal septal grafts ameliorate learning impairments in aged rats.* Science, 1984. **225**(4661): p. 533-6.

168. Wernig, M., et al., *Neurons derived from reprogrammed fibroblasts functionally integrate into the fetal brain and improve symptoms of rats with Parkinson's disease.* Proc Natl Acad Sci U S A, 2008. **105**(15): p. 5856-61.

169. Pang, Z.P., et al., *Induction of human neuronal cells by defined transcription factors.* Nature, 2011.

170. Pfisterer, U., et al., *Direct conversion of human fibroblasts to dopaminergic neurons.* Proc Natl Acad Sci U S A, 2011. **108**(25): p. 10343-8.

171. Caiazzo, M., et al., *Direct generation of functional dopaminergic neurons from mouse and human fibroblasts.* Nature, 2011. **476**(7359): p. 224-7.

172. Liu, X., et al., *Direct reprogramming of human fibroblasts into dopaminergic neuron-like cells.* Cell Res, 2012. **22**(2): p. 321-32.

173. Kim, J., et al., *Functional integration of dopaminergic neurons directly converted from mouse fibroblasts.* Cell Stem Cell, 2011. **9**(5): p. 413-9.

174. Caiazzo, M., et al., *Direct generation of functional dopaminergic neurons from mouse and human fibroblasts.* Nature, 2011.

175. Nicholas, C.R. and A.R. Kriegstein, *Regenerative medicine: Cell reprogramming gets direct.* Nature, 2010. **463**(7284): p. 1031-2.

176. Bowman, K., et al., *Gene transfer to hemophilia A mice via oral delivery of FVIII-chitosan nanoparticles.* J Control Release, 2008. **132**(3): p. 252-9.

177. van der Lubben, I.M., et al., *Chitosan and its derivatives in mucosal drug and vaccine delivery.* Eur J Pharm Sci, 2001. **14**(3): p. 201-7.

178. Senel, S., et al., *Enhancing effect of chitosan on peptide drug delivery across buccal mucosa.* Biomaterials, 2000. **21**(20): p. 2067-71.

179. Macleod, G.S., et al., *Selective drug delivery to the colon using pectin:chitosan:hydroxypropyl methylcellulose film coated tablets.* Int J Pharm, 1999. **187**(2): p. 251-7.

180. Ramdas, M., et al., *Alginate encapsulated bioadhesive chitosan microspheres for intestinal drug delivery.* J Biomater Appl, 1999. **13**(4): p. 290-6.

181. Felt, O., P. Buri, and R. Gurny, *Chitosan: a unique polysaccharide for drug delivery.* Drug Dev Ind Pharm, 1998. **24**(11): p. 979-93.

182. Dodane, V., M. Amin Khan, and J.R. Merwin, *Effect of chitosan on epithelial permeability and structure.* Int J Pharm, 1999. **182**(1): p. 21-32.

183. Fang, N., et al., *Interactions of phospholipid bilayer with chitosan: effect of molecular weight and pH.* Biomacromolecules, 2001. **2**(4): p. 1161-8.

184. Thanou, M., J.C. Verhoef, and H.E. Junginger, *Oral drug absorption enhancement by chitosan and its derivatives.* Adv Drug Deliv Rev, 2001. **52**(2): p. 117-26.

185. Hirano, S., *Chitin biotechnology applications.* Biotechnol Annu Rev, 1996. **2**: p. 237-58.

186. Dhawan, S., A.K. Singla, and V.R. Sinha, *Evaluation of mucoadhesive properties of chitosan microspheres prepared by different methods.* AAPS PharmSciTech, 2004. **5**(4): p. e67.

187. Chew, J.L., et al., *Chitosan nanoparticles containing plasmid DNA encoding house dust mite allergen, Der p 1 for oral vaccination in mice.* Vaccine, 2003. **21**(21-22): p. 2720-9.

188. Leong, K.W., et al., *DNA-polycation nanospheres as non-viral gene delivery vehicles.* J Control Release, 1998. **53**(1-3): p. 183-93.

189. Mao, H.Q., et al., *Chitosan-DNA nanoparticles as gene carriers: synthesis, characterization and transfection efficiency.* J Control Release, 2001. **70**(3): p. 399-421.

190. Kiang, T., et al., *Formulation of chitosan-DNA nanoparticles with poly(propyl acrylic acid) enhances gene expression.* Journal of Biomaterials Science-Polymer Edition, 2004. **15**(11): p. 1405-1421.

191. Bowman, K., et al. *Non-viral Gene Therapy for Hemophilia A Through Oral Delivery of Chitosan Nanoparticles*. in *The 31st International Symposium on Controlled Release of Bioactive Materials*. 2004. Hawaii: Controlled Release Society.

192. Wong, K., et al., *PEI-g-chitosan, a novel gene delivery system with transfection efficiency comparable to polyethylenimine in vitro and after liver administration in vivo.* Bioconjug Chem, 2006. **17**(1): p. 152-8.

193. MacLaughlin, F.C., et al., *Chitosan and depolymerized chitosan oligomers as condensing carriers for in vivo plasmid delivery.* J Control Release, 1998. **56**(1-3): p. 259-72.

194. Richardson, S.C., H.V. Kolbe, and R. Duncan, *Potential of low molecular mass chitosan as a DNA delivery system: biocompatibility, body distribution and ability to complex and protect DNA.* Int J Pharm, 1999. **178**(2): p. 231-43.

195. Thanou, M., J.C. Verhoef, and H.E. Junginger, *Chitosan and its derivatives as intestinal absorption enhancers.* Adv Drug Deliv Rev, 2001. **50 Suppl 1**: p. S91-101.

196. Lee, K.Y., et al., *Preparation of chitosan self-aggregates as a gene delivery system.* Journal of Controlled Release, 1998. **51**(2-3): p. 213-220.

197. Douglas, K.L., C.A. Piccirillo, and M. Tabrizian, *Effects of alginate inclusion on the vector properties of chitosan-based nanoparticles.* J Control Release, 2006. **115**(3): p. 354-61.

198. Peng, S.F., et al., *Effects of incorporation of poly(gamma-glutamic acid) in chitosan/DNA complex nanoparticles on cellular uptake and transfection efficiency.* Biomaterials, 2009. **30**(9): p. 1797-808.

199. Lin, C. and J.F. Engbersen, *Effect of chemical functionalities in poly(amido amine)s for non-viral gene transfection.* J Control Release, 2008. **132**(3): p. 267-72.

200. Chen, Z.Y., et al., *Silencing of episomal transgene expression by plasmid bacterial DNA elements in vivo.* Gene Ther, 2004. **11**(10): p. 856-64.

201. Chen, Z.Y., et al., *Minicircle DNA vectors devoid of bacterial DNA result in persistent and high-level transgene expression in vivo.* Mol Ther, 2003. **8**(3): p. 495-500.

202. Chen, Z.Y., C.Y. He, and M.A. Kay, *Improved production and purification of minicircle DNA vector free of plasmid bacterial sequences and capable of persistent transgene expression in vivo.* Hum Gene Ther, 2005. **16**(1): p. 126-31.

203. Shigematsu, H., et al., *Randomized, double-blind, placebo-controlled clinical trial of hepatocyte growth factor plasmid for critical limb ischemia.* Gene Ther, 2010. **17**(9): p. 1152-61.

204. Nathwani, A.C., et al., *Adenovirus-associated virus vector-mediated gene transfer in hemophilia B.* N Engl J Med, 2011. **365**(25): p. 2357-65.

205. Morishita, R., et al., *Phase I/IIa clinical trial of therapeutic angiogenesis using hepatocyte growth factor gene transfer to treat critical limb ischemia.* Arterioscler Thromb Vasc Biol, 2011. **31**(3): p. 713-20.

206. Bennett, J., et al., *AAV2 gene therapy readministration in three adults with congenital blindness.* Sci Transl Med, 2012. **4**(120): p. 120ra15.

207. Davis, M.E., et al., *Evidence of RNAi in humans from systemically administered siRNA via targeted nanoparticles.* Nature, 2010. **464**(7291): p. 1067-70.

208. Tang, B.C., et al., *Biodegradable polymer nanoparticles that rapidly penetrate the human mucus barrier.* Proc Natl Acad Sci U S A, 2009. **106**(46): p. 19268-73.

209. Lai, S.K., Y.Y. Wang, and J. Hanes, *Mucus-penetrating nanoparticles for drug and gene delivery to mucosal tissues.* Adv Drug Deliv Rev, 2009. **61**(2): p. 158-71.

210. Fernandez, C.A., et al., *Metabolically stabilized long-circulating PEGylated polyacridine peptide polyplexes mediate hydrodynamically stimulated gene expression in liver.* Gene Ther, 2011. **18**(1): p. 23-37.

211. Pack, D.W., et al., *Design and development of polymers for gene delivery.* Nat Rev Drug Discov, 2005. **4**(7): p. 581-93.

212. Kim, J., et al., *Microfluidic approaches for gene delivery and gene therapy.* Lab Chip, 2011. **11**(23): p. 3941-8.

213. Debus, H., M. Beck-Broichsitter, and T. Kissel, *Optimized preparation of pDNA/poly(ethylene imine) polyplexes using a microfluidic system.* Lab Chip, 2012. **12**(14): p. 2498-506.

214. Qin, D., Y. Xia, and G.M. Whitesides, *Soft lithography for micro- and nanoscale patterning.* Nature Protocols, 2010. **5**(3): p. 491-502.

215. Song, H., D.L. Chen, and R.F. Ismagilov, *Reactions in droplets in microfluidic channels.* Angew Chem Int Ed Engl, 2006. **45**(44): p. 7336-56.

216. DeMello, A.J., *Control and detection of chemical reactions in microfluidic systems.* Nature, 2006. **442**(7101): p. 394-402.

217. Khalil, I.A., et al., *High density of octaarginine stimulates macropinocytosis leading to efficient intracellular trafficking for gene expression.* Journal of Biological Chemistry, 2006. **281**(6): p. 3544-51.

218. Martens, T.F., et al., *Measuring the intravitreal mobility of nanomedicines with single-particle tracking microscopy.* Nanomedicine (Lond), 2013.

219. Adler, A.F., et al., *Nonviral direct conversion of primary mouse embryonic fibroblasts to neuronal cells.* Mol Ther Nucleic Acids, 2012. **1**: p. e32.

220. Wang, Y., et al., *Stability issue of nanosuspensions in drug delivery.* J Control Release, 2013.

221. Fischer, D., et al., *In vitro cytotoxicity testing of polycations: influence of polymer structure on cell viability and hemolysis.* Biomaterials, 2003. **24**(7): p. 1121-31.

222. Zauner, W., N.A. Farrow, and A.M. Haines, *In vitro uptake of polystyrene microspheres: effect of particle size, cell line and cell density.* J Control Release, 2001. **71**(1): p. 39-51.

223. Grigsby, C.L., Y.P. Ho, and K.W. Leong, *Understanding nonviral nucleic acid delivery with quantum dot-FRET nanosensors.* Nanomedicine (Lond), 2012. **7**(4): p. 565-77.

224. Han, S.S., L.A. Williams, and K.C. Eggan, *Constructing and deconstructing stem cell models of neurological disease.* Neuron, 2011. **70**(4): p. 626-44.

225. Urbaniak Hunter, K., C. Yarbrough, and J. Ciacci, *Gene- and cell-based approaches for neurodegenerative disease.* Adv Exp Med Biol, 2010. **671**: p. 117-30.

226. Okita, K., T. Ichisaka, and S. Yamanaka, *Generation of germline-competent induced pluripotent stem cells.* Nature, 2007. **448**(7151): p. 313-7.

227. Pang, Z.P.P., et al., *Induction of human neuronal cells by defined transcription factors.* Nature, 2011. **476**(7359): p. 220-U122.

228. Pfisterer, U., et al., *Direct conversion of human fibroblasts to dopaminergic neurons.* Proceedings of the National Academy of Sciences of the United States of America, 2011. **108**(25): p. 10343-10348.

229. Kim, J., et al., *Functional Integration of Dopaminergic Neurons Directly Converted from Mouse Fibroblasts.* Cell Stem Cell, 2011. **9**(5): p. 413-419.

230. Addis, R.C., et al., *Efficient conversion of astrocytes to functional midbrain dopaminergic neurons using a single polycistronic vector.* PLoS One, 2011. **6**(12): p. e28719.

231. Son, E.Y., et al., *Conversion of Mouse and Human Fibroblasts into Functional Spinal Motor Neurons.* Cell Stem Cell, 2011. **9**(3): p. 205-218.

232. Qiang, L., et al., *Directed conversion of Alzheimer's disease patient skin fibroblasts into functional neurons.* Cell, 2011. **146**(3): p. 359-71.

233. Marro, S., et al., *Direct Lineage Conversion of Terminally Differentiated Hepatocytes to Functional Neurons.* Cell Stem Cell, 2011. **9**(4): p. 374-382.

234. Ambasudhan, R., et al., *Direct Reprogramming of Adult Human Fibroblasts to Functional Neurons under Defined Conditions.* Cell Stem Cell, 2011. **9**(2): p. 113-118.

235. Yoo, A.S., et al., *MicroRNA-mediated conversion of human fibroblasts to neurons.* Nature, 2011. **476**(7359): p. 228-31.

236. Biasco, L., C. Baricordi, and A. Aiuti, *Retroviral Integrations in Gene Therapy Trials.* Mol Ther, 2012.

237. Montserrat, N., et al., *Simple Generation of Human Induced Pluripotent Stem Cells Using Poly-beta-amino Esters As the Non-viral Gene Delivery System.* Journal of Biological Chemistry, 2011. **286**(14).

238. Lee, C.H., et al., *The generation of iPS cells using non-viral magnetic nanoparticle based transfection.* Biomaterials, 2011. **32**(28): p. 6683-6691.

239. Okita, K., et al., *Generation of Mouse Induced Pluripotent Stem Cells Without Viral Vectors.* Science, 2008. **322**(5903): p. 949-953.

240. Jia, F., et al., *A nonviral minicircle vector for deriving human iPS cells.* Nat Methods, 2010. **7**(3): p. 197-9.

241. Gonzalez, F., et al., *Generation of mouse-induced pluripotent stem cells by transient expression of a single nonviral polycistronic vector.* Proc Natl Acad Sci U S A, 2009. **106**(22): p. 8918-22.

242. Adler, A.F., et al., *High-throughput screening of microscale pitted substrate topographies for enhanced nonviral transfection efficiency in primary human fibroblasts.* Biomaterials, 2011. **32**(14): p. 3611-9.

243. Yim, E.K., S.W. Pang, and K.W. Leong, *Synthetic nanostructures inducing differentiation of human mesenchymal stem cells into neuronal lineage.* Exp Cell Res, 2007. **313**(9): p. 1820-9.

244. Ankam, S., et al., *Substrate topography and size determine the fate of human embryonic stem cells to neuronal or glial lineage.* Acta Biomater, 2013. **9**(1): p. 4535-45.

245. Teo, B.K., et al., *The effect of micro and nanotopography on endocytosis in drug and gene delivery systems.* Biomaterials, 2011. **32**(36): p. 9866-75.

246. Nathanson, J.L., et al., *Preferential labeling of inhibitory and excitatory cortical neurons by endogenous tropism of adeno-associated virus and lentivirus vectors.* Neuroscience, 2009. **161**(2): p. 441-50.

247. Wheeler, D.G. and E. Cooper, *Depolarization strongly induces human cytomegalovirus major immediate-early promoter/enhancer activity in neurons.* Journal of Biological Chemistry, 2001. **276**(34): p. 31978-85.

248. Kugler, S., E. Kilic, and M. Bahr, *Human synapsin 1 gene promoter confers highly neuron-specific long-term transgene expression from an adenoviral vector in the adult rat brain depending on the transduced area.* Gene Ther, 2003. **10**(4): p. 337-47.

249. Hioki, H., et al., *Efficient gene transduction of neurons by lentivirus with enhanced neuron-specific promoters.* Gene Ther, 2007. **14**(11): p. 872-82.

250. Jordan, M. and F.M. Wurm, *Co-transfer of multiple plasmids/viruses as an attractive method to introduce several genes in mammalian cells*, in *New Comprehensive Biochemistry*, S.C. Makrides, Editor. 2003, Elsevier. p. 337-348.

251. Vierbuchen, T. and M. Wernig, *Direct lineage conversions: unnatural but useful?* Nat Biotechnol, 2011. **29**(10): p. 892-907.

252. Yang, N., et al., *Induced Neuronal Cells: How to Make and Define a Neuron.* Cell Stem Cell, 2011. **9**(6): p. 517-525.

253. Citri, A., et al., *Comprehensive qPCR profiling of gene expression in single neuronal cells.* Nat Protoc, 2012. **7**(1): p. 118-27.

254. Kaji, K., et al., *Virus-free induction of pluripotency and subsequent excision of reprogramming factors.* Nature, 2009. **458**(7239): p. 771-U112.

255. Lauret, E. and R. Baserga, *Inhibition of gene expression at the translational level by cotransfection with competitor plasmids.* DNA, 1988. **7**(3): p. 151-6.

256. Noctor, S.C., et al., *Neurons derived from radial glial cells establish radial units in neocortex.* Nature, 2001. **409**(6821): p. 714-20.

257. Chua, J.S., et al., *Extending neurites sense the depth of the underlying topography during neuronal differentiation and contact guidance.* Biomaterials, 2014. **35**(27): p. 7750-61.

258. Kulangara, K., et al., *The effect of substrate topography on direct reprogramming of fibroblasts to induced neurons.* Biomaterials, 2014. **35**(20): p. 5327-36.

259. Ladewig, J., et al., *Small molecules enable highly efficient neuronal conversion of human fibroblasts.* Nat Methods, 2012.

260. Rodnitzky, R.L., *Upcoming treatments in Parkinson's disease, including gene therapy.* Parkinsonism Relat Disord, 2012. **18 Suppl 1**: p. S37-40.

261. Feng, R., et al., *PU.1 and C/EBPalpha/beta convert fibroblasts into macrophage-like cells.* Proc Natl Acad Sci U S A, 2008. **105**(16): p. 6057-62.

262. Kajimura, S., et al., *Initiation of myoblast to brown fat switch by a PRDM16-C/EBP-beta transcriptional complex.* Nature, 2009. **460**(7259): p. 1154-8.

263. Ieda, M., et al., *Direct Reprogramming of Fibroblasts into Functional Cardiomyocytes by Defined Factors.* Cell, 2010. **142**(3): p. 375-386.

264. Sekiya, S. and A. Suzuki, *Direct conversion of mouse fibroblasts to hepatocyte-like cells by defined factors.* Nature, 2011. **475**(7356): p. 390-3.

265. Huang, P., et al., *Induction of functional hepatocyte-like cells from mouse fibroblasts by defined factors.* Nature, 2011. **475**(7356): p. 386-9.

Biography

Christopher Lawrence Grigsby was born in Minneapolis, Minnesota on November 12th, 1982. He graduated from the University of California, Berkeley with a Bachelor of Science degree in Bioengineering in May 2005. Following graduation, he joined Prof. David G. Gardner's group at the UCSF Diabetes Center as a research associate. After two years, he matriculated at Duke University to join Prof. Kam W. Leong's group in the Department of Biomedical Engineering. While at Duke University, Christopher's research focused on the design and application of nonviral gene delivery technologies. He was first supported by a Duke Center for Tissue and Biomolecular Engineering training grant, and subsequently by a predoctoral fellowship from the American Heart Association. He also received fellowship awards from the Whitaker International Program and US Fulbright Program to conduct research at the Mechanobiology Institute at the National University of Singapore. His work contributed to the following publications:

1. Lu M, Ho YP, **Grigsby CL**, Nawaz AA, Leong KW, Huang TJ (2014). A three-dimensional hydrodynamic focusing method for polyplex synthesis. ACS Nano. 8(1):332-9

2. **Grigsby CL**, Ho YP, Lin C, Engbersen JFJ, Leong KW (2013). Microfluidic preparation of polymer-nucleic acid nanocomplexes improves nonviral gene transfer. Sci Rep. 3:3155

3. Adler AF*, **Grigsby CL***, Kulangara K, Wang H, Yasuda R, Leong KW (2012). Nonviral direct conversion of mouse embryonic fibroblasts to neuronal cells. Mol Ther Nuc Acids. 1:e32

4. **Grigsby CL**, Ho YP, Leong KW (2012). Understanding nonviral nucleic acid delivery with quantum dot-FRET nanosensors. Nanomedicine. 7(4):565-77

5. Loo Y, **Grigsby CL**, Yamanaka YJ, Chellappan, MK, Jiang X, Mao HQ, Leong KW (2012). Comparative study of nanoparticle-mediated transfection in different GI epithelium co-culture models. J Cont Rel. 160(1):48-56

6. Chen S, Law CS, **Grigsby CL**, Olsen K, Hong TT, Zhang Y, Yeghiazarians Y, Gardner DG (2011). Cardiomyocyte-specific deletion of the vitamin D receptor gene results in cardiac hypertrophy. Circulation. 124(17):1838-47

7. Ho YP, **Grigsby CL**, Zhao F, Leong KW (2011). Tuning physical properties of nanocomplexes through microfluidics-assisted confinement. Nano Lett. 11(5):2178-82

8. Chen S, Law CS, **Grigsby CL**, Olsen K, Gardner DG (2010). A role for the cell cycle phosphatase Cdc25a in vitamin D-dependent inhibition of adult rat vascular smooth muscle cell proliferation. J Steroid Biochem Mol Biol. 122(5):326-32

9. **Grigsby CL** and Leong KW (2010). Balancing protection and release of DNA: tools to address a bottleneck of non-viral gene delivery. J R Soc Interface. 7 Suppl 1:S67-82

10. Chen S, **Grigsby CL**, Law CS, Ni X, Nekrep N, Olsen KC, Humphreys MH, Gardner DG (2009). Tonicity-dependent induction of Sgk1 expression has a potential role in dehydration-induced natriuresis in rodents. J Clin Invest. 119(6):1647-58

11. Chen S, Glenn DJ, Ni W, **Grigsby CL**, Olsen KC, Nishimoto M, Law CS, Gardner DG (2008). Expression of the vitamin D receptor is increased in the hypertrophic heart. Hypertension. 52(6):1106-12

12. Chen S, Olsen KC, **Grigsby CL**, Gardner DG (2007). Vitamin D activates type A natriuretic peptide receptor gene transcription in inner medullary collecting duct cells. Kidney Int. 72(3):300-6

13. Gardner DG, Chen S, Glenn DG, **Grigsby CL** (2007). Molecular biology of the natriuretic peptide system: implications for physiology and hypertension. Hypertension. 49(3):419-26